AD-780 657

SEISMIC PHENOMENA CONNECTED WITH
EARTHQUAKES AND EXPLOSIONS

David G. Harkrider

California Institute of Technology

Prepared for:

Air Force Office of Scientific Research
Advanced Research Projects Agency

14 September 1973

SECURITY CLASSIFICATION OF THIS PAGE (When Data Entered)

REPORT DOCUMENTATION PAGE		READ INSTRUCTIONS BEFORE COMPLETING FORM
1. REPORT NUMBER AFOSR - TR - 74 - 0854	2. GOVT ACCESSION NO.	3. RECIPIENT'S CATALOG NUMBER AD-780657
4. TITLE (and Subtitle) Seismic Phenomena Connected with Earthquakes and Explosions		5. TYPE OF REPORT & PERIOD COVERED Semi-Annual Technical Report 15 March 1973 - 14. Sept. 1973
		6. PERFORMING ORG. REPORT NUMBER
7. AUTHOR(s) David G. Harkrider		8. CONTRACT OR GRANT NUMBER(s) F44620-72-C-0078
9. PERFORMING ORGANIZATION NAME AND ADDRESS California Institute of Technology Seismological Laboratory P.O. Bin 2 - Arroyo Annex, Pasadena, CA. 91109		10. PROGRAM ELEMENT, PROJECT, TASK AREA & WORK UNIT NUMBERS ARPA Order 1827, Amend. 6 3F10 Program Code
11. CONTROLLING OFFICE NAME AND ADDRESS AFOSR 1400 Wilson Blvd. (NPG) Arlington, VA. 22209		12. REPORT DATE 1973
		13. NUMBER OF PAGES 118
14. MONITORING AGENCY NAME & ADDRESS(if different from Controlling Office)		15. SECURITY CLASS. (of this report) Unclassified
		15a. DECLASSIFICATION. DOWNGRADING SCHEDULE

16. DISTRIBUTION STATEMENT (of this Report)

Approved for public release; distribution unlimited.

17. DISTRIBUTION STATEMENT (of the abstract entered in Block 20, if different from Report)

18. SUPPLEMENTARY NOTES

19. KEY WORDS (Continue on reverse side if necessary and identify by block number)

detection	shear velocities	crustal structure
discrimination	earthquake models	
seismic sources	earth models	

20. ABSTRACT (Continue on reverse side if necessary and identify by block number)

Several studies have been completed on the shear velocity distribution in the crust and mantle. These are important in determining, correcting, and interpreting surface wave magnitudes (M_s). We show that PL contaminates studies of SV.

A major effort has been made to determine the earthquake source time history. For this purpose we have used S, P and surface waves and have been able to obtain good matches between theoretical and observed seismograms. Source functions have been derived from several shallow and

20. Abstract Cont'd.

deep focus events.

Scaling laws are derived for various realistic explosion and tectonic sources. We also determined theoretical $M_s - m_b$ curves and show that effective upper limits exist for both m_b and M_s. We suggest that published differences in P and S corner frequencies may be an artifact of the data processing.

We have determined the average crustal structure between NTS and mid-Arizona.

AFOSR - TR - 74 - 0854

California Institute of Technology
Division of Geological and Planetary Sciences
Seismological Laboratory
Pasadena, California 91109

AD780657

SEMI-ANNUAL TECHNICAL REPORT

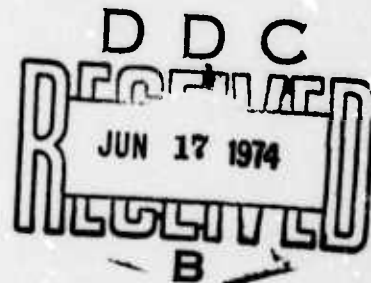15 March 1973 - 14 September 1973

ARPA Order No.: 1827, Amendment 6
Program Code: 3F10
Name of Contractor: California Institute of Technology
Effective Date of Contract: 15 March 1972
Contract Expiration Date: 14 March 1974
Amount of Contract: $228,862
Contract Number: F44620-72-C-0078
Principal Investigator
 and Telephone Number: Don L. Anderson
 (213) 795-8806
Program Manager and William J. Best
 Telephone Number: (202) 6ᵒᵘ-5456
Short Title of Work: Seismic   nomena Connected with
 Earthquakes and Explosions

DDC
RECEIVED
JUN 17 1974
B

Sponsored by
Advanced Research Projects Agency
ARPA Order No. 1827

CONTENTS

i

I. Summary

A major problem in evaluating M_s vs. m_b as an earthquake-explosion discriminant is the question of what characterizes earthquake source time histories. A major controversy in seismology is whether P- and S-wave source histories are different for individual events. This difference is suggested by spectral estimates of the corner frequencies for P- and S-waves for a variety of observed earthquakes.

Sections V and III address the problem of seismic source time histories using two different approaches. The first uses volume source models of tectonic release and obtains numerically their P- and S-wave spectra which for these models show a difference in the P- and S-wave corner frequencies. The second approach is to obtain the earthquake P-wave source history from comparison of theoretical and observed seismograms. This history is then used as the S-wave history to obtain theoretical seismograms which are compared with S-wave observations of the same events. Some of these comparisons are shown in Figure 1.

Section V discusses with numerical examples the source spectra for two relaxation volume source models, one representing the tectonic release associated with underground explosions and the other a model of earthquakes associated with a unilateral propagating rupture in a tectonic region. The azimuthal dependence of the source radiation fields is discussed as a function of frequency, both on the basis of selected amplitude spectra and of selected radiation patterns. Phase spectra are shown which illustrate the complexity of the radiated fields. Scaling laws are given and numerically demonstrated for the different P- and S-wave spectral corner frequencies. The difficulties involved with determining these corner frequencies from the amplitude spectra is also discussed.

Simulated M_s vs. m_b curves are determined from the source spectra and discussed in terms of scaling by the various source parameters. See, for example, Figure 2. Effective upper limits to m_b and M_s are shown.

Finally, theoretical spectrum and seismograms are compared with

ARGENTINA

| P-Waves | SH-Waves |

BEC

BLA

OXF

SCP

10 sec.

JCT

AAM
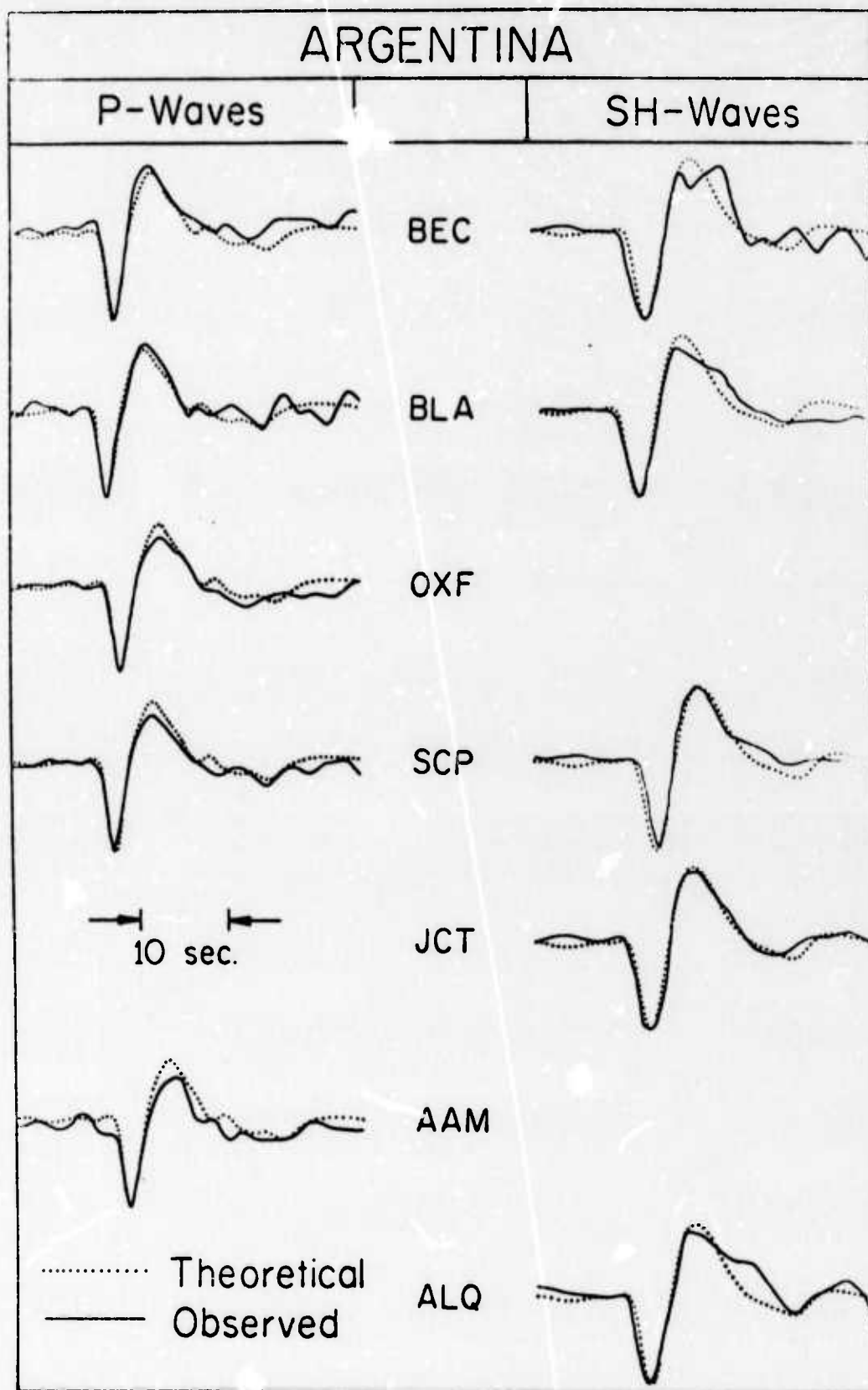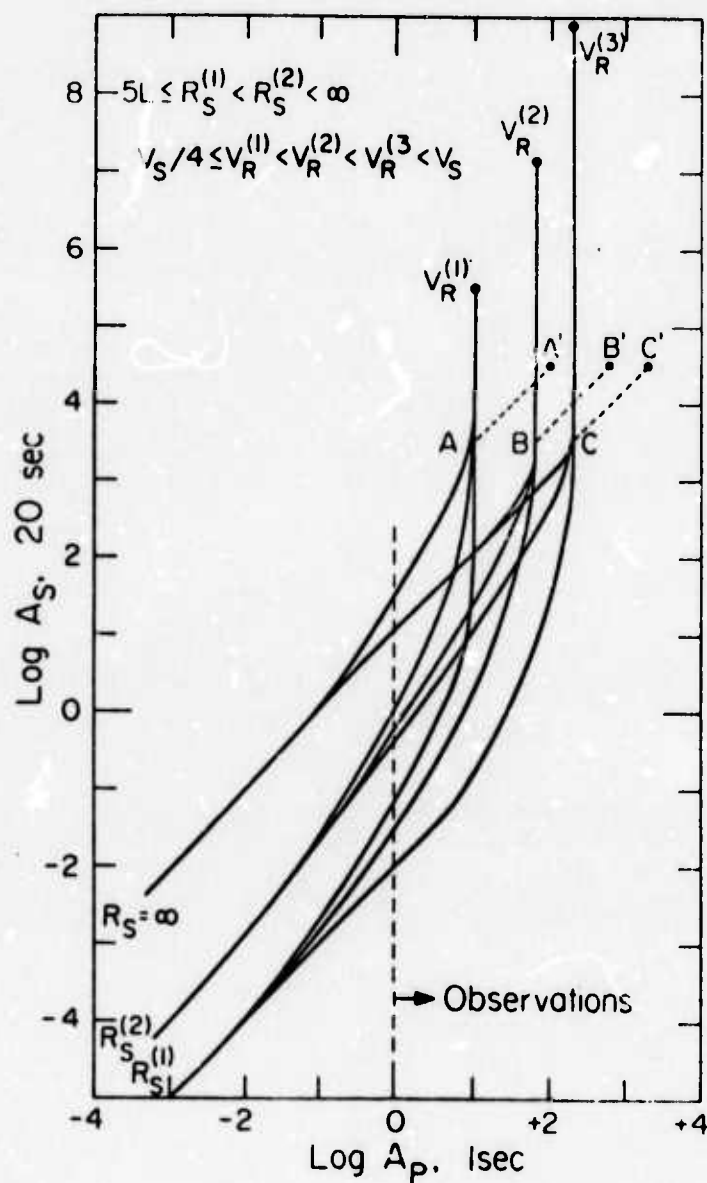
·········· Theoretical

—— Observed

ALQ

Fig. 1

Fig. 2 . Plot of S spectral amplitude at 20 seconds versus
P spectral amplitude at 1 second period. Simulation of m_b / M_s plots.

observations of the Harris Ranch earthquake of 27 October 1969 in order
to estimate its source parameters. The difference between assuming an
infinite versus finite tectonic region is shown in the frequency and
time domain. The amplitude spectrum and seismogram data both suggest
a finite tectonic release region for this event.

In section III, teleseismic P- and S-wave arrivals from three
deep focus earthquakes of roughly magnitude 6 are analyzed for differences
in their respective source time histories. The earthquakes and distances
are chosen in order to minimize the effects of near surface structure.
The signals are analyzed in the time domain so that information about
the sequence and duration of the transient pulses are preserved. The
source time history derived from the P-waves is used to predict syn-
thetic S-wave shapes that match the observations. The good agreement
(see Figure 1) implies that the P- and S-wave source time histories for
each event are essentially the same with no significant difference in
P- and S-wave spectral corner frequencies. This is in contrast to the
Wyss and Molnar (1972) study which indicates a difference in the spectral
corner frequencies of P and S for highly similar data. Providing that
both analyses are correct, this indicates that the corner frequency
difference is only weakly constrained by the original time data and
raises the possibility that the difference is an artifact of the data
processing. The occurrence of a strong PL phase in the Western Brazil
S-waves demonstrates that even for deep focus earthquakes at ranges
greater than 50°, crustal structure can distort the wave shape and
consequently its Fourier spectrum. Future studies on source histories
in either the frequency or time domain should be coupled with a careful
examination of the seismograms to screen out data contaminated by later
arrivals such as PL.

Since knowledge of the crustal structure is essential in determining
explosion and earthquake source functions, section IV demonstrates a
method of using amplitudes and arrival times of body waves and Rayleigh
waves from NTS events to determine an average crustal model from NTS
to mid-Arizona. A comparison of synthetic with observed body waves
using previous refraction studies as a starting P-wave structure was
used as a compressional velocity constraint for the lower part of the
crust. Since the observed Rayleigh waves were sampling approximately

the upper 20 km of crust, analysis of the Rayleigh waves from NTS events was used to determine the average shear structure for the upper part of the crust along the profile. Two velocity and density structures are found which fit the Rayleigh and body wave data equally well. A typical example of the agreement between theoretical and observed wave forms is shown in Figure 3 for the BOXCAR event.

We now have powerful capabilities to determine source and path properties in both the time and frequency domain for both body waves and surface waves. These techniques have been spelled out in a series of papers and technical reports by Helmberger, Harkrider, and their colleagues. Generalizations of both dislocation and relaxation source models are presently being implemented by these investigators and also by Kanamori.
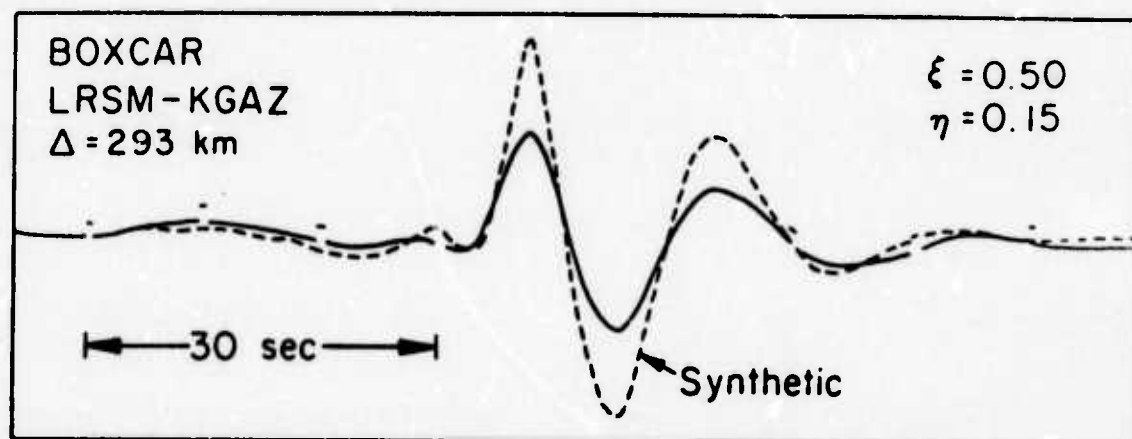
Fig. 3. Synthetic and observed Rayleigh waves from BOXCAR.

II-7

II. ABSTRACTS OF PUBLICATIONS AND REPORTS
     DURING THIS CONTRACT PERIOD.

Mitchell, B. J., "Surface Wave Attenuation and Crustal Anelasticity in Central North America," Seismol. Soc. America Bull., 63, 1057-1071, 1973.

The southeastern Missouri earthquake of October 21, 1964 generated fundamental- and higher-mode Love and Rayleigh waves which were recorded at numerous North American stations. Love-wave amplitude radiation patterns were determined and found to be consistent with theoretical patterns predicted by a fault-plane solution previously inferred from Rayleigh-wave data.

The radiation patterns were used to estimate the source spectrum and values for Love-wave attenuation coefficients for the mid-continent of North America by a least-squares iterative process. The source spectrum derived from Love-wave amplitudes exhibits a peak at periods between 5 and 9 sec and decreases to a lower DC level at longer periods, in agreement with the source spectrum determined previously for Rayleigh waves. The Love-wave attenuation coefficients decrease rapidly from about 0.0018 km at a period of 4 sec to about 0.0001 km at a period of 20 sec. At periods between 20 and 40 sec the values seem to remain nearly constant.

The crust in the mid-continent of North America is characterized by relatively low Q_β values, 75 to 300, in its upper portion. At depths between 15 and 20 km, Q_β increases sharply and decreases again at greater depths. The decrease can be explained as being due to increasing temperature in a homogeneous material, but the sharp increase requires a change in the chemical constitution of the material at mid-crustal depths.

Kurita, T., "Regional Variations in the Structure of the Crust in the Central United States from P Wave Spectra," Seismol. Soc. America Bull., 63, 1663-1687, 1973.

Regional variations in the crustal structure in the central United States has been inferred from the complex transfer ratio of long period P waves recorded at four WWSSN stations, SHA, OXF, FLO, and MDS. The crustal structure in this region is approximated by a stack of horizontal parallel layers except possibly the area around FLO where the structure is rather complicated. Deep discontinuities in the crust may possibly be replaced by transitional layers up to 10 km thick. The depth to the MOHO is about 33 km near the Gulf of Mexico, deepens to about 41 km near the intersection of the Gulf Coastal Plain and the Interior Plain, reaches about 47 km or more in the midst of the Interior Plain, and rises to about 41 km toward the intersection of the Interior Plain and the Superior Upland. The thickness of the silicic upper crust, having a velocity of about 6.0 to 6.5 km/sec in each of the regions above is about 15, 30, 35, and 30 km respectively, whereas the thickness of the mafic lower crust is about 10 km throughout the entire region. The velocity of the lower crust is about 6.9 to 7.0 km/sec except probably for the area around FLO where about 7.4 km/sec velocity is more likely. The existence of a near-surface layer with a velocity of about 4.7 to 5.4 km/sec and having a thickness of 1 to 3 km is a prevailing feature. A sedimentary layer with a velocity of about 3.0 km/sec and having a thickness of about 3 km on the Gulf of Mexico is confined to the Gulf Coastal Plain and tapering out to the north. When

two or more crustal models are appropriate for a limited region, the crustal effect may be eliminated from observed spectra with sufficient accuracy by assuming either of the models.

Niazi, Mansour, "SH Travel-Times and Lateral Heterogeneities in the Lower Mantle," Seismol. Soc. America Bull., 63, 2035-2046, 1973.

The horizontal long period seismograms of two shallow earthquakes in Turkey and Iran recorded in selected azimuths are combined for travel time studies of SH-wave beyond angular distance of 40 degrees. The observed travel times along two profiles which sample deep mantle in the vicinity of Iceland and the North Pole show monotonically increasing differences beyond 65 degrees, indicating lateral heterogeneity in the lower mantle. The travel time difference becomes as large as 7 sec at 95 degrees, implying a variation as much as 0.06 km/sec, or about 1%, in the shear wave velocity near 2500 km depth. Inversion of observations, adjusted to surface foci, results in an average lower mantle structure with lower shear velocities than those given by Jeffreys. The difference exceeds 0.1 km/sec at the core boundary.

The arrival time and signature of S waves recorded in Greenland show anomalous features which may be related to deep seated anomalous zones associated with Mid-Atlantic Ridge system.

Helmberger, D. V., "Numerical Seismograms of Long Period Body Waves from 17 to 40°," Seismol. Soc. America Bull., 63, 633-646, 1973.

Long period wave propagation in the upper mantle is investigated by constructing synthetic seismograms for proposed models. A model consisting of spherical layers is assumed. Generalized ray theory and the Cagniard-deHoop method is used to obtain the transient response. Preliminary calculations on producing the phases P and PP by ray summation out to periods of 50 sec is demonstrated, and synthetic seismograms for the long period WWSS and LRSM instruments are constructed.

Models containing prominent transition zones as well as smooth models predict a maximum in the P amplitude near 20°. The LRSM synthetics are quite similar for the various models since the instrument is relatively narrow band, peaked at 20 sec. The upper mantle appears smooth at wavelengths greater than 200 km. On the other hand, the WWSS synthetics are very exciting for models containing structure. The triplications are apparent and the various pulses contain different periods.

The amplitude of the P phase at 30° is down to about 25 percent of its 20° maximum. The amplitude of the PP phase at 35° is comparable to P. Near 35° the PP phase grows rapidly reaching about twice the P phase amplitude near 40°. Models containing sharp transition zones produce high frequency interferences at neighboring ranges. A profile of observations is presented for comparison.

Mitchell, B. J., and D. V. Helmberger, "Shear Velocities at the Base of the Mantle from Observations of S and ScS," Jour. Geophys. Research, 78, 6009-6020, 1973.

The observed amplitude ratios of transversely polarized shear waves, ScSH/SH, include a minimum at a distance of about 68°. Synthetic seismograms computed for a Jeffreys-Bullen model and for models with negative linear velocity gradients at the base of the mantle fail to explain this feature. Various positive linear velocity gradients above the core-mantle boundary explain the amplitude ratio minimum as well as an apparent difference in arrival times of the transversely and radially polarized core reactions, ScS. Good agreement between the observed and computed amplitude ratios cannot be achieved without assigning low Q values to the lower mantle or a small shear velocity value to the outer core.

At epicentral distances greater than 70°, a substantial portion of the energy recorded as a horizontally polarized ScS wave bottoms at various depths in the high velocity region rather than at the core-mantle interface. These precursory arrivals are in phase with the core reflections on the transverse component and out of phase with them on the radial component. This causes an apparent time differential by which the transversely polarized ScS wave seems to arrive slightly earlier than the radially polarized ScS wave.

High velocity regions between 40 and 70 km thick, containing increases from 0.3 to 0.5 km/sec above that of a Jeffreys velocity model yield the best explanation to the combined amplitude and differential time data.

Jordan, T. H., and D. L. Anderson, "Earth Structure from Free Oscillations and Travel Times," Royal Astron. Soc. Geophys. Jour., in press.

An extensive set of reliable gross Earth data has been inverted to obtain a new estimate of the radial variations of seismic velocities and density in the Earth. The basic data set includes the observed mass and moment of inertia, the average periods of free oscillation (taken mainly from the Dziewonski-Gilbert study), and five new sets of differential travel-time data. The differential travel-time data consists of the times of PcP-P and ScS-S, which contain information about mantle structure, and the times of $P'_{AB}-P'_{DF}$ and $P'_{BC}-P'_{DF}$, which are sensitive to core structure. A simple but realistic starting model was constructed using a number of physical assumptions, such as requiring the Adams-Williamson relation to hold in the lower mantle and core. The data were inverted using an iterative linear estimation algorithm. By using baseline-insensitive differential travel times and averaged eigen-periods, a considerable improvement in both the quality of the fit and the resolving power of the data set has been realized. The spheroidal and toroidal data are fit on the average to 0.04 and 0.08 percent, respectively. The final model, designated model B1, also agrees with Rayleigh and Love wave phase and group velocity data.

The ray-theoretical travel times of P waves computed from model B1 are about 0.8 seconds later than the 1968 Seismological Tables with residuals decreasing with distance, in agreement with Cleary and Hales (1968) and other recent studies. The computed PcP, PKP, and PK1KP times are generally within 0.5 seconds of the times obtained in recent studies. The travel times of S computed from B1 are 5 to 10 seconds later than the Jeffreys-Bullen Tables in the distance range $30°$ to $95°$, with residuals increasing with distance. These S times are in general agreement with the more recent data of Kogan (1960), Ibrahim and Nuttli (1967), Lehmann (1964), Cleary (1969), and Bolt et al. (1970).

Model B1 is characterized by an upper mantle with a high, 4.8 km/sec, S_n velocity and a normal, 3.33 gm/cm^3, density. A low-velocity zone for S_n is required by the data, but a possible low-velocity zone for compressional waves cannot be resolved by the basic data set. The upper mantle transition zone contains two first-order discontinuities at depths of 420 km and 671 km. Between these discontinuities the shear velocity decreases with depth. The radius of the core, fixed by PcP-P times and previous mode inversions, is 3485 km, and the radius of the inner core - outer core boundary is 1215 km. There are no other first-order discontinuities in the core model. The shear velocity in the inner core is about 3.5 km/sec.

Gile, W. W., and R. A. Taylor, "Photon-Coupled Generator," submitted to Electronic Design.

Using a photon-electron conversion technique, a method has been developed

to provide time mark identification on strip chart recorders, etc. The procedures can simultaneously generate time marks from a single power source on several recorders with complete isolation from interaction.

Wiggins, R. A., and D. V. Helmberger, "Synthetic Seismogram Computation by Expansion in Generalized Rays," submitted to Royal Astron. Soc. Geophys. Jour.

The exact formulation of generalized ray theory computations of synthetic seismograms for realistic earth models is relatively complex and expensive. The expense can be reduced considerably by a proper organization of the computational procedures. The expense is reduced far more dramatically by introducing an approximation of the transmission coefficients and a careful selection of the rays to be included. The incorporation of such procedures leads to programs which are economically feasible to use to aid in the interpretation of body waves and near source surface and leaky mode waves.

Abstracts of papers presented at meetings during this contract period

Seismological Society of America, 1973 Joint Annual Meeting, May 16-19, Colorado School of Mines, Golden, Colorado

Burdick, L. J., and D. V. Helmberger, "Time Functions Appropriate for Deep Earthquakes."

One important feature of seismic dislocation theory is that it does not predict different corner frequencies for P and S waves. There should be a single time history of displacement on the fault which when corrected for directivity, earth structure, Q, and instrument response, matches the actual observations of P and S. The first two effects can be eliminated by choosing a small deep event with simple waveform on both the short and long period WWSS records. Applying the Q operator and instrument response to an assumed time function we searched by trial and error until a match to the observations was obtained. We found that a ramp dislocation function with a relatively high rise time of .4 sec fit the observed periods of P and S for a magnitude 5.5 event. Adding a small overshoot provided a still better fit to overall wave shape.

Mellman, G. R., and D. V. Helmberger, "High Frequency Attenuation by a Thin High Velocity Layer."

Wave propagation has been studied using the method of Cagniard and de Hoop in an elastic medium consisting of a thin high velocity layer overlying a low velocity zone. It was found that diffraction effects are present, leading to high frequency attenuation in the geometric shadow zone. Attenuation is increased as the thickness of the thin high velocity layer is increased. Comparison of results obtained by omitting the high velocity layer but using an average Q operator show that effects of the high velocity layer are similar to Q effects, with the equivalent Q for a given layer thickness varying as a function of source-receiver distance. These attenuation effects are explained in terms of deformation of the Cagniard contour.

American Geophysical Union, Fifty-Fourth Annual Meeting, April 16-20, 1973, Washington, D.C.

Hart, R. S., "Lower Mantle S-Velocities from Nuclear Explosions."

A new technique has been employed in determining shear wave travel-times from nuclear explosions. This method uses the theoretically determined waveform to separate the true shear arrival from P-wave precursors. The dominant

shear wave from an explosion, actually a pS arrival, has a stable, character-
istic form which permits the use of peak-times, with a theoretical correction
to first arrival, to measure the true travel-time. The resulting data, for a
given event, has a scatter of less than two seconds.

The range of interest was between 25° and 90° from explosions in Nevada,
the Aleutians, Novaya Zemlya, and Eastern Kazakistan. S wave residuals
varied between plus one and plus six seconds with respect to the Jeffreys-
Bullen tables throughout the distance range examined. These new shear data
are interpreted in terms of a new S-velocity structure for the lower mantle.

Minster, J. B., T. Jordan, P. Molnar, E. Haines, "Numerical Modelling of
Instantaneous Plate Tectonics."

A self-consistent plate tectonic model is constructed from the observations
of relative velocities between plates at plate margins through a systematic
inversion procedure.

The data inverted are measurements of the magnitudes (spreading rates),
and directions (transform fault orientations and slip vectors of earthquakes)
of relative velocity vectors between plates. The overdetermined linearized
system of equations relating changes in the pole positions and rates of
rotation to first order changes in the relative velocity vectors is inverted
by the maximum likelihood procedure. The use of Gaussian statistics is
justified. Because we use a linear theory we can determine the uncertainties
in the model induced by small errors in the data, and also study the relative
importances of the data. We have also inverted the azimuths of 25 volcanic
chains, distributed over nine plates, under the assumption that they were
caused by hot spots fixed in the mantle. With the exception of Iceland,
very good fits were obtained, yielding a model for plate motions over the
mantle. The velocity of the Pacific plate over the Hawaiian hot spot for
this model is 8.9 cm/y.

Kanamori, H., "Interpretation of Near-Field Seismograms in Terms of Fault
Parameters."

de-Hoop-Haskell representations have been used to calculate synthetic
seismograms at short epicentral distances. These synthetic seismograms
are compared with the observed long-period strong-motion records to deter-
mine various fault parameters such as the dislocation and the dislocation
velocity. For most moderate-size Japanese earthquakes including the 1943
Tottori and the 1948 Fukui earthquakes, a dislocation velocity of 50 cm/sec
is obtained, while for the 1952 Kern County earthquake, a dislocation velocity
of about 2 to 3 m/sec is suggested. Since the particle velocity is ultimately
related to the tectonic stress, the above difference suggests a significant

difference in the stress level in the respective hypocentral regions. For the 1933 Long Beach earthquake,the dislocation velocity is estimated to be about 10 to 20 cm/sec. This value is much lower than that for the Kern County earthquake, and is comparable to that for the 1966 Parkfield earthquake. This low dislocation velocity may be characteristic of strike-slip earthquakes in California. Since the tectonic stress presumably controls the high-frequency acceleration in the epicentral area, the determination of the dislocation velocity for various regions is important for estimating the possible maximum ground accelerations in the individual region.

III. TIME FUNCTIONS APPROPRIATE FOR DEEP EARTHQUAKES

By L. J. Burdick & D. V. Helmberger

ABSTRACT

The seismic signatures of isolated body phases from many deep focus earthquakes were analyzed in the time domain. Most shocks were found to be multiple events when examined in detail. The time history derived from P-waves for single events predict synthetic S-wave shapes that match the observations, indicating compatibility with shear dislocation theory. Several other features of source functions in the time domain have been brought to light.

INTRODUCTION

Recent studies on P- and S-spectra such as Hanks and Wyss (1972), Wyss and Molnar, and Molnar et al.(1974) indicate that on the average the spectral corner frequency (Brune, 1970) of P-waves is significantly higher than that of S-waves. Savage (1972) demonstrated that these results are incompatible with shear dislocation theory. Since the Haskell (1964) dislocation model has the advantage of being both logically straightforward and mathematically simple, it seems worthwhile to focus sharply on this discrepancy to be certain that it reflects a breakdown in the model. Accordingly, in this study, we have attempted to isolate in the time domain any differences between P- and S-sources beyond those predicted by shear dislocation theory to make sure such differences exist and, if they do, to understand why.

The spectral corner frequency studies have made use of three different types of observations: local (Molnar et al., 1974), shallow teleseismic (Hanks & Wyss, 1972) and deep teleseismic (Molnar & Wyss, 1972). The local high frequency events were recorded near the epicenter on horizontal instruments. This recording geometry provides a natural prejudice against P-waves. In the case of shallow events, the spectra were severely contaminated by free surface effects (Helmberger, 1974) which casts some doubt upon the results. The results from the deep events were the most significant and the ones which we elected to reexamine in this study. But, in contrast to the previous study of deep events, we chose to compare the P- and S-sources in the time domain.

Transforming a time series into the frequency domain for analysis does provide many computational advantages, but it also masks information about the sequence and duration of transient pulses. However, an analysis in the time domain preserves this information. Therefore, a comparison of the P- and S-wave-forms should help to isolate on the record precisely when and how the S pulse departs from the shape predicted by shear dislocation theory.

We have used a two-stage procedure in studying the P- and S-waves. First, we determined the far-field time history from digitized P-waves by deconvolution. Next, we generated synthetic S-waves assuming the same time history for comparison with observations. We chose this course over the more obvious one of deconvolving to obtain the S-source and comparing with the P-source for these reasons. Our technique permits direct comparison of calculated results with unprocessed data, and it permits us

to circumvent the large uncertainties associated with deconvolution. That
is, when a bandpass filter like a seismic instrument is deconvolved from
a signal such as the P-wave-form, the uncertain data well off the filter
peak is heavily emphasized. But when the result is reconvolved with the
filter in producing the synthetic S, the uncertain data is again
deemphasized.

OBSERVATIONS

The data set consists of observations of three deep events from three
source regions. The events were selected on the basis of their size, the
character of their wave-forms and their location relative to observing
stations. The three earthquakes all have a body wave magnitude of roughly
six. At this size they are large enough to provide strong teleseismic
signals, but small enough to simplify the predictions of shear dislocation
theory as will be explained later. The wave-forms of both the P and the
S were required to be well defined and impulsive in character, leaving no
doubt as to the onset and termination of the phase. Finally, the events
had to occur at an epicentral distance of 50° to 80° from a small array of
WWSS stations. Acting together, these three conditions served to severely
limit the available data set. An extensive search of the WWSS records
was required to produce the three events used in this study. The pertinent
source information is given in Table 1 and the station data in Table 2.

The S observations were rotated into SH and SV components and the
better resolved of the two was selected for the study. SH is ordinarily
preferable since it contains no converted phases. However, since its
radiation pattern is orthogonal to P, whenever the P-wave is strong and

clear, the S is primarily SV. Consequently, SV-waves were used for the Western Brazil and Fiji events and SH for only the Argentina event.

CALCULATION OF SYNTHETICS

Computation of a synthetic seismogram involves modeling the effects of rupture propagation, attenuation, instrument response and earth structure on some specified source time function. In shear dislocation theory, the effects of rupture propagation can be modeled by convolving a boxcar function of duration

$$\Delta t = \frac{L}{2}\left(\frac{1}{V_r} - \frac{\cos \delta}{(\alpha,\beta)}\right)$$

with the source time history. L is the fault length, V_r the rupture velocity, δ the angle between the rupture direction and the ray direction and (α,β) is either the P- or S-velocity, depending on the respective wave type. Mikumo (1971) demonstrated empirically that the azimuthal variation of the rupture effect disappears for earthquakes of magnitude six or less. If the azimuthal dependence vanishes, the wave type dependence also vanishes which implies that for the three events used in this study the P-source function and rupture effects should be identical with the S. This result of shear dislocation theory is the one which we tested by computing synthetic S-waves from P-source functions.[*] Any significant difference between the observed and synthetic S-waves should indicate

[*] From this point forward, the term "source function" includes the rupture effect.

either a difference in P- and S-sources beyond those predicted by theory or earth structure which has not been accounted for.

Past work has shown that the Q operator for the earth is nearly independent of frequency (Attewell and Ramona, 1966). The Fourier amplitude at some point along the ray path defined by x may be written as a function of frequency ω and wave velocity c as

$$A(\omega) = \exp\left(-\omega\int\frac{dx}{2cQ(x)}\right)$$

The expression can be further simplified by replacing $Q(x)$ with a constant average Q and obtaining

$$A(\omega) = \exp\left(-\omega\frac{T}{Q}\right)$$

where T is the travel time (Carpenter, 1967). The quantity T/Q is a near constant (Helmberger, 1973)[a] and was assumed in this study to be .55 for P and 2.2 for S (Anderson et al., 1965). The time domain pulses of the Q filters are shown on the right of Figure 1.

The pulse next to the filters is the delta function response of the WWSS long period Benioff. The steady state response of the instrument and Q filter pulses have been tested by convolving them with infinite sinusoids of various frequencies. The agreement with the expected Fourier amplitudes is most satisfactory.

The earth structure correction for deep earthquakes such as these can be handled almost as simply as the rupture effect. The free surface

effects are negligible; the mantle structure effects become
negligible if the observed rays bottom in the smooth lower mantle
(Helmberger, 1973)[b], which leaves only the structure near the receiver.
It would be unreasonably tedious to attempt to model the structure near
every station which was used, but an approximation to the amplitudes and
arrival times of all the important near-source reflected phases, except
one, can be computed using the Haskell unilayered crust model and plane
wave theory. The theory breaks down for the one case of SV coupled PL
since the ray parameter for this phase is relatively large. The PL phase
is extremely difficult to model using even more sophisticated techniques
because it is highly sensitive to variations in crustal structure.
Consequently, no attempt has been made to synthesize the PL phase.
Fortunately, only one of the three earthquakes contained a possible PL
arrival and it occurred late enough in the wave to be easily discriminated
from source information. The delta function responses of the crust for P,
SH and SV incident plane waves are shown on the left of Figure 2. The
system responses derived by performing a double convolution involving the
instrument, Q operator and crustal responses are displayed on the right.

DETERMINATION OF THE TIME FUNCTION

The most obvious way to find the source function given the P
observation and system response is to deconvolve. Accordingly, for each
of the three earthquakes, the P-system response was deconvolved from
several high quality P observations. The resulting time functions were
cross correlated and averaged at the time of peak correlation. The
observing stations were chosen in tight patterns, so that if there was an

azimuthally varying difference in the P- and S-sources, it would be
emphasized rather than smoothed by the averaging. The results are shown
in Figure 3. The dotted standard deviation line gives some indication of
the variation of the deconvolved pulses. The middle column gives the
integral of the time function which should correspond to the average motion
on the fault somewhat smoothed by rupture effects. The right-hand column
shows the Fourier transform of the source function in a frequency band
appropriate for the sampling rate and signal length. The three sources
show significant variation in structure and, as demonstrated most clearly
in the middle column, they show a feature somewhat similar to an overshoot.

RESULTS

The deconvolution and averaging technique was tested by convolving
the source functions with the P-system responses to reproduce the P-wave-
forms. The results on the left of Figures 4 and 5 indicate that we have
produced a satisfactory representation of the P-source. The synthetic S-
waves on the right of the figures were computed by convolving P-source
with the S-system function. For the Argentina and Fiji events there is
no significant difference between the observed and synthetic S-waves. The
synthetic of the Western Brazil S does diverge from the observations, but
this may be linked to an SV coupled PL arrival. The relatively high
frequency pulse arrives roughly ten seconds after onset. This is too
large a time span for the fault to be still radiating but does correspond
to PL arrival time. Also note the wide variation in form over the
compact station array. This is again characteristic of the PL phase.

DISCUSSION

The close agreement between the observed and synthetic S-waves for the Argentine and Fiji events indicates that, for magnitude six earthquakes at teleseismic distances, the P- and S-source functions are nearly identical as predicted by the Haskell dislocation model. Contrastingly, the Wyss and Molnar (1972) study indicated a difference in the spectral corner of P and S for highly similar data. Providing that both analyses are correct, this indicates that the corner frequency difference is only weakly constrained by the original time domain data and raises the possibility of the difference being an artifact of the data processing. The occurrence of a strong PL phase in the Western Brazil S-wave demonstrates that even for deep earthquakes at ranges greater than 50°, earth structure can distort the wave-shape and the Fourier spectrum. Any future studies of this type in either the frequency or time domain should be coupled with a careful examination of the seismograms to screen out data contaminated by not only PL, but PcP and ScS as well.

As was noted, an important advantage of the time domain is that information about sequence and duration is preserved. That is, the time function of the Western Brazil quake in Figure 3 clearly indicates that there were two high frequency events. This information is, however, not apparent from the amplitude spectrum. What is apparent is that the two peaks enhance the short periods relative to the long. In a corner frequency study this would have the surprising effect of decreasing the estimated source dimension. A time domain study would permit the events to be analyzed separately yielding two sets of source parameters. The difficulties associated with double sources may warrant some attention

since, of five deep earthquakes analyzed in this and a subsequent study, three have been shown to contain more than one event.

One other feature of the source function that merits some attention is the overshoot-like phenomenon. It does not appear to be a spurious effect of the data processing for two reasons. First, the feature does not appear when the same procedure is used on shallow earthquakes; and second, the phenomenon is directly observable in the phase pP. It is not difficult to see that, if the time functions shown in Figure 3 were strongly filtered by propagating twice through the low Q layers at the earth's surface, the main peak would be more strongly affected than the backswing. The pulse would have roughly equal area up and down swings. The instrument response to such a pulse would have three swings instead of two. The bottom two traces of Figure 6 show synthetic pP arrivals from the Western Brazil source. The overshoot was artifically removed in the lower trace. The top two traces show observed pP phases.

There are at least three possible explanations for the backswing. First, it may represent actual return motion on the fault. Burridge (1969) obtained a theoretical result for motion on a frictionless fault which did overshoot and return. He reasoned that in real earthquakes friction would prevent this from happening. Perhaps for deep events, there is melting on the fault which keeps friction from playing an important role. Second, the backswing may reflect motion on the surface between the down-going plate and the mantle. Fault plane studies have indicated that most deep shocks occur inside the plate. The mantle plate surface appears to allow relatively smooth motion. But this surface is still a plane of weakness which may interact with a rupture in the plate. A coupled set

of motions like those shown in Figure 7 would explain the sense of motion of the initial swing and the backswing for all three events. Note that the long slow backswing is consistent with the mantle plate coupling being weak in nature. The third possible explanation is that the backswing is a volume source effect (Archambeau, 1968) and should not be interpreted at all as motion on a fault surface.

CONCLUSIONS

As predicted by the Haskell shear dislocation theory, there are no strongly resolved differences between P- and S-sources on long period seismograms for deep events of magnitude six. This study has also shown that seismic sources should in many, if not most, instances be considered as sums of simpler events which may even have different fault planes.

Acknowledgments

The authors thank Ralph Wiggins for his advice and for the use of his deconvolution program. This research was supported by the Advanced Research Projects Agency at the Department of Defense and was monitored by the Air Forace Office of Scientific Research under contracts F44620-72-C-0078 and F44620-72-C-0083.

REFERENCES

Anderson, D. L., A. Ben-Menahem, and C. B. Archambeau (1965). Attenuation
of seismic energy in the upper mantle, *J. Geophys. Res.* 70, 1441-1448.

Archambeau, C. B. (1968). General theory of elastodynamic source fields,
Rev. Geophys. 6, 241.

Brune, J. N. (1970). Tectonic stress and the spectra of seismic shear
waves from earthquakes, *J. Geophys. Res.* 75, 4997-5009.

Burridge, R. (1969). The numerical solution of certain integral equations
with non-integrable kernels arising in the theory of crack propagation
and elastic wave diffraction. *Phil. Trans. Roy. Soc. (London)* 265,
353-381.

Carpenter, E. W. (1967). Teleseismic signals calculated for underground,
underwater, and atmospheric explosions, *Geophys.* 32, 17-32.

Hanks, T. C. and M. Wyss (1972). The use of body wave spectra in the
determination of seismic parameters, *Bull. Seism. Soc. Am.* 62,
561-589.

Haskell, N. A. (1964) Total energy and energy spectral density of elastic
wave radiation from propagating faults, *Bull.Seism. Soc. Am.* 54.

Helmberger, D. V. (1973a). On the structure of the low velocity zone,
Geophys. J. Roy. Astr. Soc. 33, in press.

Helmberger, D. V. (1973b) Numerical seismograms of long-period body waves
from seventeen to forty degrees, *Bull.Seism. Soc. Am.* 63, 633-646.

Helmberger, D. V. (1974) Generalized ray theory for shear dislocations,
Bull. Seism. Soc. Am. 63, in press.

Mikumo, T. (1971) Source process of deep and intermediate earthquakes as
inferred from long-period P and S waveforms, deep-focus and

intermediate depth earthquakes around Japan, *J. Phys. Earth.* 19, 303-319.

Molnar, P., B. E. Tucker, and J. N. Brune (1974). Corner frequencies of P and S waves and models of earthquake sources, <u>Bull. Seism. Soc. Am.</u>, <u>63</u>, 2091-2104.

Savage, J. C. (1972). Relation of corner frequency to fault dimension, *J. Geophys. Res.* 77, 3788.

Wyss, M. and T. C. Hanks (1972). The source parameters of the San Fernando earthquake inferred from teleseismic body waves, *Bull. Seism. Soc. Am.* 62, 591.

Wyss, M. and P. Molnar (1974). Source parameters of intermediate and deep focus earthquakes in the Tonga Arc, *Phys. Earth Plan. Int.* in press.

Table 1

Location	Latitude	Longitude	Date	Time	Depth	Magnitude
Argentina	27.4 S	63.3 W	1/17/67	1:7:54.3	590 km	5.5
Fiji	21.1 S	179.2 W	3/17/66	15:50:33.1	639 km	6.2
W. Brazil	9.1 S	71.4 W	3/11/65	1:39:3.1	593 km	6.2

Table 2

Event	Observing Stations	Distance	Azimuth
Argentina	BLA	66.3°	345°
	QXF	66.3°	337°
	JCT	67.3°	326°
	SCP	69.2°	348°
	AAM	71.9°	344°
	ALQ	74.2°	324°
	BEC	76.4°	358°
Fiji	BAG	69.8°	296°
	ANP	73.7°	305°
	HKC	78.0°	300°
W. Brazil	LUB	51.3°	327.2°
	ALQ	54.9°	324.8°
	TUC	55.8°	319.5°
	RCD	60.3°	334.1°

FIGURE CAPTIONS

Figure   1.   Delta function response of the WWSS Long period instrument and attenuation filters.

Figure   2.   Delta function response for the crust and earth-instrument system.

Figure   3.   Source functions deconvolved from averaged P-waves are displayed on the left. The dislocation history across the fault produced by integration are displayed in the middle column. The corresponding amplitude spectra are given on the right.

Figure   4.   A comparison of the synthetic P and S waveforms with the observed signals.

Figure   5.   Same as Figure 4.

Figure   6.   A comparison of the synthetic pP phases computed with and without overshoot (artificially removed) with the observed pP signals.

Figure   7.   A hypothetical set of planes along which a high frequency shock inside the plate might couple to a low frequency shock on the plate boundary.

WWSS L. P.
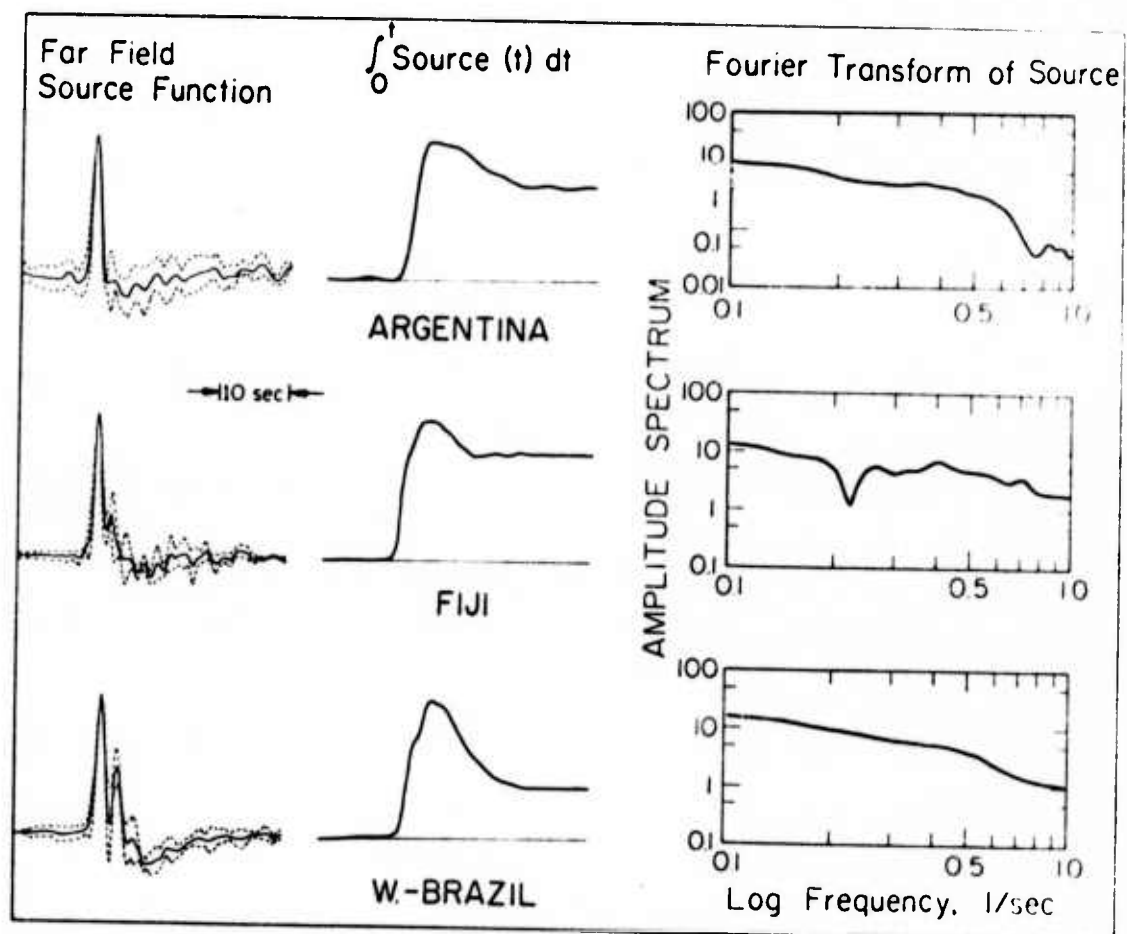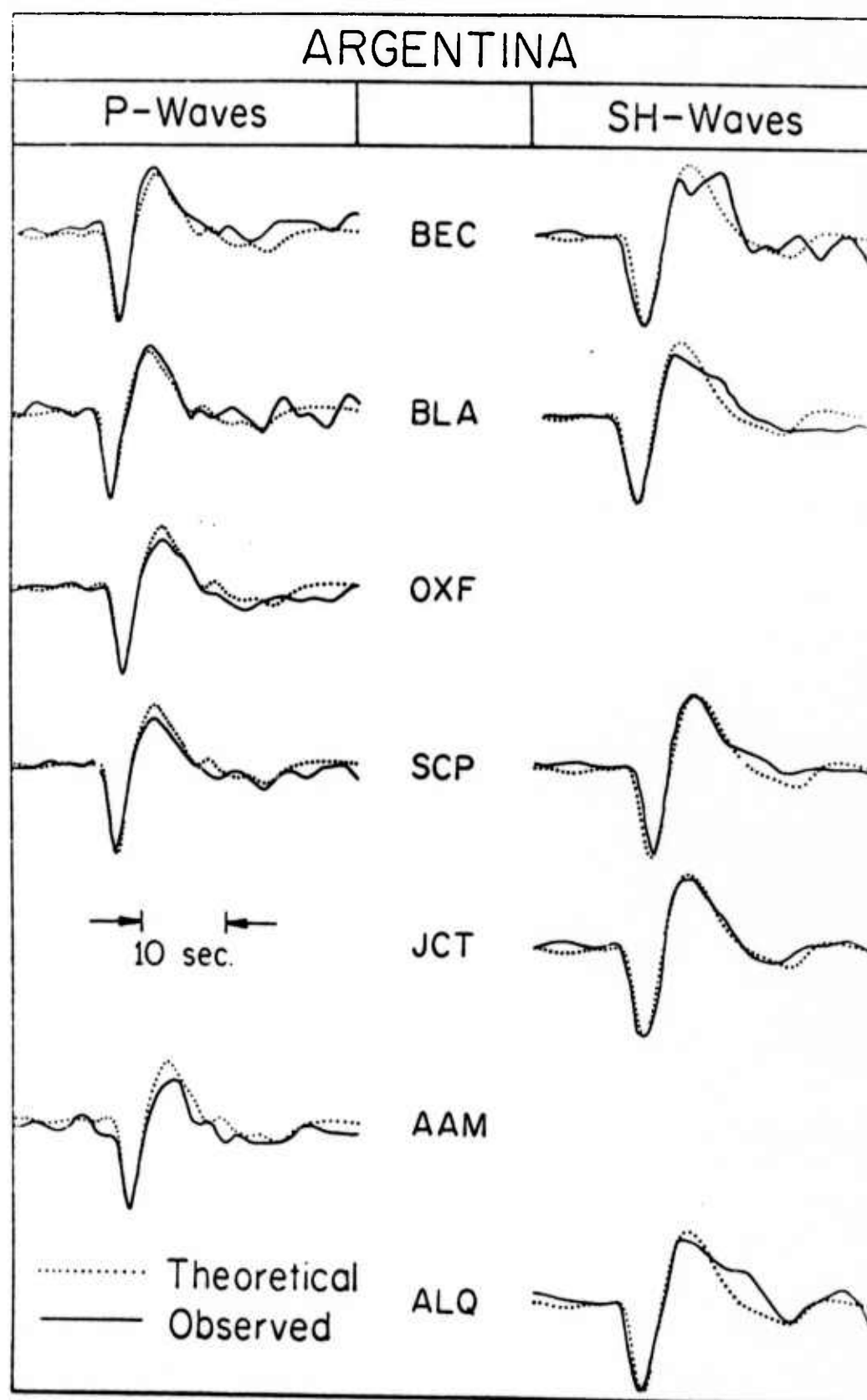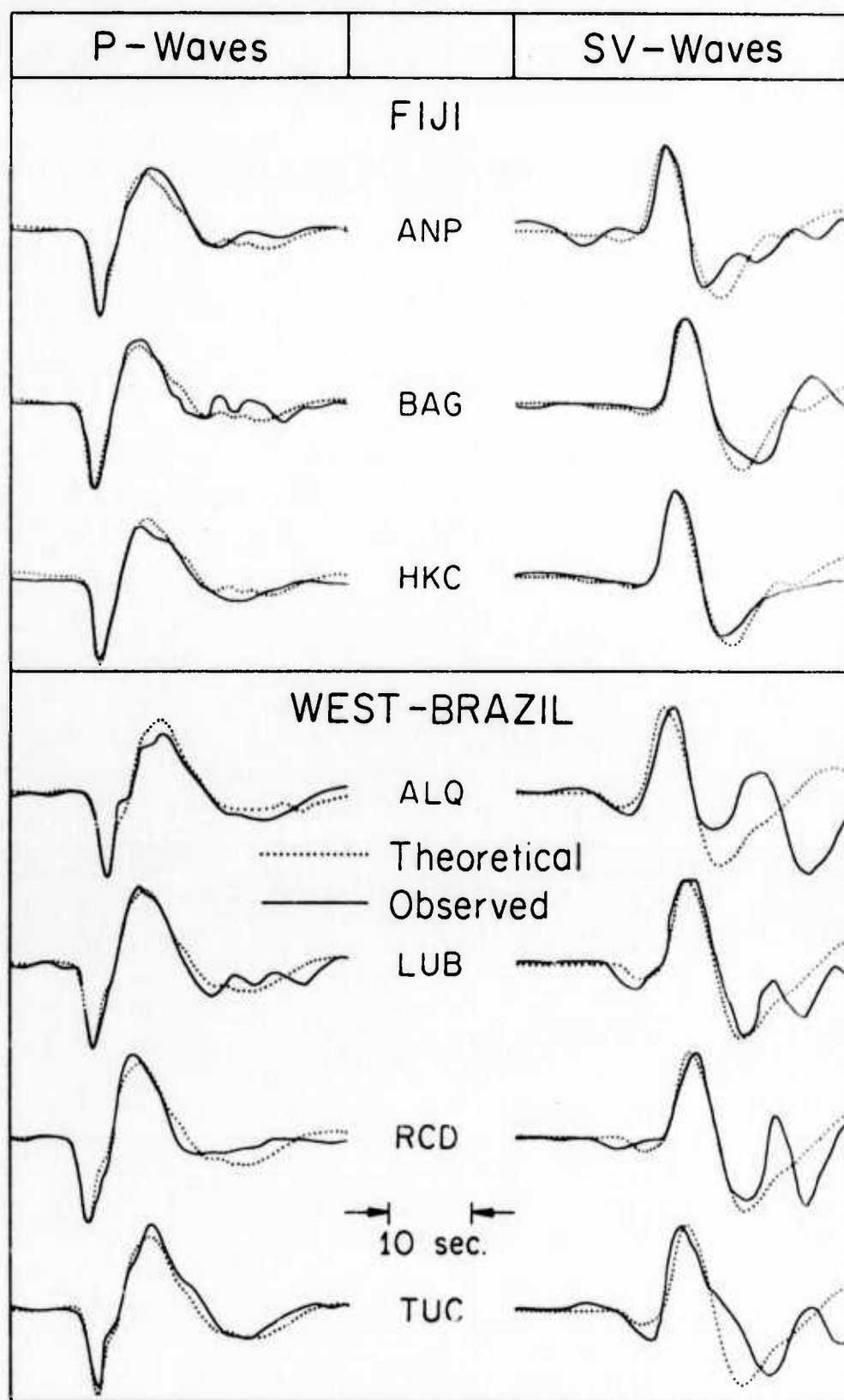
"Q" Filters

P

S

→|10 sec|←
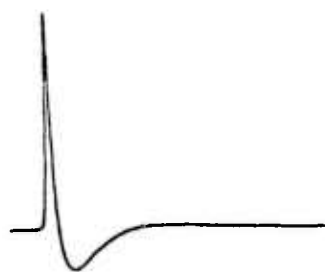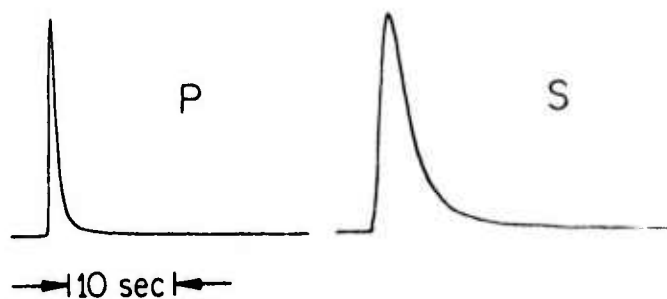
Figure 1.

Figure 2

Figure 3

ARGENTINA

P-Waves | SH-Waves

BEC
BLA
OXF
SCP
JCT
AAM
ALQ

10 sec.

.... Theoretical
———— Observed

Fig. 4

Figure 5

pP Phases OBSERVED
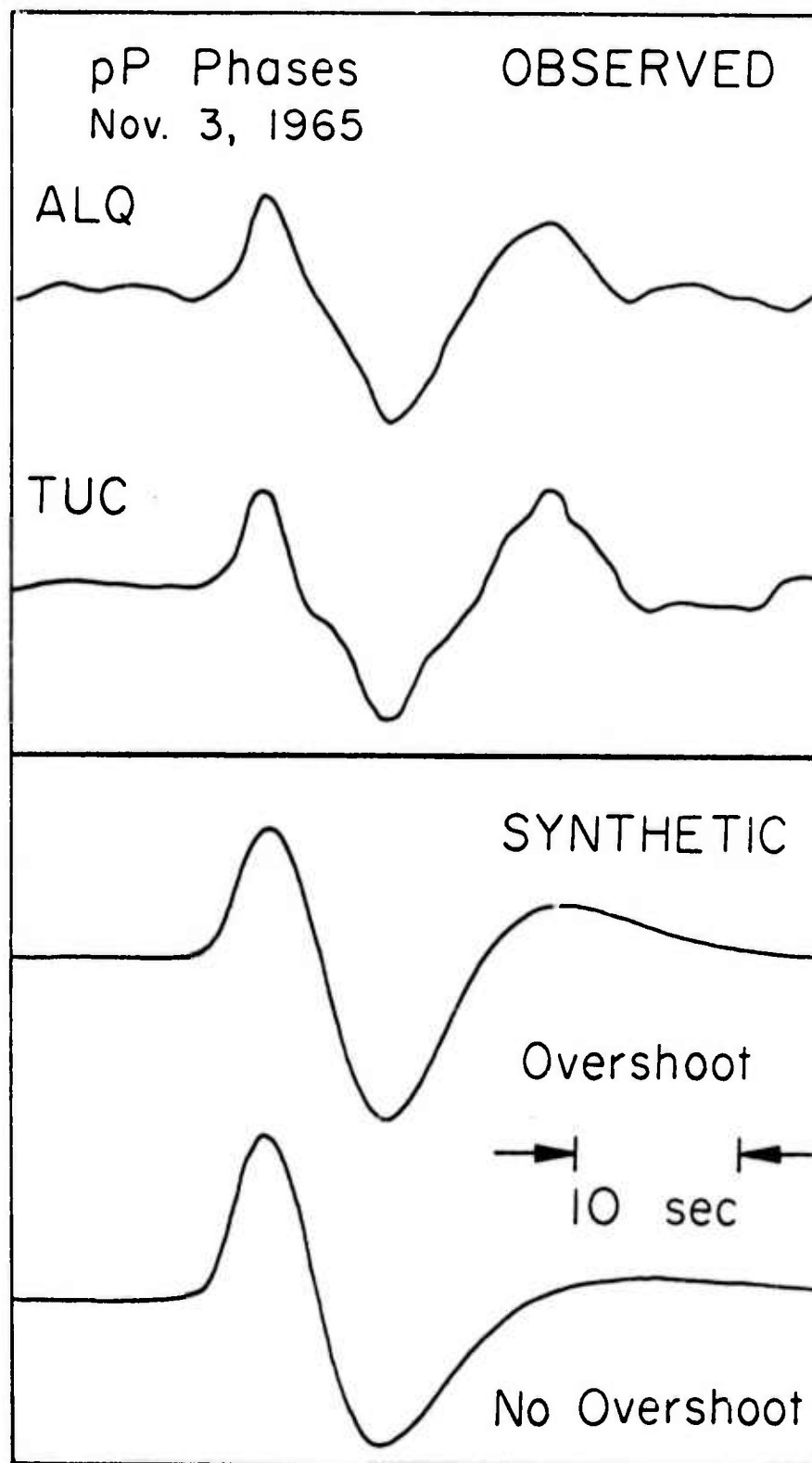Nov. 3, 1965
ALQ
TUC
SYNTHETIC
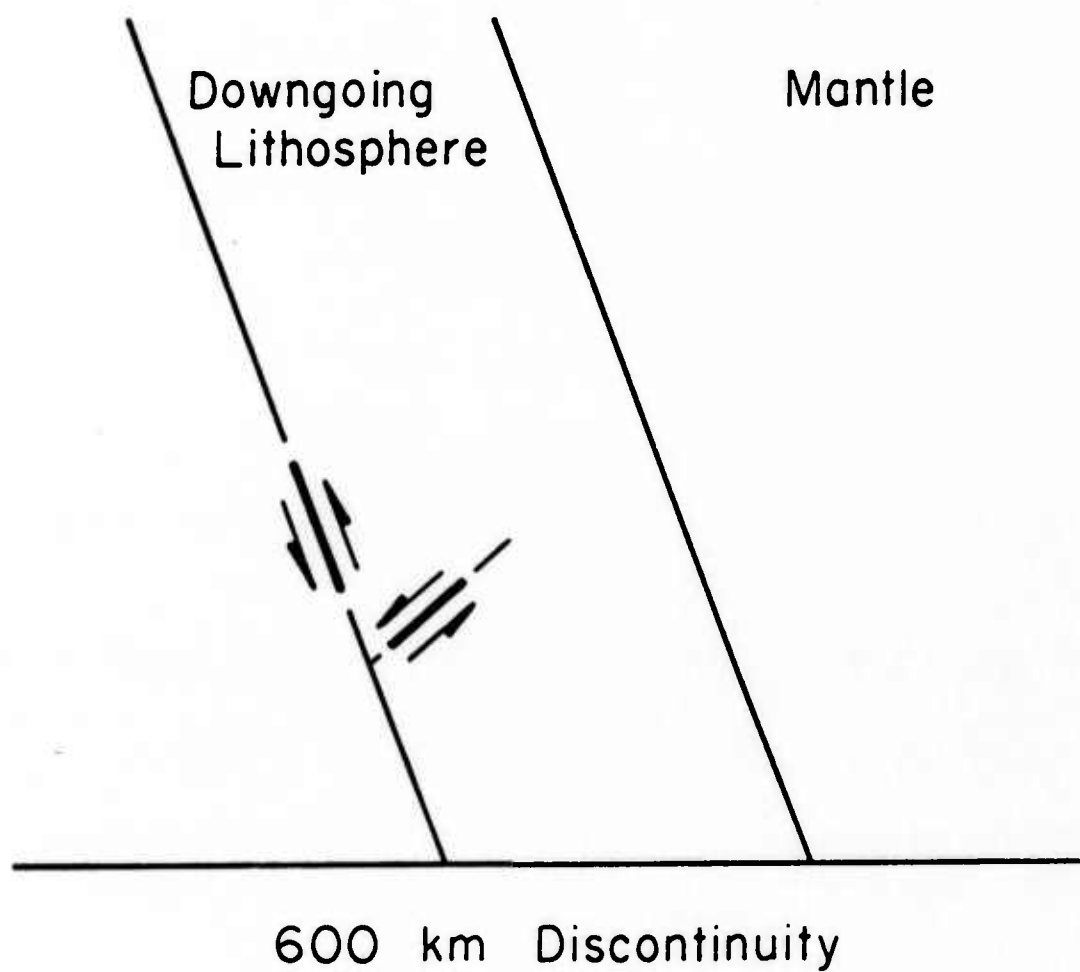Overshoot
10 sec
No Overshoot
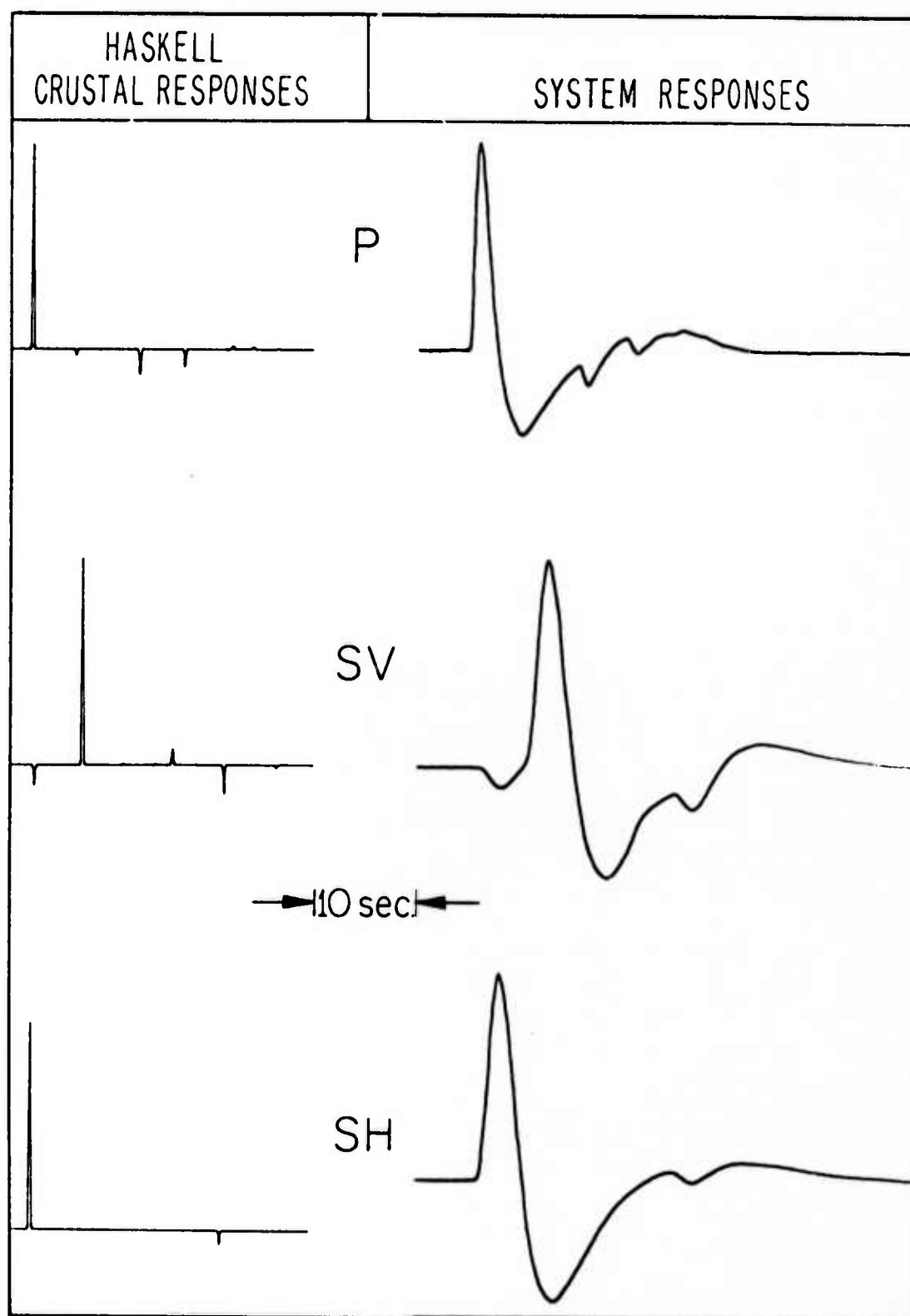
Figure 6

Figure 7.

IV. Interpretation of Body and Rayleigh Waves

from NTS to Tucson

Charles A. Langston and Donald V. Helmberger

ABSTRACT

A linear array of eight Caltech portable broad-band seismograph traiter
was set out from NTS to near Phoenix, Arizona, for the pre-announced
ground nuclear test, Oscuro, on September 21, 1972. Travel time and amplitude
information were used to find an average crustal model by calculating synthetic
seismograms using the Cagniard-de Hoop method. Rayleigh waves from other nuclear
events at NTS, as recorded at the Tucson WWSS station, were examined as a control
for determining the structure of the top half of the crust. Group velocity
curves were found and synthetic Rayleigh waves calculated for Tucson and
Kingman (LRSM). The formations and characteristics of Pn, a reflected Pn, and
the Pg phases are examined. Pg is demonstrated to be composed of the primary
P reflection from the mantle and contains multiple arrivals of P-SV conversions.
Comparisons of synthetic and observed seismograms indicate a crustal thickness
of 30 km with a Poisson's ratio of .23. The crust-mantle transition appears
to be sharp jumping from 6.1 to 7.9 km/sec. The amplitude behavior of Pn
shows little evidence of any lid structure.

Introduction

In previous years determination of crustal structure through long-range
refraction lines has been largely limited to the techniques of travel time
analysis and qualitative observations of amplitude information. Many crustal
models found from these methods have been published and have been very useful
in determining the broad characteristics of the earth's crust and tectonic
development. It was the hope of many investigators, however, that these studies
could be checked by constructing synthetic seismograms and comparing these
with the observations. In this way interpretations could be verified and
further refinements made in the model.

In this paper a refraction line from NTS running into mid-Arizona is
studied. Previous refraction work by Diment, et al. (1961), was done along
the same profile and serves both as a starting point in this study and as a
supplement to our interpretations.

Using the Cagniard-de Hoop method of calculating synthetic seismograms
(Helmberger, 1968), synthetics were fitted to the observed refraction
records in an effort to determine the crustal structure more accurately
than previously done. In addition, Rayleigh waves were examined from
previous nuclear explosions at NTS as recorded at the WWSS station at Tucson
along the same line. Dispersion curves for several intermediate explosions
were obtained and two synthetic records calculated using the Thompson-Haskell
layer-matrix technique as developed by Harkrider (1964). These two techniques
of using body waves and Rayleigh waves were played against each other in an
effort to constrain the crustal model.

Another primary goal of this study is to examine and explain the function of the Pg phase. The Cagniard-de Hoop method proved to be well suited for such interpretation.

Data Reduction

An array of eight Caltech portable seismograph trailers was set out along a southeast trending line from NTS to Luke AFB, Arizona, for the preannounced underground nuclear test, Oscuro, which occurred on September 21, 1972 (Figure 1). The line was in the southeastern part of the Basin and Range province and follows regional topographic and structural trends. Previous refraction work, by Diment, et al. (1961), has been done along the northeast half of the present line from NTS to Kingman, Arizona.

Data from the blast is displayed in figures 2 and 3. Two distinct phases are seen, Pn and Pg, having apparent velocities of 7.9 and 6.1 km/sec, respectively. Also, there is a hint of another phase, designated Pn′, coming in after Pn and before Pg for the three farthest stations with an apparent velocity comparable to Pn. More will be said about these phases later.

First order station corrections for elevation and geology were calculated by first consulting geologic and topographic maps. Using a datum of 700 meters and assuming the crystalline rocks have a compressional velocity of 5.9 km/sec and sediments, 3.0 km/sec, travel time corrections were no greater than 0.2 sec (Table 1). The data were read to accuracies of 0.2 sec for Pn and 0.5 sec for Pg and Pn. The travel times were then fitted with a least-squares line to find the apparant velocities. Ranges were calculated by computer using

the geographical coordinates of the source and receivers. Figure 4 shows the resulting travel time curves.

Data Inversion

............ntially, the method of data inversion used in this paper is the following. Using the travel times a simple layered earth model can be made provided the interpretations of the observed phases are correct. This serves as a starting model for the calculation of synthetic seismograms. The amplitude behavior of the synthetics are examined and compared to the data and a further iteration performed on the model until a satisfactory match is obtained.

Body Waves

Body wave synthetic seismograms were computed by the Cagniard-de Hoop method. The object was to fit the first 10 to 25 seconds (the Pn and Pg phases) of the observations as closely as possible.

The first problem encountered in calculating synthetics was finding a suitable source time function. In dealing with linear elastic wave theory the seismogram can be decomposed into several parts as the following equation illustrates:

$$S_R(t) - M(t) * I(t) * S(t)$$

where $S_R(t)$ is the trace of the seismogram; $M(t)$, the impulse response of the layered earth structure; $I(t)$, the impulse response of the instrument; $S(t)$,

the effective point source time function; and *, the convolution operator.
S(t) was not known so the following approximate method was used. We suppose
that a simple headwave acts as the time integral of the direct wave or
source history. One can then take the Pn phase off the seismogram, differentiate
it, and obtain I(t) * S(t). This was done using station 5. In the upper
right-hand corner of Figure 2 the pulse used in all the body wave synthetic
seismogram calculations is displayed. Included in the S(t) is the interaction
with the free surface such as pP and any contributions from fine structure
near the surface. We will assume that S(t) is invariant over the small range
in ray parameters considered.

The first crustal model computed was Diment's et al. (1961) proposed model
(their Figure 8) as shown in Table 3. Figure 5 shows the synthetic seismograms
obtained. The synthetics disagree with the observations mainly because of
the 8.1 km/sec layer which caused a large reflection to come in at the onset.
The amplitude of this reflection (looking at stations 4 to 8) is comparable
to the rest of the record. The third pulse in seismogram 8 starts with the
reflection from the 6.15 - 7.81 km/sec interface which is comparable in travel
time to the Pg phase in the observation. Taking out the 8.1 km/sec layer
produces synthetics which compare fairly good in relative amplitudes of both
Pn and Pg but are off a few seconds in travel time because of the different
velocities observed in this study.

Before a better model was attempted, however, it was realized that this
profile was deficient in resolving the structure of the upper half of the crust.
Diment et al. (1961), found that for close-in distances to NTS the crust pre-
dominately yielded velocities of 6.15 km/sec. Because this gave a localized

velocity structure it was felt that it may not be applicable to the entire
profile. To get an idea of how the upper part of the crust acted, on the
average, Rayleigh waves from NTS events as recorded at the WWSS station at
Tucson were analyzed. Tucson was ideal since it lay on the same line as the
profile.

Rayleigh Waves

Nine low-intermediate events were examined (Table 2). A typical record
is displayed in the lower half of Figure 6. Group velocity curves for the
nine events were determined by the peak-and-trough method. This assumes there
is no group delay at the source, small amplitude variations on the record
and that the wave is well dispersed. The assumption of small amplitude
variations seems to be the weakest but will be tested by constructing a
synthetic Rayleigh wave.

Peaks and troughs were counted using the digitizer and plotted versus
travel time. A cubic was fitted through each data set by least-squares,
analytically differentiated to find the period arrival-time curve, and
using the calculated distance arrive at the group velocity dispersion curve.
The curves for the nine events were nested together and an "average" curve
drawn between the extremes. The accuracy of the final averaged curve is taken
to be the spread in the nested curves. Figure 7 shows the obtained dispersion
curves.

Inversion of the averaged curve was done by trial and error. Using the
Thompson-Haskel layer matrice method as developed by Harkrider (1964) dispersion
curves were calculated from various models. The body wave data was used as a

constraint for the lower part of the crust since the Rayleigh waves were only sampling approximately the upper 20 km. An attempt was made to hold Poisson's ratio at 0.25 so that the shear velocity would determine the compressional velocity. The velocity constraints on the models, however, required that the shear velocity vary somewhat independently of the compressional velocity. This ultimately produced a Poisson's ratio of 0.23 for the main part of the crust in the final models.

Models

The models obtained are displayed in Table 3. Two models were found to fit the Rayleigh and body wave data equally well. Model A is most like Diment et al. (1961), model with the major differences being in velocity and overall thickness. The second and third layers of model B should be interpreted as an increasing velocity gradient as seen by the Rayleigh waves and not as discrete layering.

The most important aspect of these two models is that lower velocity materials in the upper~~half~~ portion of the crust are thin and that the crust, largely, behaves like one 6.1 km/sec layer. Both models explain the data equally well and both are just as plausible. If any preferred model is to be taken it should be model A just because of its simplicity.

Rayleigh Waves

A Rayleigh wave synthetic seismogram was calculated for the event Dumont.

The time source function (Helmberger and Harkrider, 1972)

$$S(t) = t^\xi \epsilon^{-nt}$$

was used, where the parameters ξ and n were found by trial and error to be 0.7 and 1.0 respectively. The fit (Figure 6) is remarkable considering the assumptions made in the analysis. Group arrivals are in complete agreement and relative amplitudes are good. The seismograms of Figure 8 have not been normalized to each other.

As a test of the model closer to NTS the event Boxcar, as recorded at the LRSM station KGAZ, Kingman, Arizona, was used. Source parameters were obtained for this event by Helmberger and Harkrider (1972). The synthetic obtained (Figure 8) is in good agreement with respect to group arrivals and relative amplitudes but had to be shifted four seconds back in time to line up with the observation. This is a discrepancy of about 0.1 km/sec in overall group velocity and indicates that the crust may have slightly smaller velocities in the northwest portion of the profile.

Body Waves

Body wave synthetics were calculated for model B and are displayed in Figure 2. The travel times and relative amplitudes fit well and even wave shapes are good in some cases. The observed records have not been normalized. The synthetics are normalized with respect to maximum amplitudes attained by each. The good agreement of Pn waveshapes, especially at station 5 is an indication that the assumption of I(t) *S(t) was good in the calculations.

Discussion

Through the examination of the amplitude behavior of the synthetics a few points about the fine structure of the crust and propagation effects can be made.

Perhaps the most interesting and obvious point to be made from these synthetics concerns the formation of the Pg phase. The calculated Pg phase includes the primary reflection from the Moho, as defined in this profile, as the first arrival with the first crustal multiple arriving a few seconds afterward and contributing almost as much energy. Also included are rays which traverse one leg as SV waves. The most important conversions are those associated with the surface layer and contribute perhaps 10% of the energy in the calculated Pg phase. Obviously, at some stations, the synthetics do not match the observations in peak amplitudes. This deficiency is interpreted as a lack of including near surface (upper five kilometers) ringing effects or multiple rays which occur in the upper layers. This effect will be strongly dependent on local geology and, hence, cannot be modeled adequately by the techniques used here.

The crustal waveguide explanation as deduced by others, for example, Press and Gutenberg (1956) and Shurbet (1960), seems to be fundamentally correct. However, there is still a problem in determining just what are the waveguide boundaries. In this profile the entire crust behaves largely as one layer with compressional wave velocity 6.1 km/sec. The corresponding Pg phase observed here is slightly faster than the 5.9 km/sec apparent velocity more commonly observed due to having the waveguide composed of the Moho and free surface. Other crustal structures will change the character of the phase.

For instance, in an area with an intermediate layer, such as the so-called Conrad discontinuity, the Pg phase will be complicated through the interaction of the Moho and the intermediate boundary. Another modeling study, similar to this one, for mid-continent crust would be needed to resolve the problem.

As shown on Figure 2 the relative amplitude behavior of Pn between observations and synthetics is remarkably good. This suggests that the upper mantle under the profile is free from any significant velocity gradients, both positive and negative. Synthetic models were run for gradients of approximately 0.02 sec^{-1}. The synthetics obtained were significantly different in amplitudes as compared with the observations. A positive gradient boosted up the amplitude of Pn to values approaching the size of Pg. The negative gradient had a less drastic effect but a significant variation in apparent travel time and wave shape was observed. The conclusion is, based on the data and synthetics, that any velocity gradients in the uppermost mantle must be much less than 0.02 sec^{-1}, probably lower than 0.005 sec^{-1}, and cannot be distinguished with these observations.

The Pn' phase, as designated here, is emphasized to be only a possible interpretation. This phase is a head wave associated with the first crustal multiple. Evidence for it is slight and can be seen in Figures 2 and 3. The strongest indication of its existence are the interference effect of Pn coming out of the Pg phase, which is clear in the final synthetics and suggestive in the observations (Figure 2), and the prominent arrival at station 8 (Figure 3). The lack of coherence of this low amplitude phase may not be surprising considering that part of its path consists of a surface reflection where the local geology is very important. Reverberation near the receiver in the upper

layers for Pn may also be important.

Conclusions

Two average crustal models are presented for a profile from NTS to Phoenix, Arizona, which differ somewhat from those given by Diment et al. (1961). It is shown that a 8.1 km/sec layer 53 km from the surface does not exist. The uppermost mantle has an average compressional velocity of 7.9 km/sec and has no observable velocity gradients from the study of Pn amplitudes. The crust is 30 to 32 km thick, depending on the model used, and acts largely as one 6.1 km/sec layer. The models presented differ in that one has an increasing velocity gradient from 5.5 to 6.1 km/sec over three kilometers at the top, whereas the other, which is similar to Diment's et al. (1961) preferred model, consists of one 31 km thick 6.1 km/sec layer.

A shear velocity profile obtained by Rayleigh wave analysis taken with the compressional wave profile yields a Poisson's ratio of approximately 0.23 for the crust.

Synthetic seismograms were calculated for both Rayleigh waves and body waves and agree very well with the observations. Calculation of a Rayleigh wave synthetic for the Boxcar event for the northwest portion of the profile indicates that the crust may have slower velocities, perhaps up to 0.1 km/sec less than those obtained over the entire profile.

The Pg phase has been experimentally verified, along this profile, as consisting mostly of the primary reflection off the Moho followed by crustal multiples. Rays with one leg of SV energy also contribute to the phase.

The Pg phase in more complicated crustal structures will be more complicated
due to the increasing number of boundaries in the crustal waveguide.

Acknowledgments

Bibliography

Diment, W. H., S. W. Stewart, and J. C. Roller (1961). Crustal structure from the Nevada Test Site to Kingman, Arizona, from seismic and gravity observations, J. Geophys. Res. 66, n. 1, 201-214.

Harkrider, D. G. (1964). Surface waves in multilayered elastic media, 1. Rayleigh and Love waves from buried sources in a multilayered elastic half-space, Bull. Seism. Soc. Am. 54, 627-679.

Helmberger, D. V. (1968). The crust-mantle transition in the Bering Sea, Bull. Seism. Soc. Am. 52, 299-319.

Helmberger, D. V. and D. G. Harkrider (1972). Seismic source descriptions of underground explosions and a depth discriminate, Geophys. J. R. astr. Soc. 31, 45-66.

Press, F. and B. Gutenberg (1956). Channel P waves g in the earth's crust, Trans. Am. Geophys. Union, 37, No. 6, 754-756.

Shurbet, D. H. (1960). The P Phase transmitted by crustal rock to intermediate distances, J. Geophys. Res. 65, 1809-1814.

Table 1

Station No.	Name	Latitude	Longitude	Distance from (km) source	Elevation (meter)	Travel Time Correction
1.	Corn Creek	36°26.32'	115°21.55'	92.91	890	-.16
2	Boulder City	35°58.71	114°50.45'	162.1	768	-.12
3	Charlie's Mine	35°42.27'	114°28.63'	207.5	713	+.18
4	Kingman	35°11.92'	114°02.41'	276.1	1140	+.11
5	Seapy's Ranch	34°46.38'	113°36.43'	337.9	640	+.19
6	Gibson's Canyon	34°26.21'	113°06.84'	395.6	658	+.19
7	Wickenburg	33°59.46'	112°40.85'	458.6	768	+.17
8	Luke AFB	33°32.35'	112°20.48'	516.5	335	+.02

Table 2

NTS Events

Name	Date	Time	Latitude	Longitude	Δ (NTS-TUC) (Km)
Oscuro	9/21/72	15:30:00.2	37.082°N	116.037°W	
Chartreuse	5/6/66	15:00:00.1	37.35°	116.32°	754.3
Commodore	5/20/67	15:00:00.2	37.13°	116.06°	720.7
Bourbon	1/20/67	17:40:04.4	37.10°	116.00°	714.6
Dumont	5/19/66	13:56:28.1	37.11°	116.06°	719.1
Duryea	4/14/66	14:13:43.1	37.24°	116.43°	752.4
Bronze	7/23/65	17:00:00.0	37.10°	116.03°	716.4
Buff	12/16/65	19:15:00.0	37.07°	116.03°	714.0
Piledriver	6/2/66	15:30:00.1	37.23°	116.06°	728.8
Corduroy	12/3/65	15:13:02.1	37.16°	116.05°	722.5
Boxcar	4/26/68		37.29°	116.46°	293 to KGAZ

Table 3

Model	Layer	Thickness (km)	P velocity (km/sec)	S velocity* (km/sec)	density* (gm/cm^3)
Diment, Stewart, Roller (1961) (taken from their figures)	1	1.7	3.0	1.7	2.3
	2	28.4	6.15	3.55	2.8
	3	24.4	7.81	4.5	3.2
	4	--	8.1	4.7	3.3
A	1	1.0	3.0	1.73	2.3
	2	31.0	6.1	3.6	2.8
	3	--	7.9	4.6	3.2
B	1	1.0	3.0	1.73	2.3
	2	1.0	5.5	3.3	2.5
	3	2.0	5.9	3.4	2.7
	4	25.5	6.1	3.6	2.8
	5	--	7.9	4.6	3.2

*S velocity and density used in calculations of synthetics not given by Diment et al. (1961).

Figure Captions

1. Index map of the stations used in this study. Open triangles show the location of the trailer array; half-open triangle, combined location of trailer and an LRSM station; solid triangle, WWSSN station.

2. Q observed and synthetic seismograms. Left-hand portion displays observed vertical component of trailer array. Right-hand side shows the final synthetics calculated from model B. The waveform in the upper right-hand corner is the $I(t) * S(t)$ used in all the synthetic seismogram calculations. Travel time lines have been drawn in for the Pg, Pn, Pn' phases. Station numbers are to the left of each seismogram and relative Pn amplitudes are to the right.

3. Observed radial components. Dotted line shows interpreted arrival of the Pn' phase.

4. Least-squares fit to Pn and Pg travel times. Dotted line for Pn' is inferred.

5. Synthetic seismograms calculated using the model given by Diment, Stewart and Rollins (1961) as displayed in Table 3.

6. Observed and synthetic Rayleigh waves for the Tucson WWSSN station. Lower half shows a typical Rayleigh wave from events at NTS. Upper half is a synthetic Rayleigh wave calculated using model B. The source parameters used are displayed in the upper right-hand corner.

7. Nested group velocity dispersion curves obtained from events at NTS.

8. Synthetic and observed Rayleigh waves from Boxcar for KGAZ. Synthetic calculated from model B. Source parameters for the synthetic are displayed in the upper right.
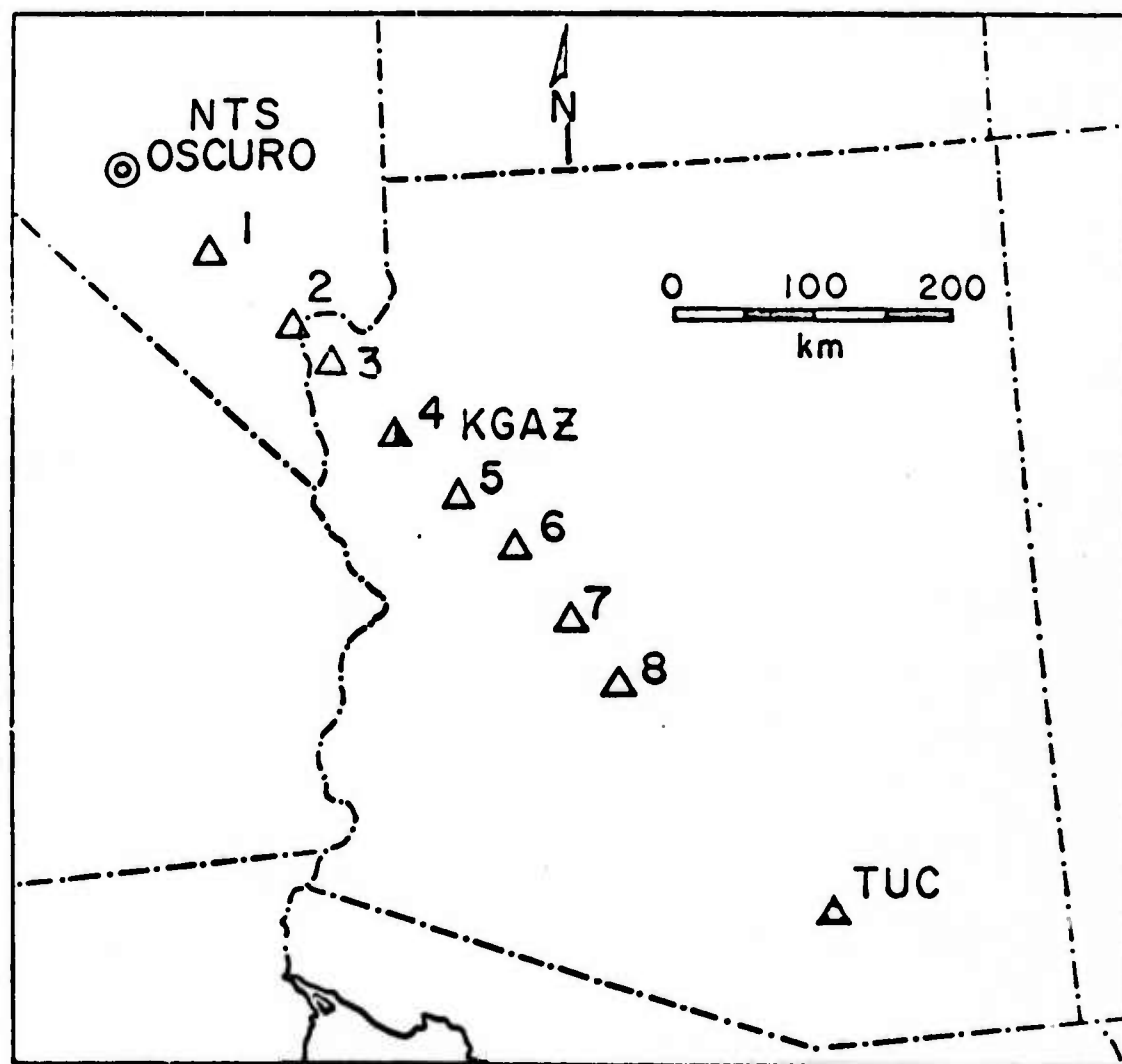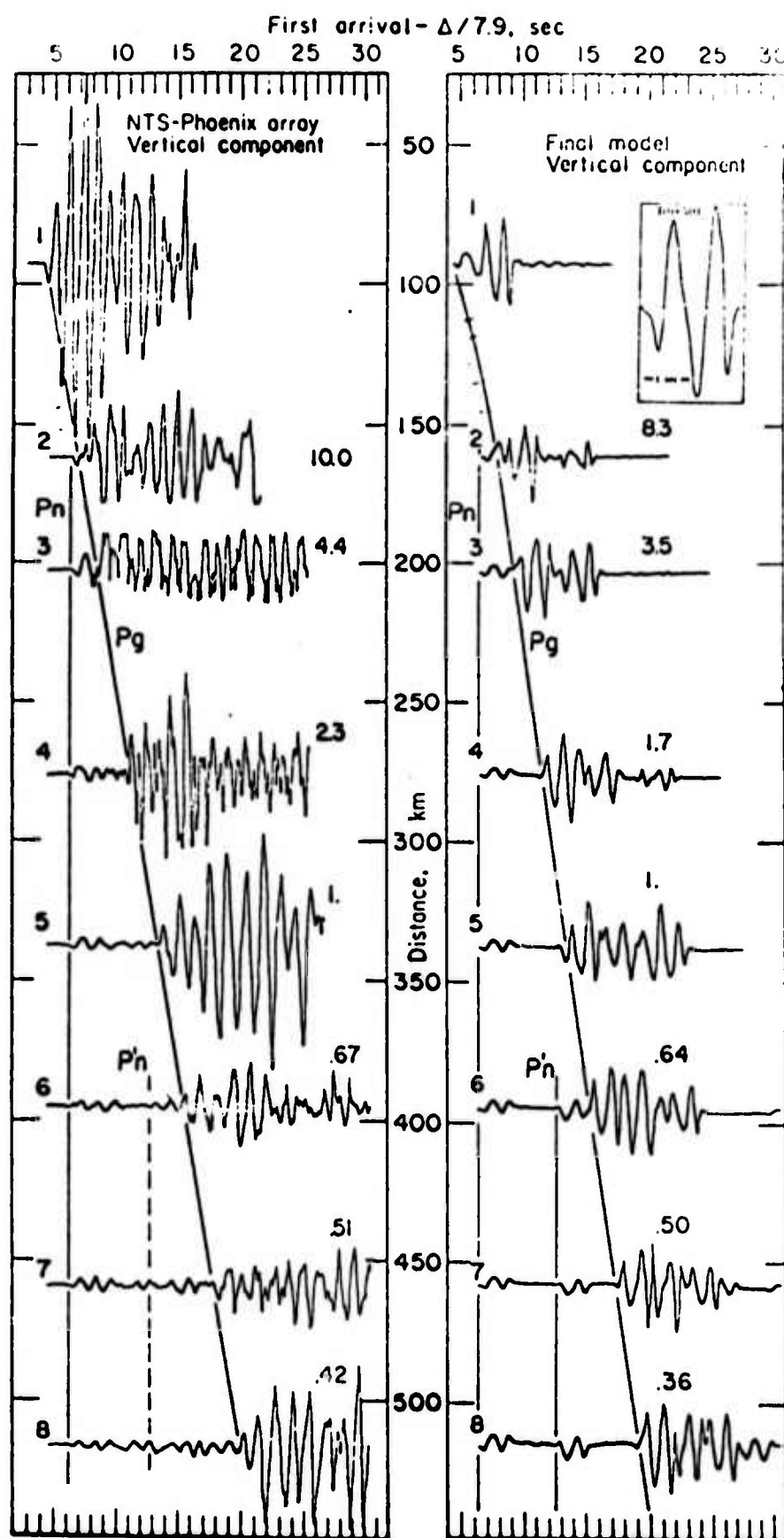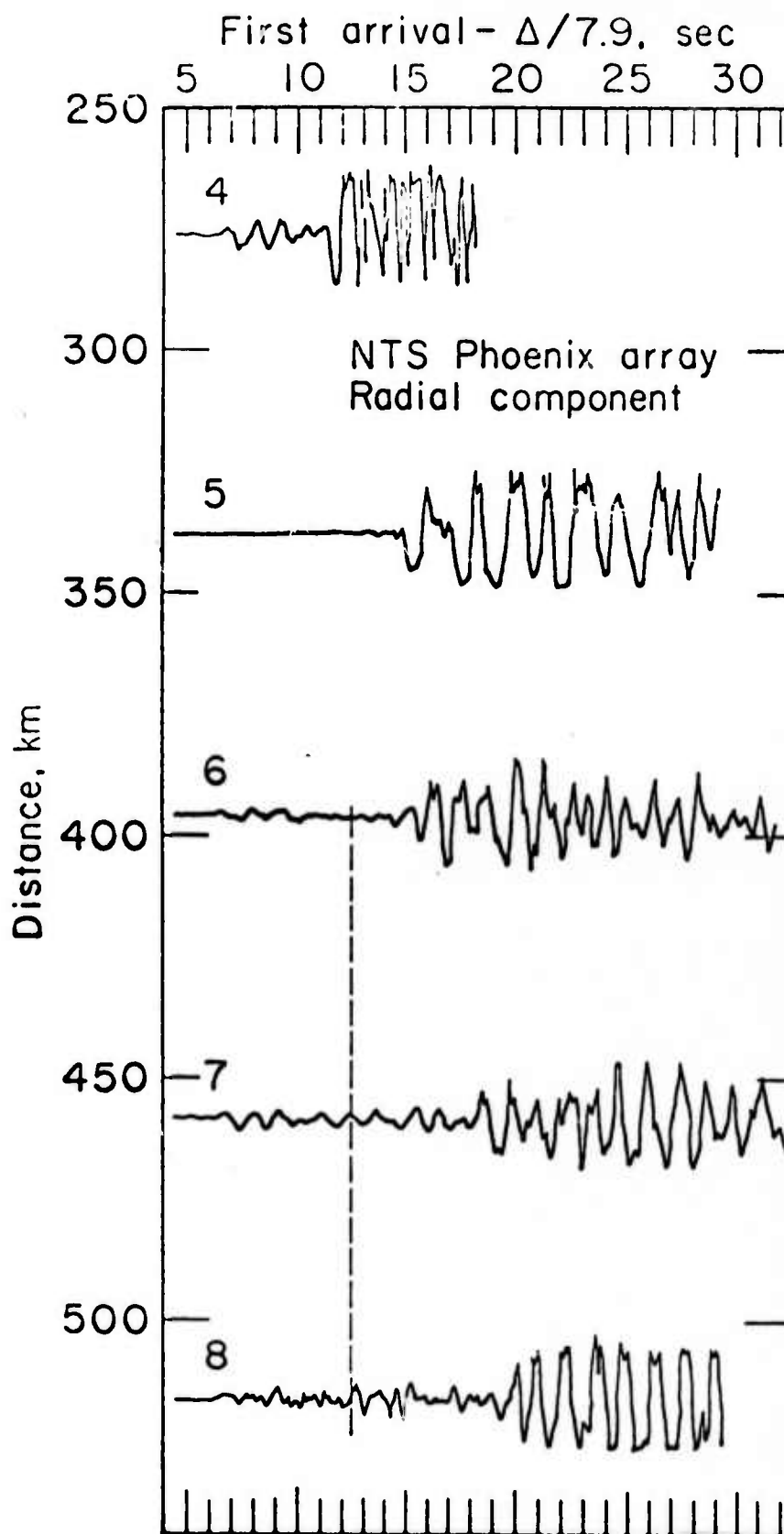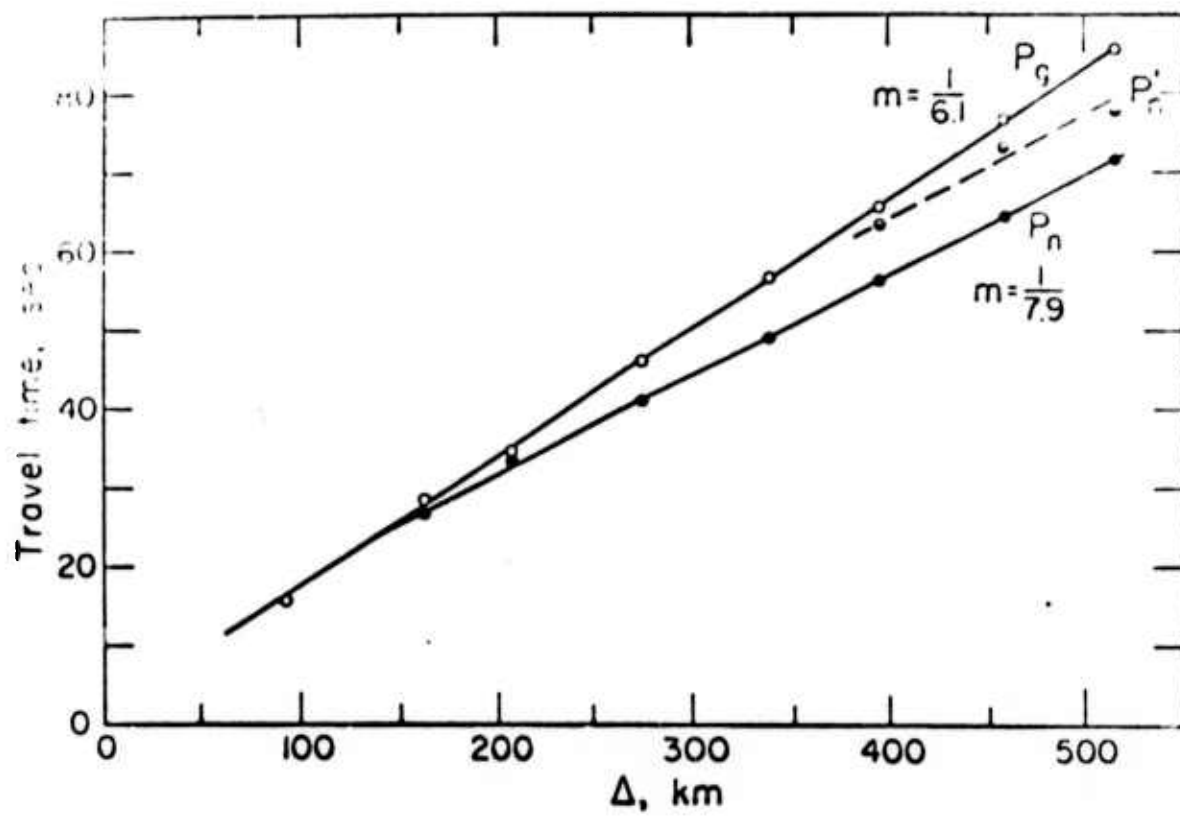
FIG. 1

First arrival - Δ/7.9, sec

NTS-Phoenix array
Vertical component

Final model
Vertical component

FIG. 12

First arrival – Δ/7.9, sec

NTS Phoenix array
Radial component

FIG. #3

FIG. 4

Fig. 5

Synthetic

$\xi = 0.7$
$\eta = 1.0$

WWNSS–
TUCSON

DUMONT
$\Delta = 719$ km

Observed

1 min.

FIG. 8 ? 6

Fig. 8.1

BOXCAR
LRSM–KGAZ
$\Delta = 293$ km

$\xi = 0.50$
$\eta = 0.15$

|←——30 sec——→|

Synthetic
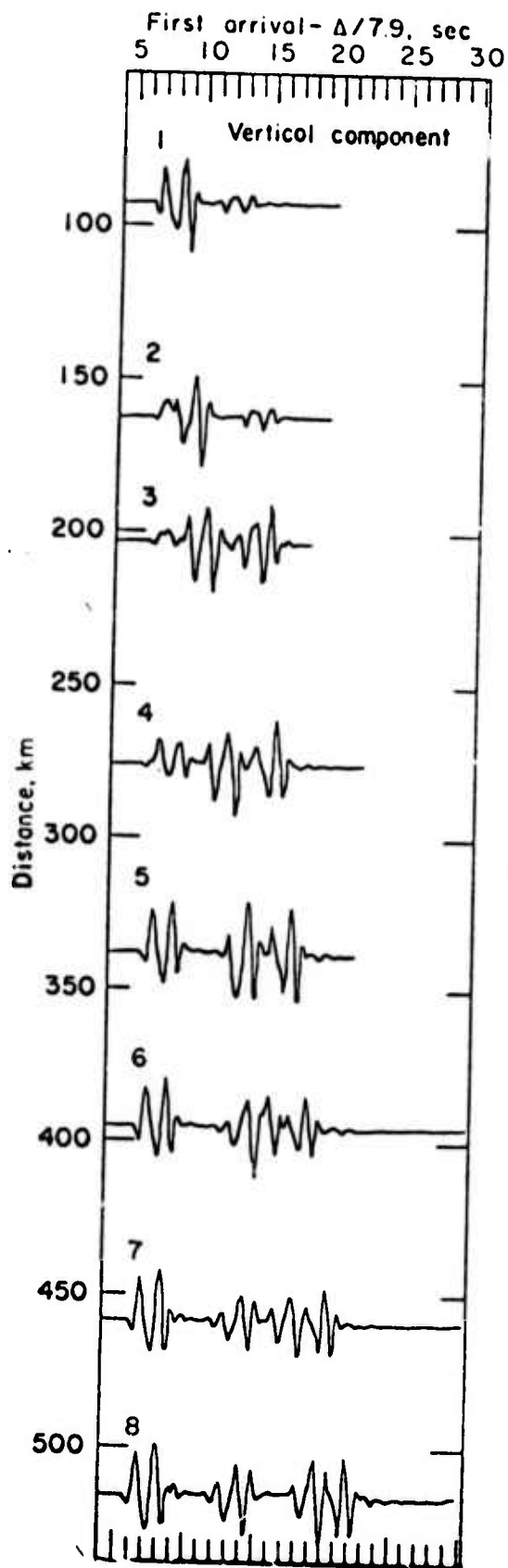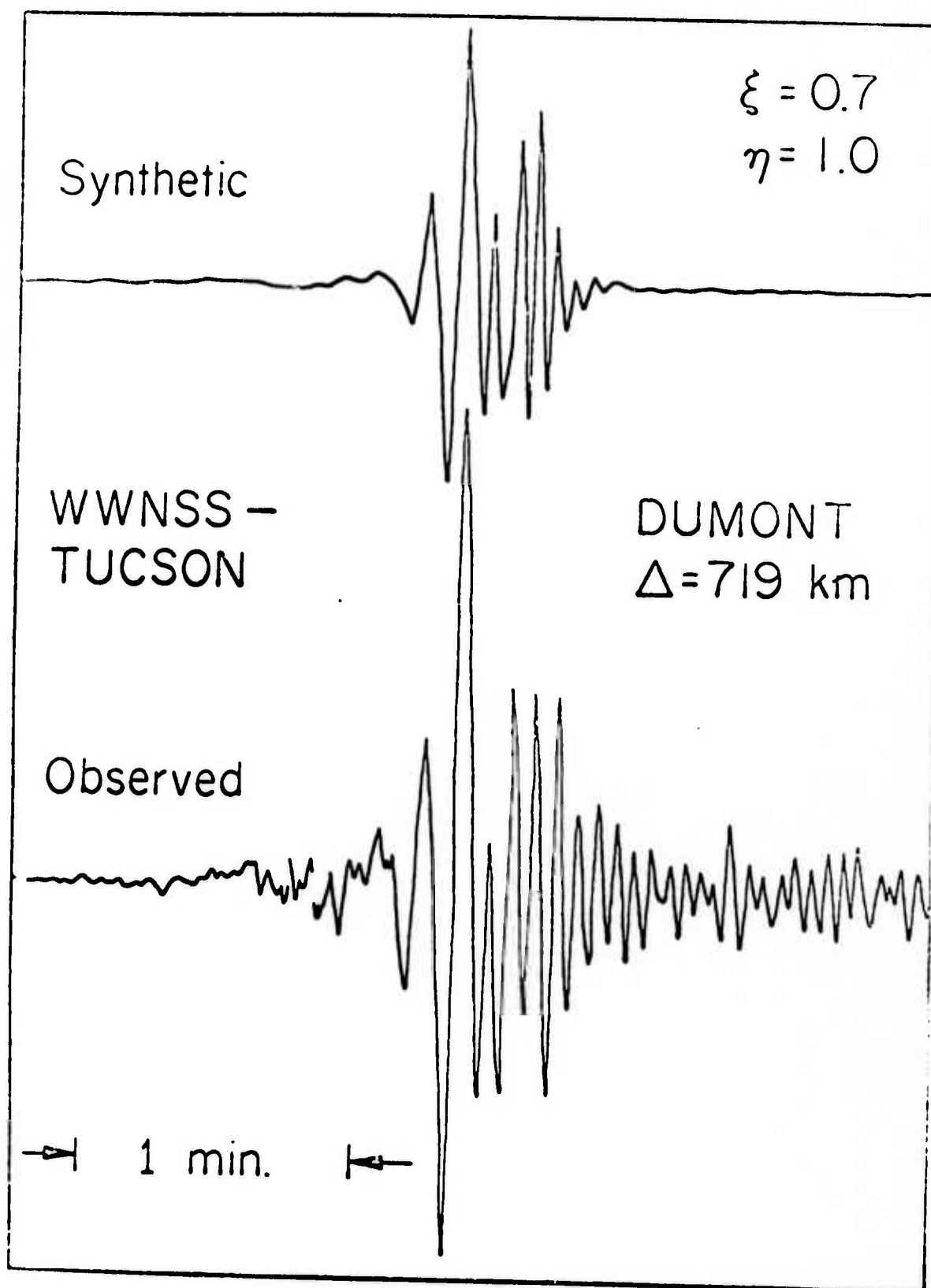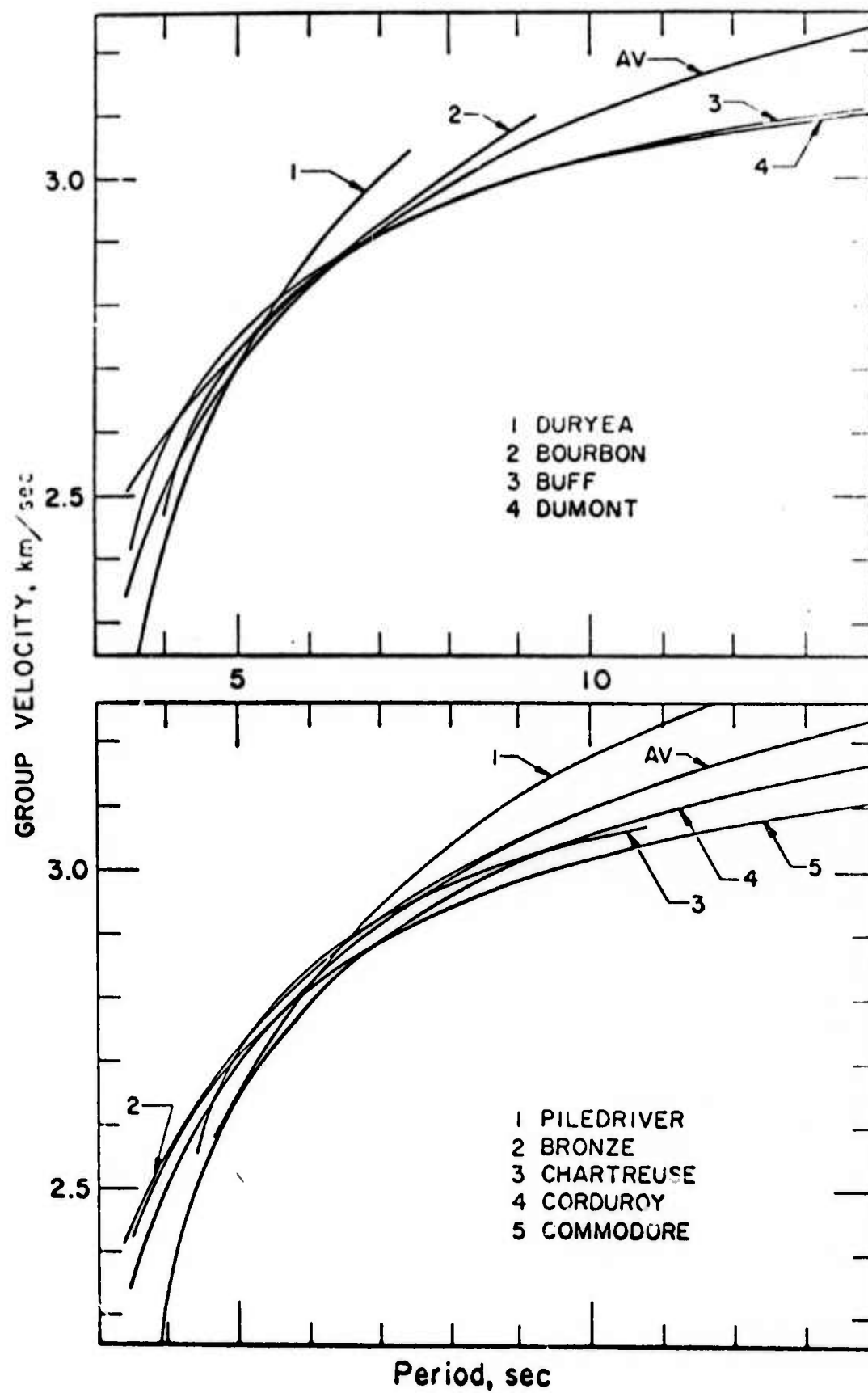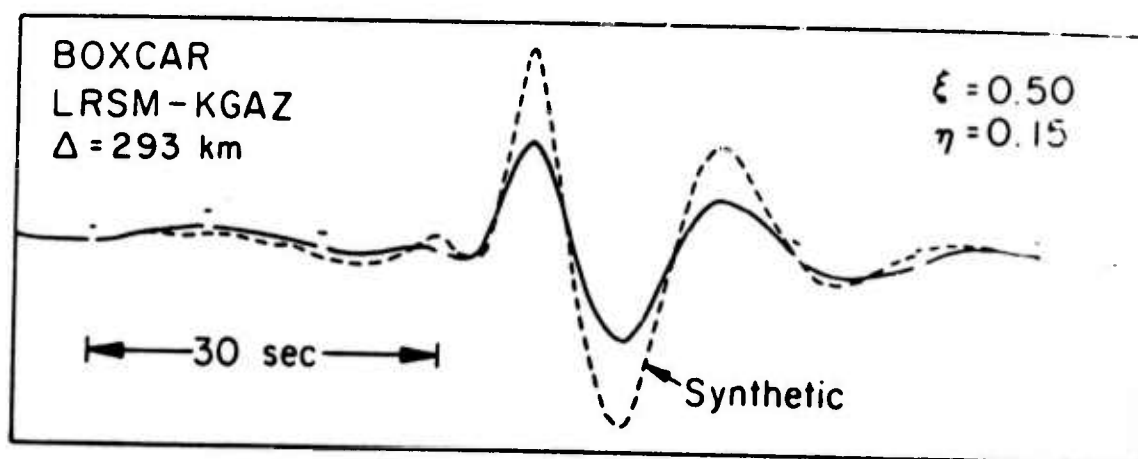
Fig. 8.

V. Numerical Applications of the Expanding Spherical Rupture and
    the Unilateral Propagating Spherical Rupture in a Prestress
    Field of Pure Shear

This section is Chapter VII of Jean-Bernard Minster's thesis (1974) titled "Elastodynamics of Failure in a Continuum." References and details cited in this section can be found in the thesis. This thesis has been submitted and successfully defended as partial fulfillment of the requirements for the Degree of Doctor of Philosophy at the California Institute of Technology, Pasadena, California.

Figure 2   is from this thesis and shows a simulation of an m_b/M_s plot for a particular relaxation source.

-347-

Chapter VII

NUMERICAL APPLICATIONS

Introduction

Theoretical work in an applied field such as geophysics is of
limited help if one does not develop simultaneously a capability to
translate mathematical expressions into numbers. We shall row present
the computed radiation field for the spherical rupture 'ode described
in section IV-2.

The most important lesson which one can draw from these numerical
applications is that even such a simple model depends on enough para-
meters so as to be, in fact, quite complex. A complete discussion of
all of its aspects is thus a major undertaking in itself. We shall
focus in this chapter on the major features of the radiation field,
which we shall discuss on the basis of selected examples.

The far-field radiation will be analyzed first, and then some of
near-field effects. Starting from the simplest model of a symmetrically
expanding sphere, we shall continue with a discussion of the effects of
unilateral rupture propagation. The azimuthal dependence of the
radiation fields will be discussed as a function of frequency, both on
the basis of selected amplitude spectra and of selected radiation
patterns. Phase spectra will be shown which further illustrate the
complexity of the radiated fields and may revive the concept of the
Z phenomenon. Finally, for the sake of completeness, a brief comparison
with the observations will be given.

We wish to emphasize in this chapter the fact that there is a

de facto trade-off between model flexibility and convenience. Of course, the dilemma must be solved according to the quality of the data to be interpreted. But in view of the complexity of this simple model, there can be no doubt that an earthquake is a very complicated phenomenon indeed, and we are probably still a long way from understanding it well.

In order to fix the ideas we shall assume throughout this chapter that the stress field is pure shear, and such that it should generate a north-south vertical strike slip fault. In the source coordinate system (see Chapter V) this corresponds to the condition $\sigma_{12}^{(o)} = \sigma_{23}^{(o)} = 0$, $\sigma_{13}^{(o)} \neq 0$. We shall in fact specify the prestrain $e = e_{13}^{(o)}$ rather than the prestress. Furthermore, whenever the rupture propagates it is assumed to propagate towards the north. Azimuths are then measured from the northern direction, and take-off angles from the downward vertical (e.g., Chapter V). The free-space radiation is computed in all cases, so that we are discussing source effects only.

VII-1   The far-field amplitude spectra

We already know from the discussion of Chapter IV that, at fixed rupture dimension, two essential parameters affect the shape of the far-field amplitude spectrum: the rupture velocity V_R controls the high frequency spectral shape, while the relaxation radius R_s determines the long-period behavior. Let us start with the simplest case of a non-propagating, expanding spherical rupture of final radius R_o.

1)   Stationary rupture with equilateral growth

In that case we know from the analytical solution that the radiation field is pure quadrupole at all frequencies. Figure VII-1-1 shows the high frequency part of the displacement amplitude spectrum computed for a sequence of several rupture velocities. The lowest rupture velocity is .3 km/sec, which is very low, and the highest one is 3.45 km/sec, which approaches the shear wave velocity, chosen at 3.5 km/sec. The figure exhibits several noteworthy features.

First of all, we note that the average slope of the spectra always tends to -3 at high frequencies. However, this asymptotic behavior is only reached at very high frequency for the S-spectra when the rupture velocity approaches V_s. This confirms the analytical results of Chapter IV, and one can see quite clearly that the S-spectrum will have a slope of -2 when $V_R = V_s$. We should note that this effect becomes strong only when V_R is greater than, say, 0.9 V_s. No such effect is observed for the P-spectrum, since V_R never approaches V_p.

On the other hand, for low rupture velocities P- and S-spectra are affected in a similar fashion. In fact, it is clear from the figure

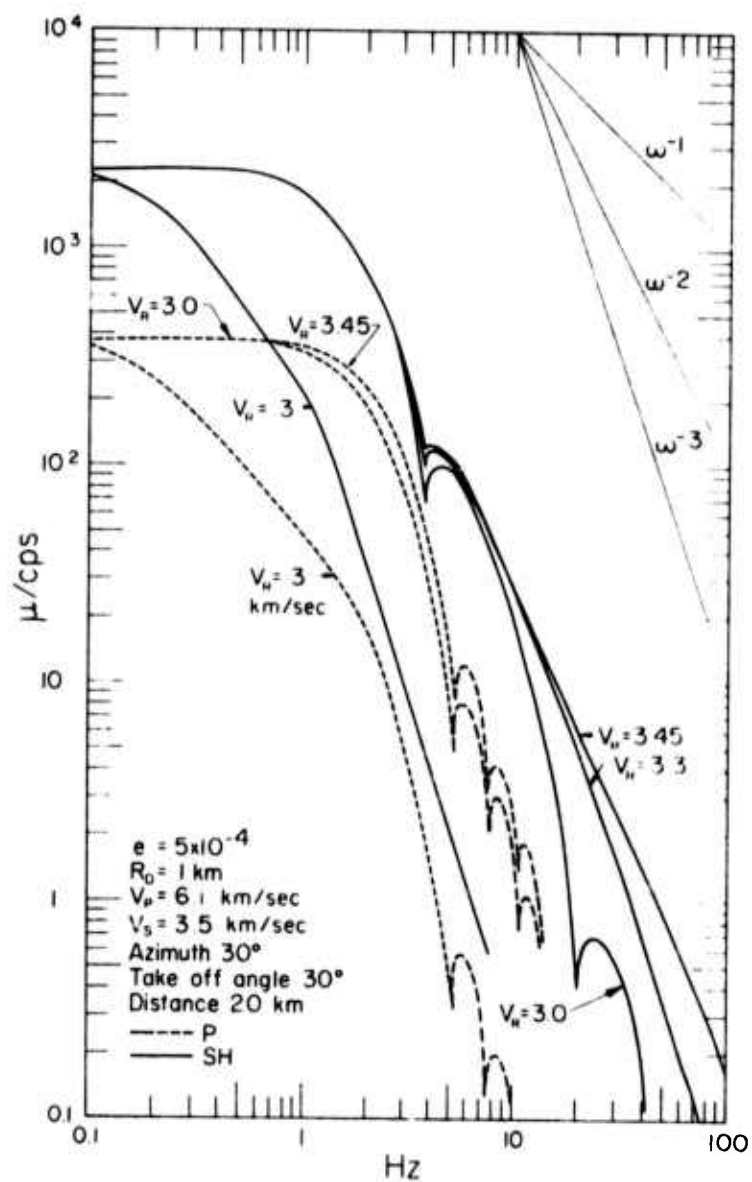Figure VII-1-1. Effect of rupture velocity on the displacement spectrum. Case of a stationary rupture with equilateral growth.

that the dependence of the spectra on V_R is nonlinear. As the rupture velocity becomes slow, we note the development of an intermediate frequency range, where the spectrum has approximately a slope of -1, before it steepens to -3 at higher frequencies. There is clearly no simple scaling law of these curves as a function of V_R ; in fact, one wonders whether a "corner frequency" may be usefully defined. If f_o is such a corner frequency, then according to the results of section IV-5, we have

$$2\pi f_o = \left(\frac{9V_R \, v^2_{(p,s)}}{R_o^3} \right)^{1/3} . \qquad \text{(VII-1-1)}$$

We may therefore compute the following values of f_o , in hertz

	P-spectrum	S-spectrum
$V_R = 3.$ km/sec	1.6	1.1
$V_R = .3$ km/sec	0.74	0.51

It is clear that (VII-1-1) yields the intersection of the high frequency asymptote with the long-period level. Should one insist in defining a corner frequency in all cases, this is a self-consistent way to do it. However, it is doubtful that such a concept is very useful for low rupture velocities.

Let us point out in passing that the frequency at which the spectrum reaches its long-period asymptote apparently scales linearly

with rupture velocity. Unfortunately, this point is rather difficult to pick on theoretical spectra (figure VII-1-1), let alone on observed spectra.

Finally, we wish to comment on the observational result that S-corner frequencies are lower than P-corner frequencies. For various reasons discussed earlier, observed spectra are rather band-limited. Now, if the spectra of figure VII-1-1 were only given in the frequency band .5 cps to 10 cps, then we see that the average high frequency slope of the S-spectrum can easily be underestimated, and thus the corner frequency will be biased towards longer periods. This bias is not present for the P-spectrum, and therefore from band limited data, the difference between S- and P-corner frequencies will exhibit a tendency to be overestimated.

Let us now turn to the long-period spectral behavior. Figure VII-1-2 shows three P-wave spectra computed for R_s = 5 km, 20 km, and $R_s = \infty$. If R_s is unbounded, the long-period spectrum is flat, as we also know from Chapter IV. On the other hand, a finite value of R_s leads to a peaked spectrum. However, even when R_s = 5 km, which is two and a half source dimensions, the peak level is very nearly equal to the "flat level." And a more acceptable value of ten source dimensions yields a spectrum which is quasi-flat over almost a decade in frequency. Of course, this only corroborates the findings of section IV-5 and we shall not repeat the discussion here.

ii) Propagating rupture, unilateral growth

The model discussed so far is adequate to model the tectonic

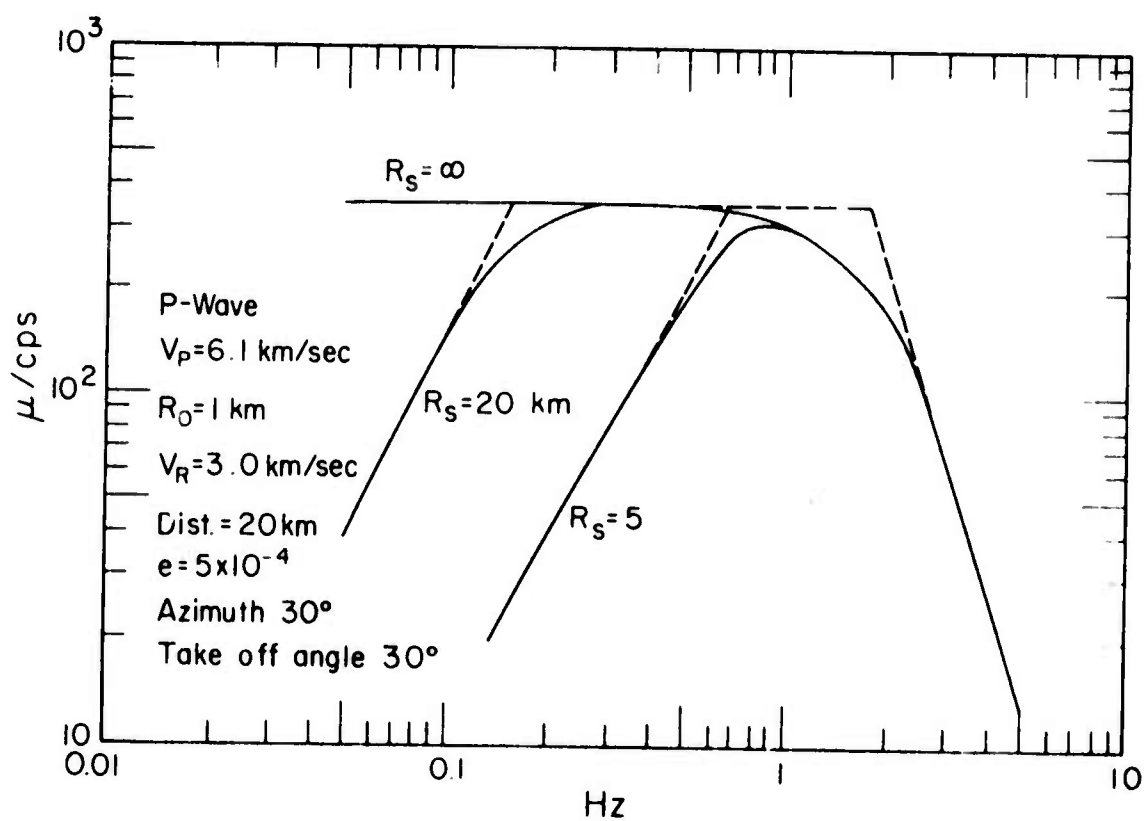Figure VII-1-2. Effect of R_s on the long period displacement amplitude spectrum. Case of equilateral growth.

release due to underground explosions. Let us now investigate the case of a rupture growing unilaterally, since this is more appropriate to model an earthquake.

Recall first that multipoles of higher degrees are excited in addition to the fundamental quadrupole, and that their effects are essentially felt at high frequencies. Figure VII-1-3 shows how these multipoles of higher degree affect the spectra--in a particular direction. The first impression is that this effect, although clearly noticeable, is not particularly large. However, under closer scrutiny, the figure reveals that the S-spectrum character has been radically changed by the additional multipoles. Indeed, because of the rapid rate of growth chosen in this case ($V_R \simeq .98 \, V_s$) the quadrupole spectrum exhibits a high frequency slope of almost -2. However, since the rupture is unilateral, the radiation field must "see" a different propagation velocity in different directions. In particular, the propagation rate in the direction indicated on the figure is certainly less than V_R. This explains why the multipoles of higher degree steepen the spectrum at high frequency. When ten multipoles are taken into account, the slope is in fact -3.

From the explanation given above, one expects this effect to be strongly dependent on azimuth; this is indeed the case, and we shall see later that this effect is very strong for back azimuths for which the azimuth makes an obtuse angle with the direction of propagation. As we pointed out in Chapter IV, one should probably add a few more multipoles (up to $\ell = 15$) in order to reach convergence. However, the computation becomes then quite lengthy, and necessitates a more
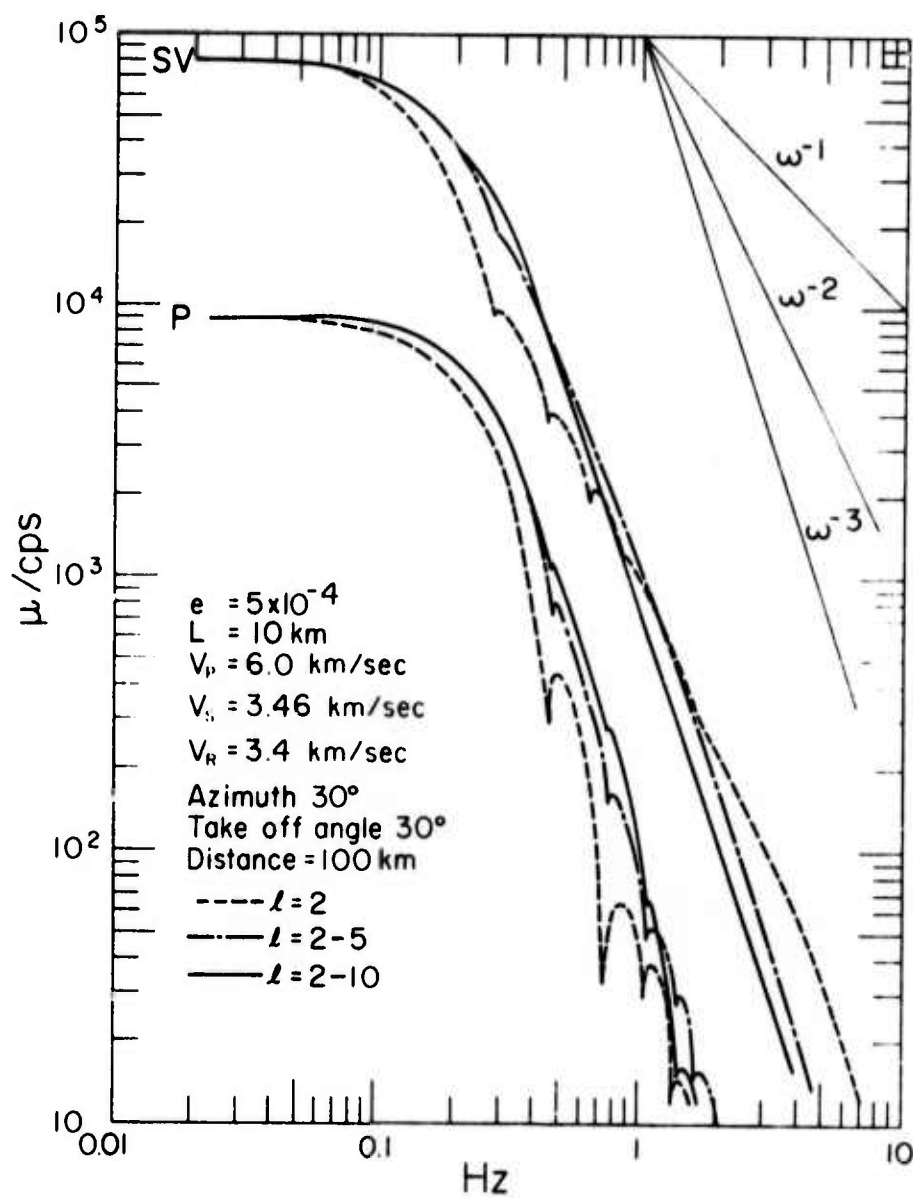
Figure VII-1-3. Effect of the multipoles of higher degree on the displacement amplitude spectrum. Case of unilateral growth.

efficient algorithm than the one we used. Convergence problems are only
critical at very high frequencies, and for azimuths close to 180°, and
we shall simply keep this in mind for the present discussion.

According to the analysis of section IV-5, if one wishes to define
a corner frequency in that case, one should simply replace R_o by L
in (VII-1-1) . This means that the corner frequency obtained at
convergence should be about twice that obtained from the quadrupole only.
Figure VII-1-3 seems to agree with this result reasonably well.
However, here again, one expects azimuthal effects to be rather strong,
and the concept of a corner frequency thereby loses some of its
usefulness.

The spectra scale with V_R and R_s much in the same way as we saw
earlier. Figures VII-1-4 through VII-1-6 show a variety of possible
spectral shapes obtained by varying these parameters. This is shown
separately for P , SV and SH spectra. Note also that these
figures correspond to an azimuth and a take-off angle of 30° each. It
seems at first glance that the spectral shape changes rapidly as a
function of R_s and V_R . However, we should point out that if
$R_s > 10L$, and if V_R is greater than, say, $V_s/3$, then the range
of possible shapes is somewhat reduced. Nevertheless, there is a
definite dependence of the general far-field spectral shape on the
rupture velocity and the relaxation radius. The parameter V_R controls
the high frequency side of the spectrum, while R_s controls the long-
period side. Furthermore, unless one goes to small values of both R_s
and V_R , there is little interference between these parameters; in
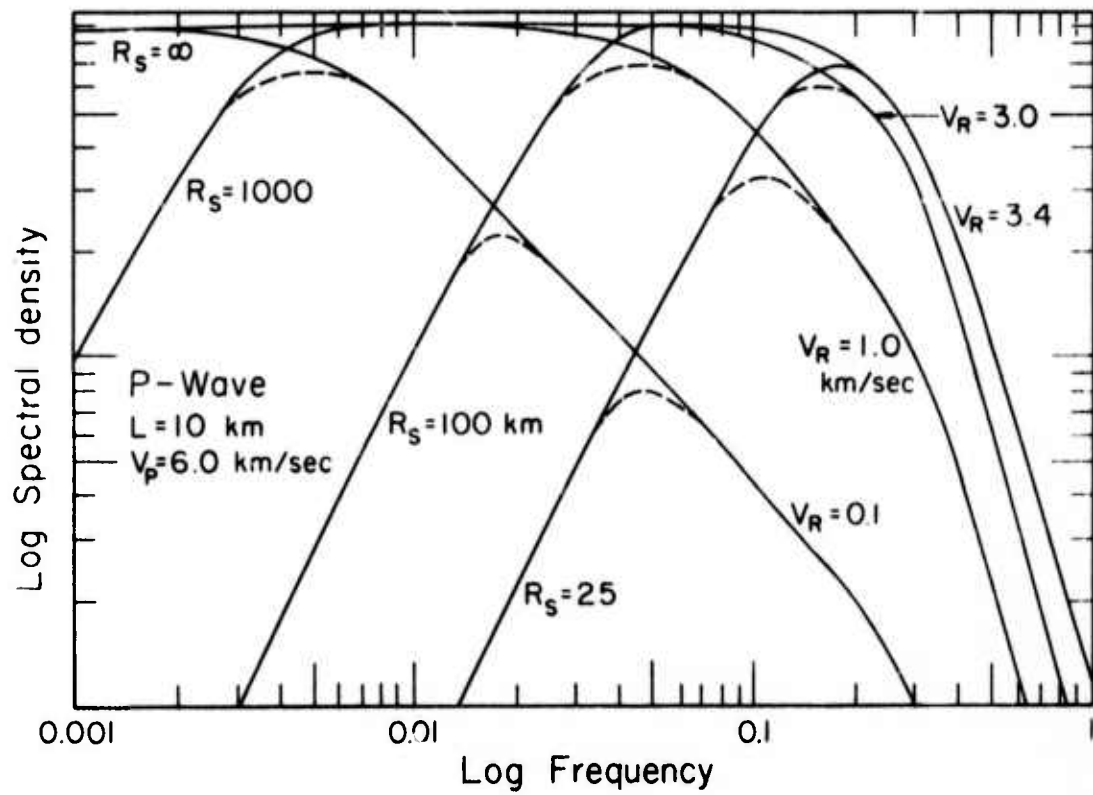particular, the spectra are rather insensitive to either one at

Figure VII-1-4. Effects of R_s and V_R on the global shape of the displacement amplitude spectrum. Unilateral growth. P-wave spectra.
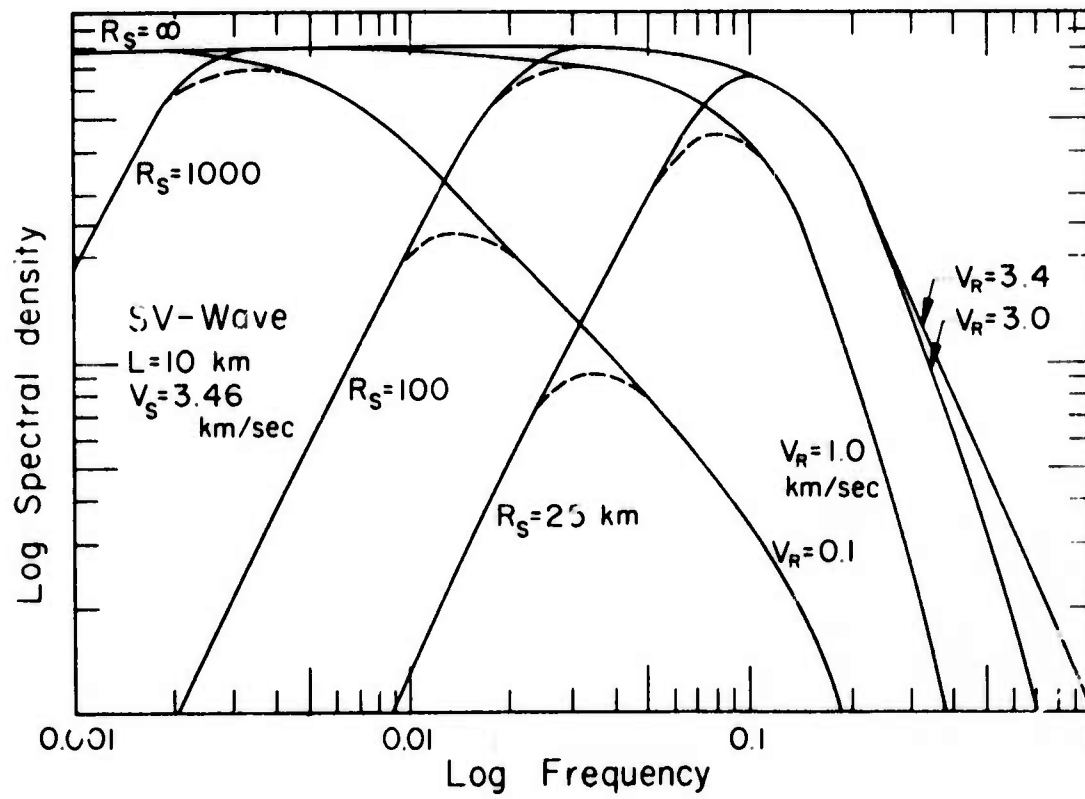
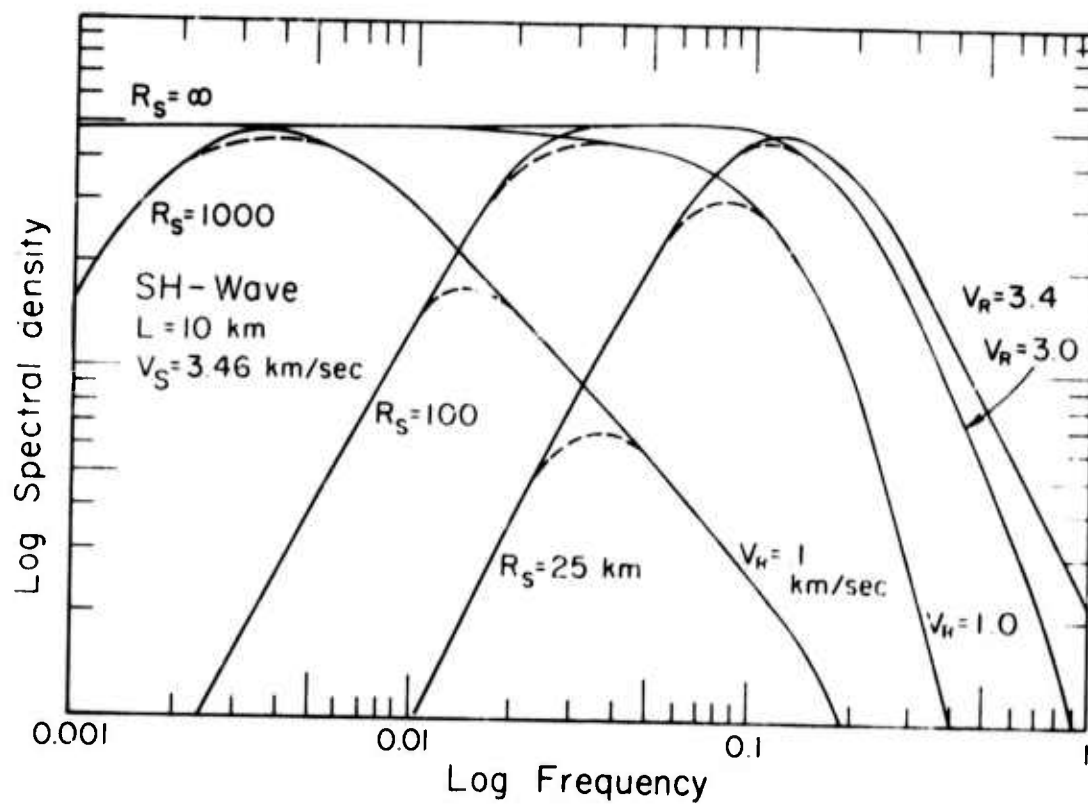Figure VII-1-5.   Same as figure VII-1-4.   SV-wave spectra.

Figure VII-1-6.   Same as figure VII-1-4.   SH-wave spectra.

intermediate frequencies.

Much simpler is the scaling with rupture length, as shown on figure VII-1-7. To simplify the matter we assume that R_s is proportional to L, which is an acceptable assumption. The calculations are plainly in agreement with the results of Chapter IV. A change in rupture length simply results in a translation of the whole far-field spectrum. In fact, increasing L by one order of magnitude results in an increase of the peak level by three orders of magnitude, and a shift by a decade in frequency towards long periods. Thus the points A, B, C are transformed into $A'B'C'$. For convenience, the segment AA' was graduated in terms of length. The figure illustrates several things. First, since the average high frequency slope of the spectra tends asymptotically to -3, the scaling as a function L consists essentially in sliding the spectra along their high frequency asymptotes. This is particularly true for the P-spectrum. Now if we assume that the body wave magnitude m_b is closely related to the P-wave spectral amplitude at 1 cps, we may conclude that, at constant prestress, m_b possesses an upper bound. The S-wave magnitude, however, could be unbounded if V_R approaches V_s since the slope of the S-spectrum may be close to -2 in that case. Of course, this opens the possibility that efficient SV to P conversion near the source--for example, at the free surface--could result in large measured values of m_b. Clearly a similar analysis can be made for the surface wave magnitude M_s, which may be related to the S-spectral amplitude at 0.05 cps. We shall return to this question below.
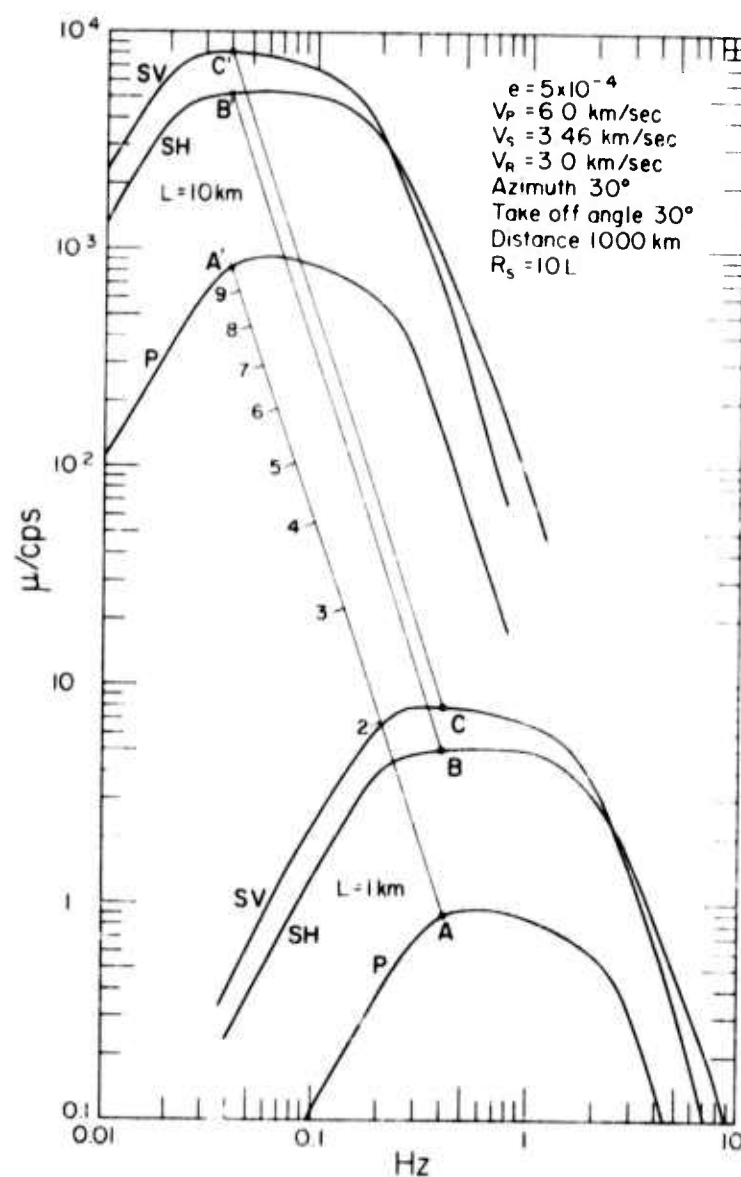
Figure VII-1-7. Scaling of the displacement spectra with rupture length.

VII-2   The near-field amplitude spectra

Discussion of the near-field spectra is somewhat less informative for several reasons. First of all, we are evaluating here a very simple model, and it is precisely in the near-field that the details of the source mechanism should be felt the most strongly. Thus near-field observations will depend very much on the fault geometry, on the history of rupture, on the complexity of the stress field (e.g., Hanks, 1973), and we do not take any of these into account. Furthermore, it is also in the near-field that most of the approximations made in Chapter IV lose some of their validity. However, we can point out several interesting general features which should hold independently of the particular model chosen.

Since near-field effects are only important at long periods, only the quadrupole term contributes to the radiation, and there is in that case no convergence problem. Let us discuss first the case of an observer lying inside the relaxation zone, that is, the case where R_s is infinite.

As we showed in Chapter IV, there is little point in talking about P- and S-waves in that case. The reason for this is clealy illustrated by figure VII-2-1. The spherical (r,θ,ϕ) components of the so-called P- and S- displacement spectra behave as ω^{-3} at long periods in that case. This is obviously unphysical since the radiated energy would be unbounded in that case. On the other hand, the total spectra--also shown on figure VII-1-2 as P+S--behave as ω^{-1} which is what should be expected for a net offset in displacement. This figure also shows that only the r component of the P-wave, and the θ and ϕ components of

Figure VII-2-1. Near-field spectra. Case of unbounded R_s.

the S-wave—SV and SH respectively—are the only components which survive at high frequency. This means, of course, that the high frequency radiation is far-field in nature, and that no near-field effects are felt at such frequencies.

Let us also point out that near-field spectral observations can be quite complicated because of interference phenomena, which give a scalloped aspect to the spectra. In addition, for example, the θ and ϕ components of the S-spectra exhibit a quasi-flat portion at intermediate frequency, while the r component, which is pure near-field, is monotonic . On the other hand, one notices that the θ and ϕ components of total radiation are not flat but exhibit a broad peak. The shape of that peak will, of course, be azimuthally dependent since the quadrupole pattern for P, SV and SH waves are different.

Figure VII-2-2 focuses on the dependence of the near-field with hypocentral distance. Only the radial component of the P-spectrum is shown, but similar results obviously hold for other components as well. Two cases are considered: for a source length of 10 km, R_s is chosen successively at 100 km and at infinity. The most obvious effect is that the greater the distance, the longer the period at which the near-field is observed. This stems from the fact that far-field terms decay with distance as r^{-1} , while near-field terms have a faster decay of r^{-2} , r^{-3} and r^{-4} . It is interesting to note that when R_s is finite, the far-field spectrum is of course peaked, but that this peak practically disappears at short distances, due to the near-field radiation. Of course, inside the relaxation zone, only the case $R_s = \infty$ is relevant.
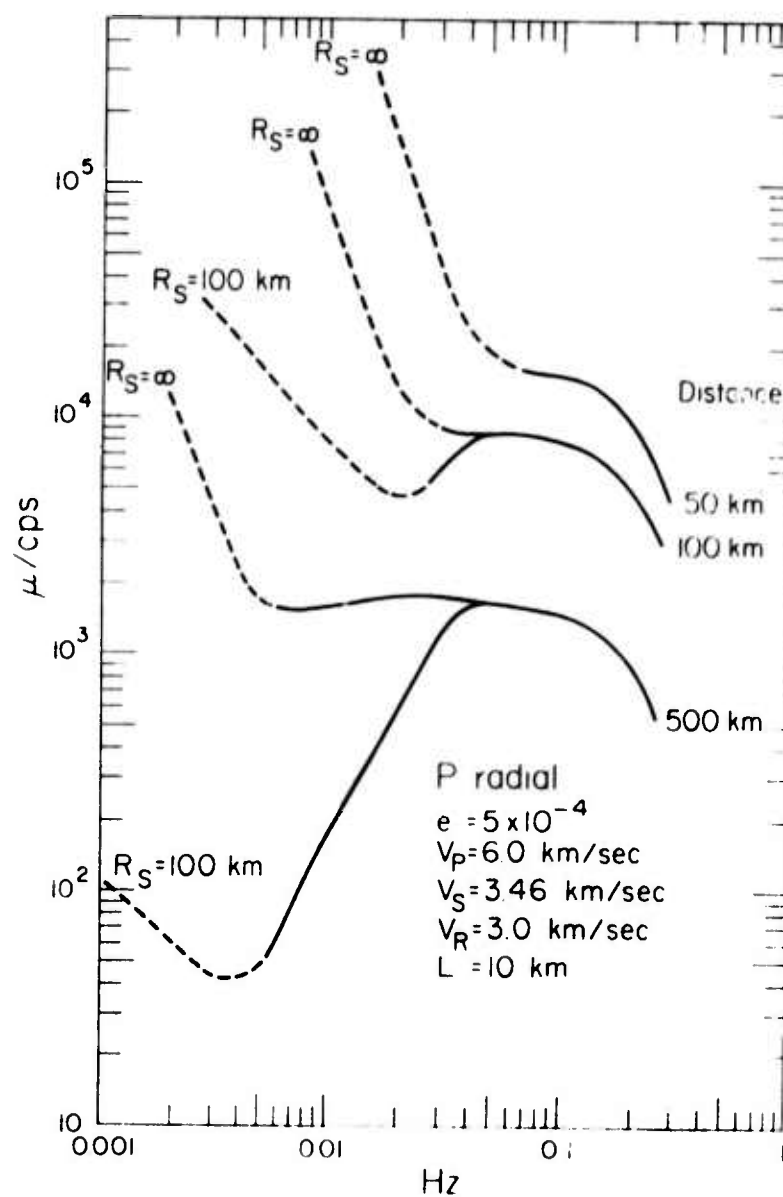
Figure VII-2-2. Dependence of the near-field on hypocentral distance.

These are the only aspects of the near-field radiation that we can usefully discuss here. More complete investigations must be undertaken on the basis of each particular event, by taking into account the details of faulting, the inhomogeneities in the vicinity in the source, etc. Such investigations have been undertaken, for example, by Hanks (1973) or Cherry, et al. (1973).

VII-3 Azimuthal effects, radiation patterns

The azimuthal dependence of the radiation fields was mentioned several times in the preceding discussion. To be complete, a description of this dependence should include a presentation of the spectra at many azimuths and many take-off angles. Similarly, three dimensional radiation patterns should be plotted on the focal sphere, using a contour representation on a stereographic projection. This is well beyond the goals of the present discussion and we shall try and show, on the basis of selected examples, how complex the radiation field really is.

1) Azimuthal dependence of the spectra

Figure VII-3-1 shows two sets of spectra computed for a propagating rupture, at the same distance, the same take-off angle, but at two complementary azimuths. The difference is striking.

First of all, there is clearly more high frequency energy radiated in the forward direction (azimuth 20°) than in the backward direction (azimuth 160°). This is accompanied by a drastic change in the character of the spectra. The spectra are indeed smooth in the forward direction and very scalloped in the backward direction. This is of course due to different interference phenomena. As we pointed out earlier, because the rupture is unilateral, the rupture velocity "seen" by the radiation field is greater in the forward direction than in the backward direction. This effect is rather more pronounced for the S-spectra than for the P-spectra, which is to be expected since V_R is closer to V_s than to V_p .
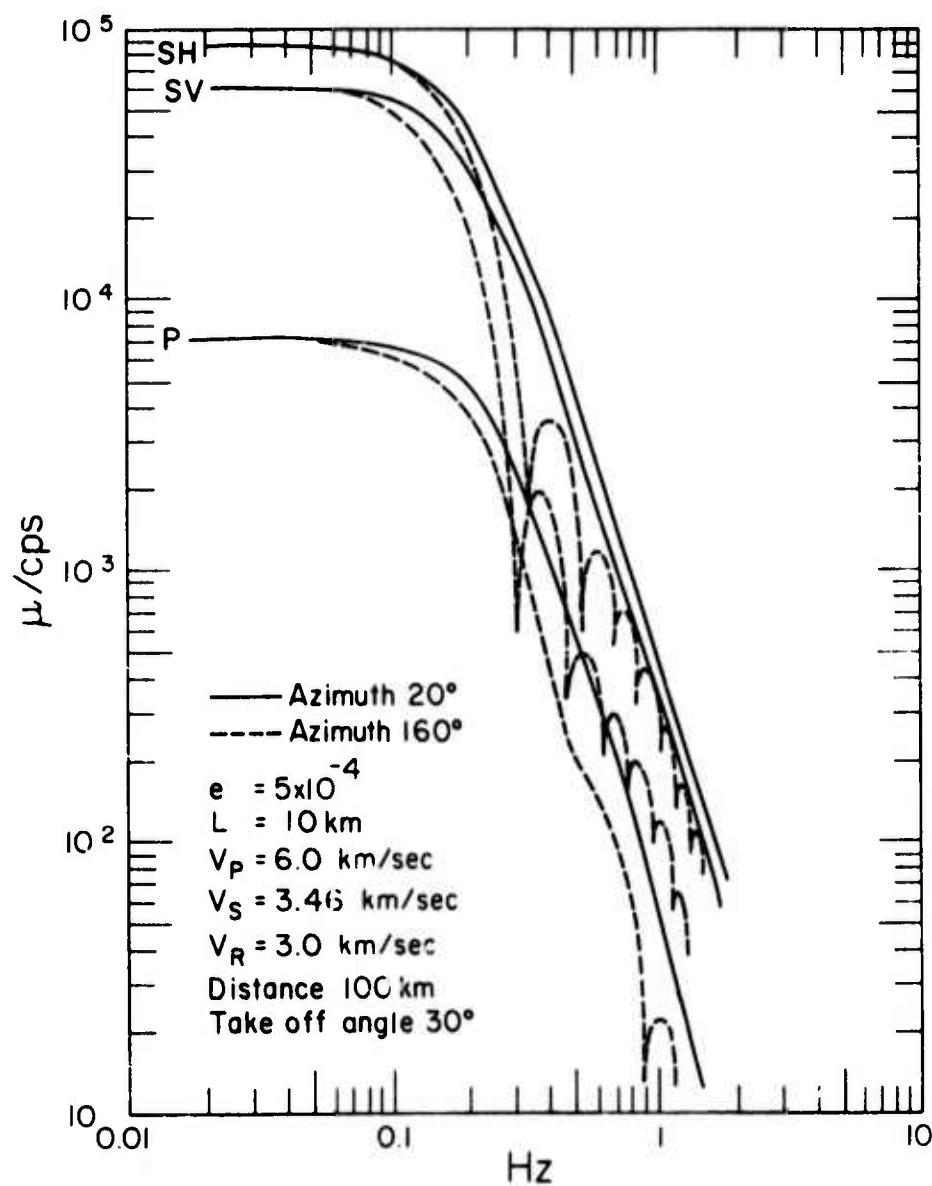
Figure VII-3-1.   Azimuthal dependence of displacement spectra.

We should comment on the remark made earlier that the convergence of the multipolar expansion is slower for back azimuths. A total of ten multipoles have been added to compute the spectra of figure VII-3-1. To check the convergence of the series, we compared the partial sum of five multipoles with figure VII-3-1. The result is that convergence is practically attained with only five terms at the forward azimuth, while ten multipoles are not quite sufficient in the other case. In fact, the details of the high-frequency spectra at azimuth 160° can be slightly modified by adding a few more multipoles, particularly for frequencies higher than 0.5 cps. Our numerical experiments indicate that the spectral levels shown on this figure are a little too high, so that the average slope will be increased by the additional terms.

Figure VII-3-1 also illustrates how the "corner frequency" may depend on azimuth. No comment is needed except to emphasize once again that such a concept can only be used in a gross sense, and that a suitable averaging over all directions should be performed in evaluating it.

ii) Radiation patterns

In order to better illustrate the azimuthal dependence of the radiated field, we computed radiation patterns at periods of 20, 10, 5, and 2 seconds. These radiation patterns for P, SV, and SH waves were computed at constant take-off angle 30°, for the same model as used in figure VII-3-1 for two rupture velocities. They are given in figures VII-3-2 through VII-3-4. In addition, because of the obvious symmetry

of the source, only one half of the pattern in given in each case. The
left-hand side of each figure corresponds to $V_R = 3$ km/sec and the
right-hand side to $V_R = 1$ km/sec . For completeness, both amplitude
and phase are shown as a function of azimuth.

The simplest patterns are obtained at long periods, where the
radiation field is dominantly quadrupole in all cases, and where no
effect of the rupture velocity can be noted. We note, however, a
slight alteration of these patterns at a period of ten seconds, and, by
comparison with figure VII-3-1, this corresponds, of course, to a
period where higher degree multipoles begin to be felt. We see that the
holes in the amplitude pattern are not as pronounced, the phase discon-
tinuities not as sharp, and we also note a very slight distortion
towards the direction of rupture propagation.

At shorter periods, these effects are much more pronounced, and
the patterns change very rapidly with frequency. At the same time,
several phenomena take place: it seems that the SH pattern at 5 seconds
possesses a rather strong monopole component, while P and SV develop
apparently dominant dipole components at the same period. We know that
this cannot be the case since the solution used for the computation
contains neither monopole nor dipole (see section IV-2). It may thus
clearly be misleading to try and deduce the multipolar content of a
radiation field from observations at one frequency, and one take-off
angle. The converse situation is also true: for instance, a dipole
could be excited such as in the solution of section IV-3, but its
contribution could be negligible at some frequencies and certain
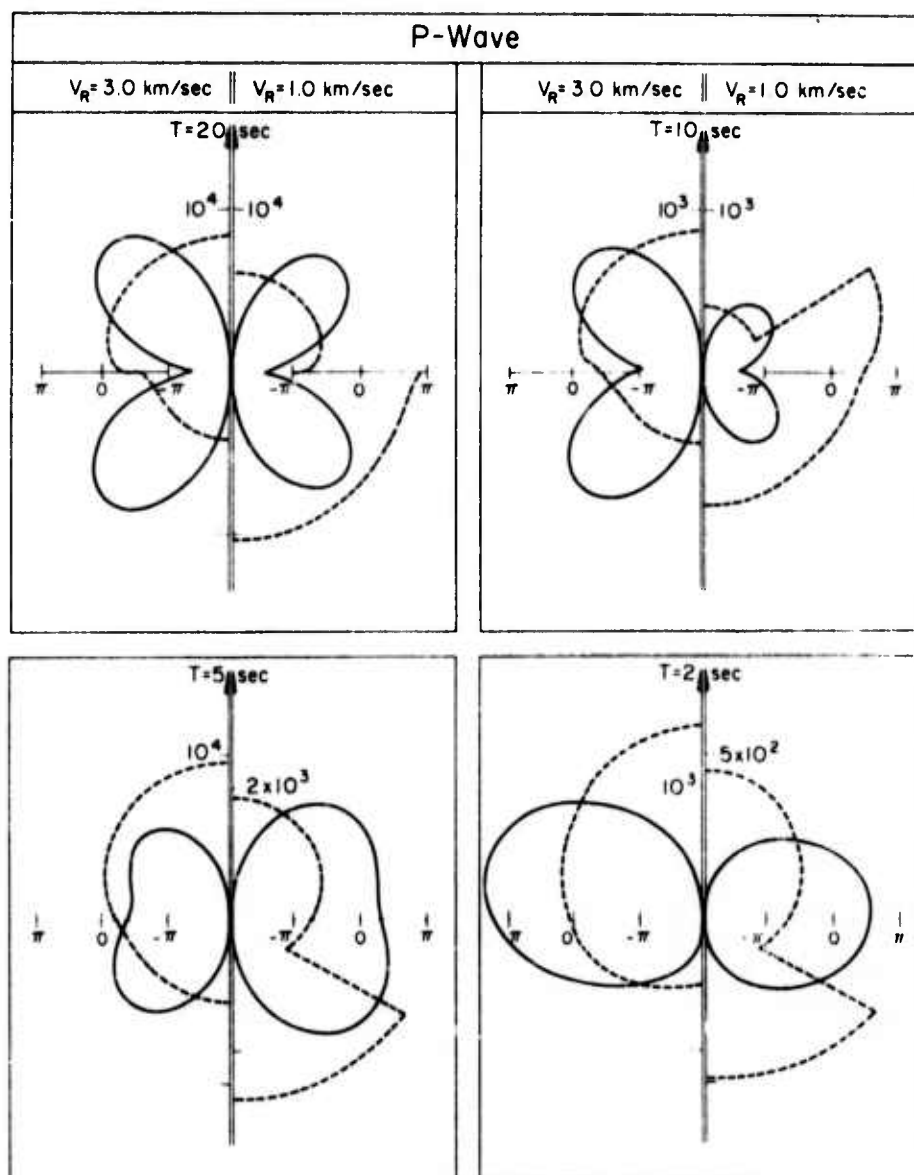directions (for instance, in the holes of the dipole spectrum).

Figure VII-3-2. P-wave radiation patterns at four periods, and for two rupture velocities. Only half-patterns are shown. The solid line is the amplitude pattern; the broken line is the phase pattern.
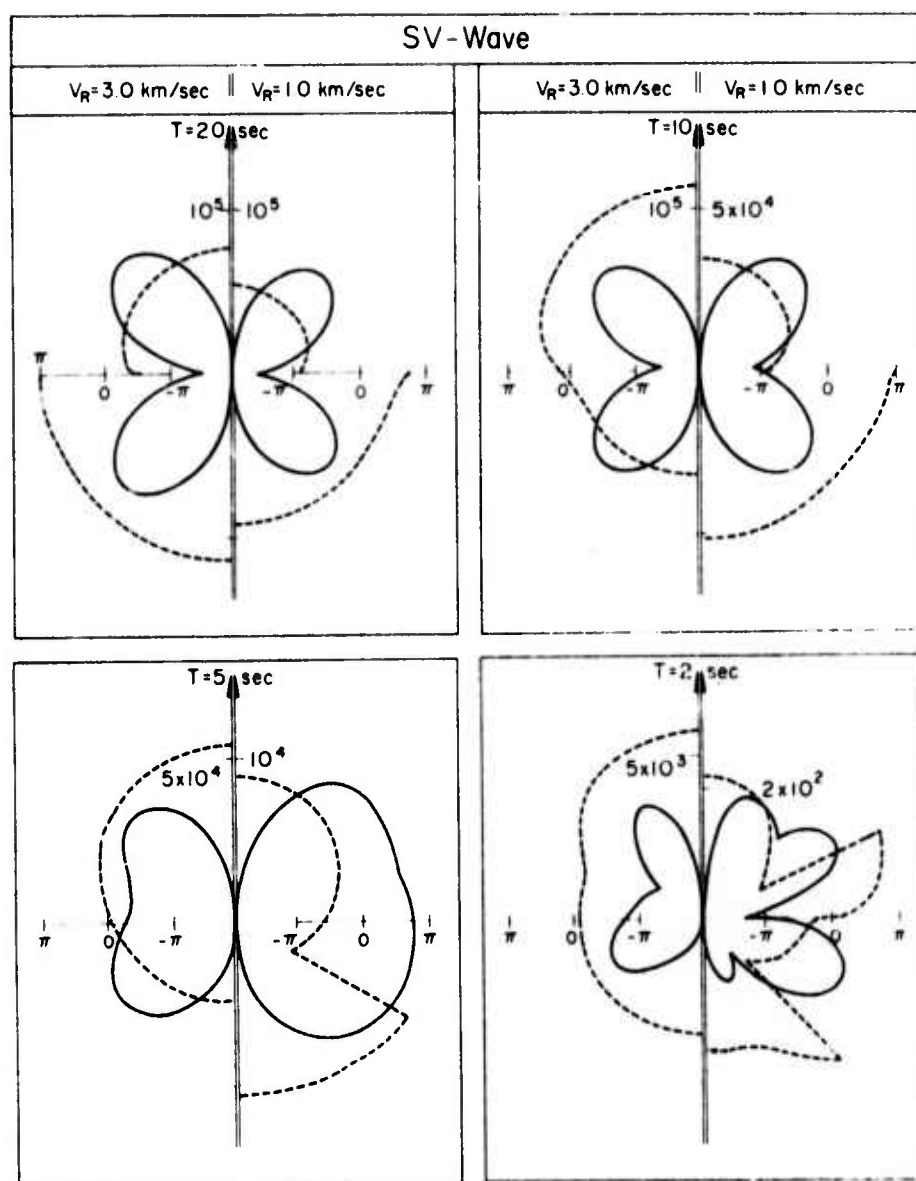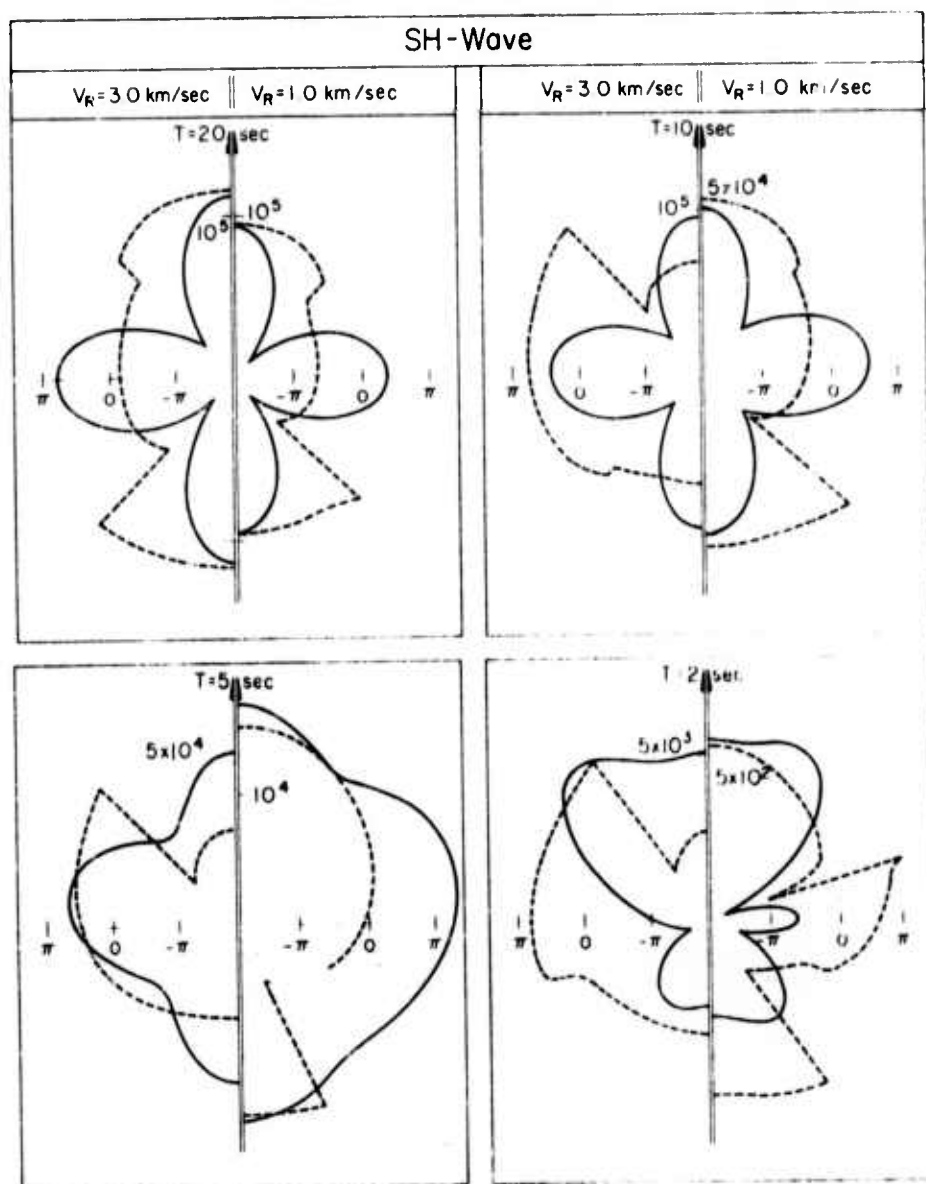
-372-

Figure VII-3-3.   Same as figure VII-3-2.   SV-wave.

Figure VII-3-4. Same as figure VII-3-2. SH-wave.

Note that the details of the SV and SH radiation patterns at two seconds and for low rupture velocity are probably not real, and would be altered by adding a few more multipoles.

In all cases we observe that more high frequency energy is radiated in the direction of rupture propagation than in the other direction, and that this effect is stronger for higher rupture velocity. All of the short period patterns are indeed distorted in a forward direction. This was to be expected, and is consistent with similar results in electromagnetism (e.g., Stratton, 1941).

It is clear from these figures that the quadrupole is no longer dominant at high frequencies. In fact, no multipole dominates. It is fascinating to see that ten multipoles, with individual patterns of great complexity, can add up to yield such simple results. This requires a very particular combination of their amplitudes and phases, which could be easily destroyed if an error is made in the calculation. We may thus consider this simplicity as an indirect check of the correctness of our calculation.

Finally, let us note that the loss of the quadrupolar character of the radiation field--at high frequencies--does not invalidate the determination of focal mechanism from first motion data. Indeed, the direction of first motions, which is a time domain concept, is essentially controlled by the very beginning of the rupture. It cannot be associated in any way with the radiation pattern at any particular frequency, which depends on the whole time series. In fact, in order to retrieve a theoretical time series from the spectra given here, one must know the phase spectra as well. This is the object of the next section.

VII-4 The phase spectra

In order to eventually be able to retrieve time domain information from spectral results--in particular, to construct synthetic seismograms --one must know the phase spectra as well at the amplitude spectra. Because the phase is rather more sensitive than the amplitude to numerical uncertainties, we only tried in this preliminary investigation to study it for frequencies lower than 1 cps. We shall recall that convergence problems started to be important for higher frequencies (see figure VII-3-1).

Although it is sufficient to know a phase angle modulo 2π , there are a number of advantages in "unwinding" the phase spectrum. This is true in particular for purposes of interpolation, and also to study the slope of the phase spectrum as a function of frequency (group delay). We also confine ourselves to the far-field case since near-field effects may be evaluated analytically (see section IV-5).

Figure VII-4-1 shows the phase spectra for various displacement components, computed at a hypocentral distance of 100 km, or ten source dimensions. The immediate observation is that, even at such a short distance, the phase spectrum is overwhelmed by the propagation term-- $k_\alpha r$. The spectra are very linear, and show very little fine structure (at least in that particular direction). The figure also shows that an additional term is present in the spectra, which depends quite strongly on the rupture velocity V_R . This is definitely a source effect, and it appears to be strong enough to be detectable in close range observations. A slow rupture velocity yields a steeper phase spectrum, and thus implies a larger group delay at the source.
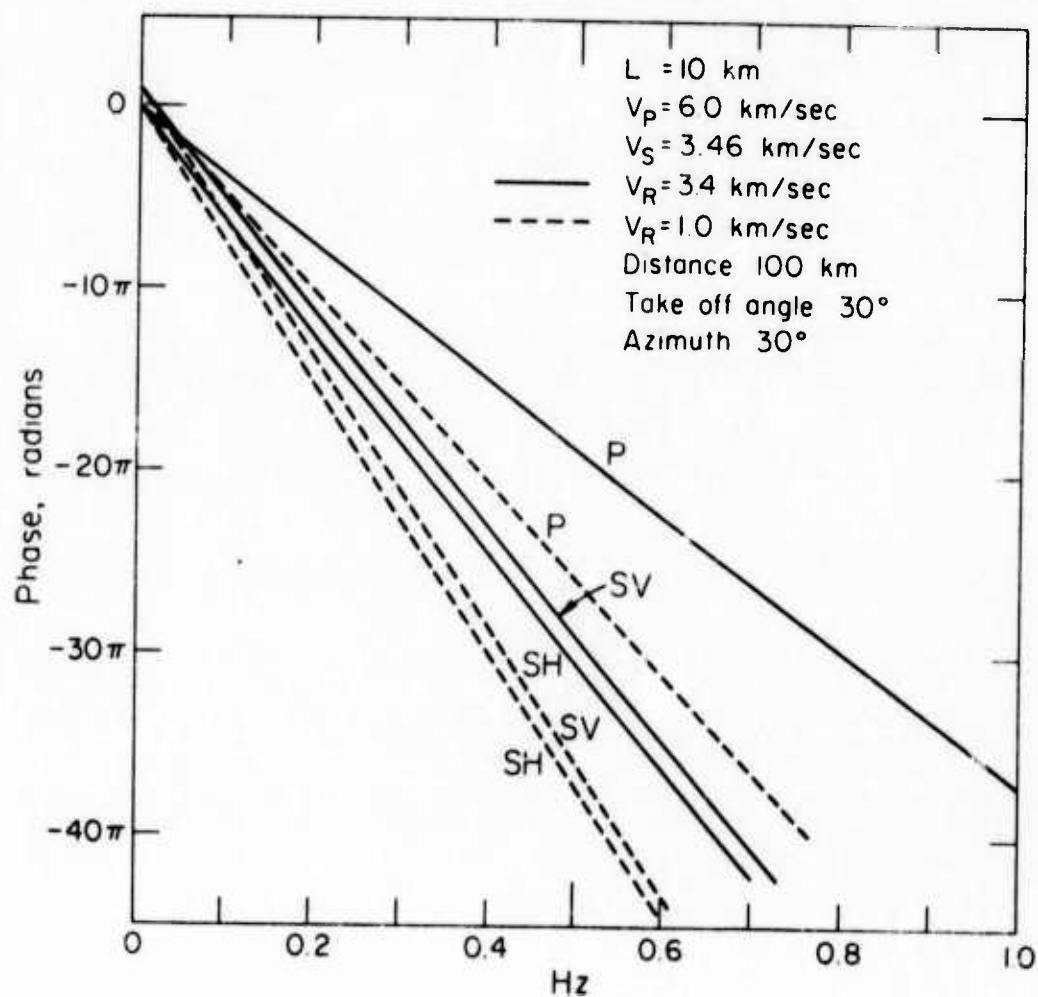
Figure VII-4-1. Far-field phase spectra computed at a distance of
ten source dimensions, and for two rupture velocities.

-377-

When the propagation term $-k_\alpha r$ is removed (figure VII-4-2), one is left with the phase at the source. This is the initial phase of an equivalent multipolar point source (see Chapter V). This reduced phase spectrum is much more interesting, and yields important information about the rupture phenomenon.

First of all, the initial phase does not depend linearly on frequency. This means that our source model is inherently dispersive. As discussed in section IV-5, one defines the group delay at the source by

$$t_g(\omega) = -\frac{\partial(\text{phase})}{\partial\omega} = \frac{-1}{2}\frac{\partial(\text{phase})}{\partial f} \qquad \text{(VII-4-1)}$$

Since the steeper slopes in figure VII-4-2 occur at long periods, we deduce that long-period radiation is rather more delayed than high frequency radiation. This delay clearly increases with decreasing rupture velocity, and it is not difficult to see that the long-period group delay is of the order of L/V_R , the rupture duration. This is quite consistent with the results of section IV-5. Recall that we found the long-period delay to be 0.75 L/V_R for a stationary source. We have confirmed this result on the basis of numerical calculations not shown here. For propagating sources (figure VII-4-2) we see that the delay is closer to L/V_R , and that it is slightly larger for S-waves than for P-waves at this particular azimuth.

Just as we predicted in Chapter IV, the group delay tends towards zero at high frequencies. This is especially clear for S-waves and for high rupture velocities. The group delay for P-waves does not converge
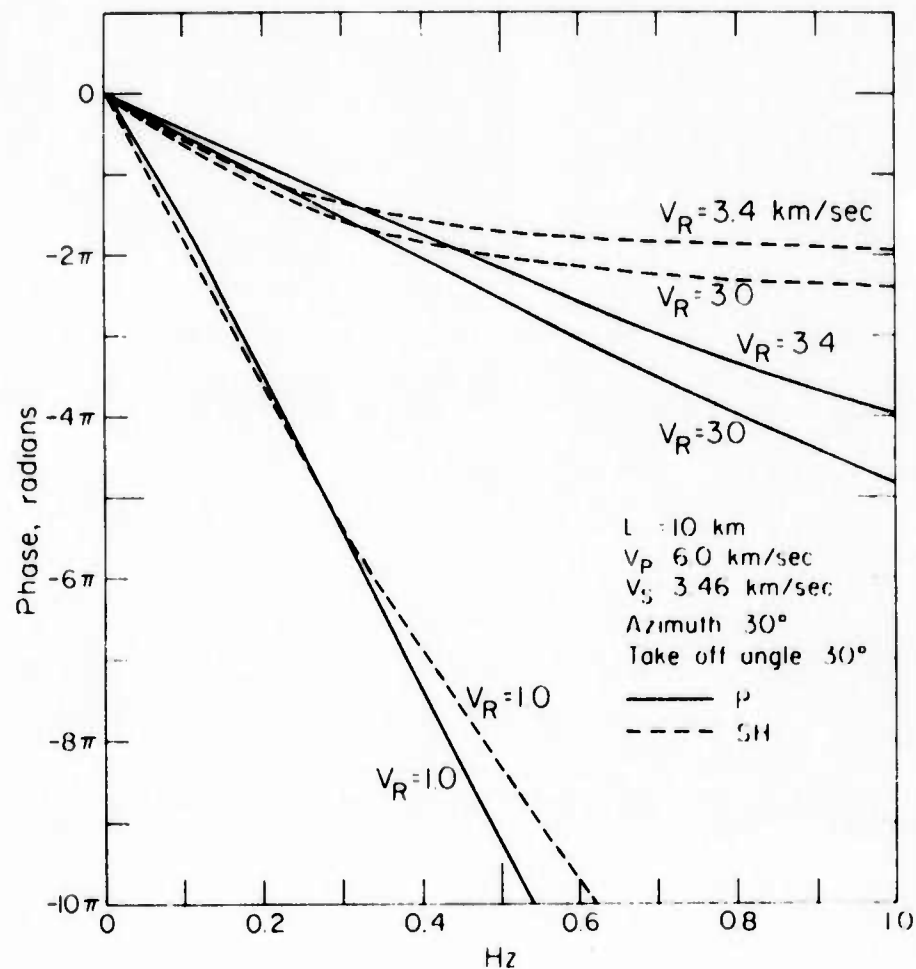
Figure VII-4-2. Far-field phase spectra corrected back to equivalent point source. Effects of rupture velocity.

-379-

to zero as rapidly, and this can be intuitively explained by not ng that V_R stays rather small compared to V_p , even when it approaches V_s . As a result, our source model is less dispersive for P-waves at low to intermediate frequencies than it is for S-waves. Of course, one wonders whether this is azimuthally dependent. Figure VII-4-3 shows phase spectra (at the source) computed for three different azimuths, and at constant take-off angle. It is immediately obvious that, just as the amplitude spectra, the phase spectra become more complicated as back azimuths. The portions marked with question marks correspond to frequency bands where the phase varies extremely rapidly with frequency. Each one of these bands is associated with a hole in the amplitude spectrum, while the regions where the phase varies smoothly with frequency are to be correlated ith peaks of the amplitude (see e.g., figure VII-3-1). When the phase varies rapidly, it can only be unwound by sampling it very densely. Because our frequency sampling was not dense enough, each one of the jumps shown in figure VII-4-3 is only known up to an undetermined number of full cycles (2π) . Furthermore, since the holes in the amplitude spectra are due to destructive inter-ference phenomena, these frequency bands are precisely those for which numerical noise is critical. On the other hand, and for exactly the same reason, little power is radiated in the same frequency bands, so that spectral details in such bands are not essential.

Outside the narrow frequency bands where the phase varies rapidly, one notices little azimuthal dependence of the slope. The strongest dependence is found for the P-wave, for which the group delay at the source is slightly smaller at forward azimuths than at back azimuths.
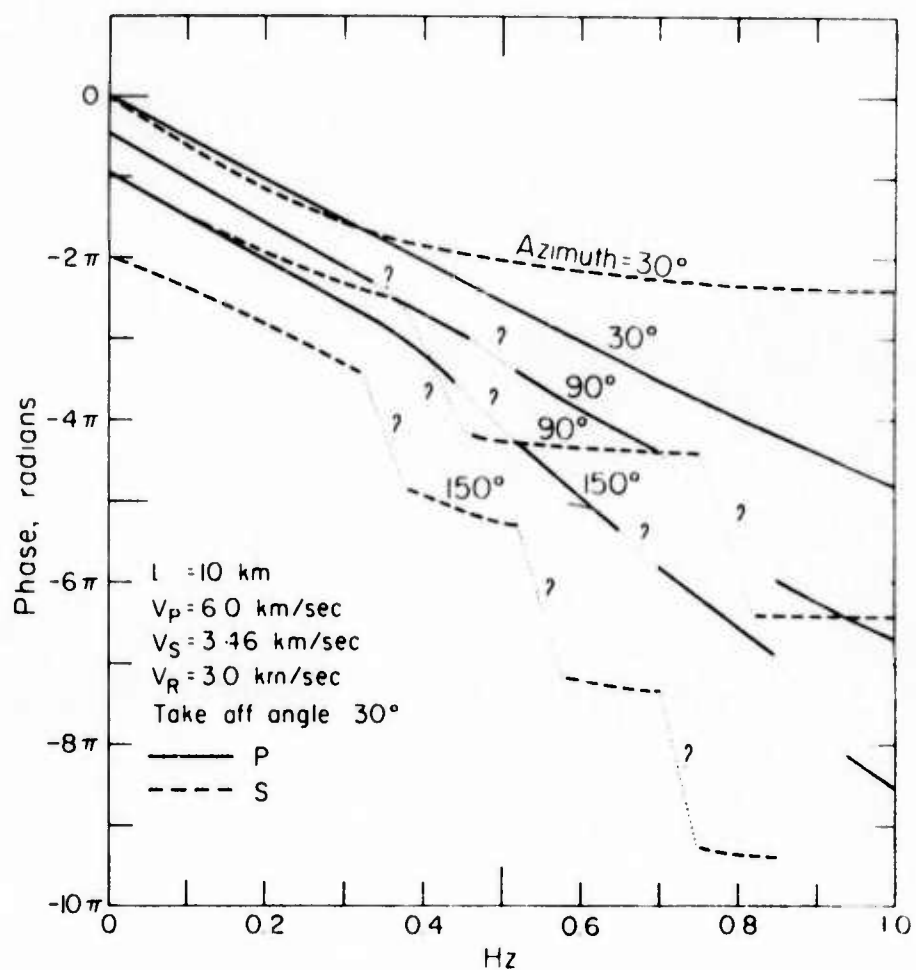
-380-

Figure VII-4-3. Far-field phase spectra corrected back to equivalent point source. Azimuthal dependence.

-381-

This is consistent with the idea advanced earlier that the radiation field "sees" a slower rupture velocity at back azimuths. Azimuthal effects seem to be smaller at long periods, which was also to be expected.

The fact that P- and S-waves may have different group delays at the source is somewhat unsettling and deserves further discussion. It seems to indicate that P- and S-waves should exhibit different apparent origin times. This effect has been called the "Z" phenomenon. The International Dictionary of Geophysics gives the following definition:

"Z phenomenon: it has been suggested that the main P and S waves may issue from some earthquake foci at times separated by the order of some seconds. Such a separation is called the Z phenomenon, but it is now thought to be much less significant than formerly."

Observational evidence for such a discrepancy in P and S apparent origin times is relatively abundant in the seismological literature prior to 1950. For example, Jeffreys (1927) found that the linear travel time equations for the direct P- and S-waves from two British earthquakes had different constant terms by two or three seconds. The S radiation appeared to have originated earlier than the P radiation. Having observed this phenomenon in several other instances, Jeffreys (1937) concluded that the two waves both originated from the rupture zone but at different times. Gutenberg and Richter (1943) developed an explanation of the phenomenon first suggested by Reid (1918) and used later by Benioff (1938). This explanation calls for a transsonic rupture velocity, that is, such that $V_s < V_R < V_p$. If this is the case, they

argue, the first arrival of the S-wave actually comes from the point on the fault which is closest to the observer, while the P-wave first arrival comes from the point of initial rupture, hence the discrepancy in origin times. As pointed out by Bullen (1963), the concept fell into disuse and thus into obscurity after the work of Richter (1950). Richter plotted P arrival times against S-P times for several Southern California earthquakes and defined the origin time as the intercept of this curve for $S-P = 0$. This method presents the advantage of yielding origin times independent of the velocity (at constant Poisson ratio), but also the procedure will hide a hypothetical Z phenomenon by a shift of the origin time. In fact, if the Z phenomenon really takes place, the origin times so obtained should be slightly too late, and thus the mean velocities deduced from them slightly too high. If one tries in turn to locate an earthquake by using this high velocity, either the solution may be difficult to find, or the hypocentral depth will be too shallow.

Figure VII-4-2 shows that no transsonic rupture velocity is required for the occurrence of the Z phenomenon. We have here a frequency dependent effect, but since we are only talking about arrival times, and since instrument responses are generally band-limited, this dependence may be neglected. From figures VII-4-2 and VII-4-3, we see that in the case $V_R = 3.0$ km/sec , $V_s = 3.5$ km/sec , the group delay for S-waves at 1 sec is practically negligible, while that for P-waves is of the order of two or three seconds. This matches Jeffreys' (1927) observations very well. Furthermore, this result is only weakly dependent on azimuth.

The phenomenon is even more pronounced for low rupture velocities. For instance, for $V_R = 1.0$ km/sec, figure VII-4-2 shows that at .5 cps

the S delay is 6.5 sec while the P delay is 9.5 sec, a Z phenomenon of three seconds.

To go even further along this line of discussion, one may wonder whether premonitory apparent changes in the V_p/V_s ratio before earthquakes (e.g., Whitcomb and others , 1973) could not be partly interpreted as a source effect. In order to create an apparent decrease of that ratio, one only needs to assume that the failure mechanism of small events preceding larger ones changes--for example, V_R may increase so that S-P decreases. Thus, the premonitory phenomenon would not be due to a wave propagation effect only, but also due to a change in the failure characteristics of the medium. The dilemma will be solved by obtaining conclusive data both from local and from teleseismic events. Although this is the object of much current research, we feel that the question is still open at this time. This is a vast subject, full of promising ramifications, and this is not the proper place for an extensive discussion.

Although it is probably too early to reach definitive conclusions, we suggest that the long forgotten Z phenomenon may have to be revived, and that only careful observations will prove or disprove it. Since it is rather difficult to retrieve the initial phase of the radiated fields with sufficient accuracy, we propose the following procedure: seismic records could be filtered by narrow band causal filters, and the S-P times could be plotted against frequency for several events with neighboring foci. Changes in group delays at the source from event to event might be observed in this fashion. This is, of course, subject to improvements, and further theoretical and numerical work is needed in

that respect.

Before leaving the subject, we should point out that only the curvature of the phase spectrum, as well as the slope difference between S and P, are of importance. The linear trend present in the spectrum will only yield a net shift in the origin time, which is of course impossible to retrieve from observations of arrival times only.

VII-5 Evaluation of the model

The examples given in the previous sections give a general idea of
the radiation fields predicted by our model. Let us now turn to an
evaluation of how this model compares with observations, and with
completely numerical models. The present section does not do justice
either to the flexibility of the model, or to the large body of observa-
tions currently available (e.g., Tucker, et al., 1973; Hanks, 1973). But,
then again, an extensive discussion would be too voluminous to insert
here.

i) Magnitude data

As mentioned earlier, the spectral shape which our model predicts,
and the scaling laws presented in this chapter permit us to discuss the
relationship between the body-wave magnitude m_b and the surface-wave
magnitude M_s . Of course, because magnitude scales have been
empirically defined from time domain observations (e.g., Richter, 1958),
a quantitative comparison can only be made by computing synthetic seismo-
grams and following the usual procedure to calculate magnitudes.
However, by plotting the S-spectral amplitude at a period of 20 seconds
against the P amplitude at one second as a function of source dimension,
one obtains an idea of the character of the m_b/M_s curve predicted by
the model. A sketch of such plots is given on figure VII-5-1, for three
relaxation radii and three rupture velocities. The axes are scaled so as
to correspond to the source and medium parameters used in the previous
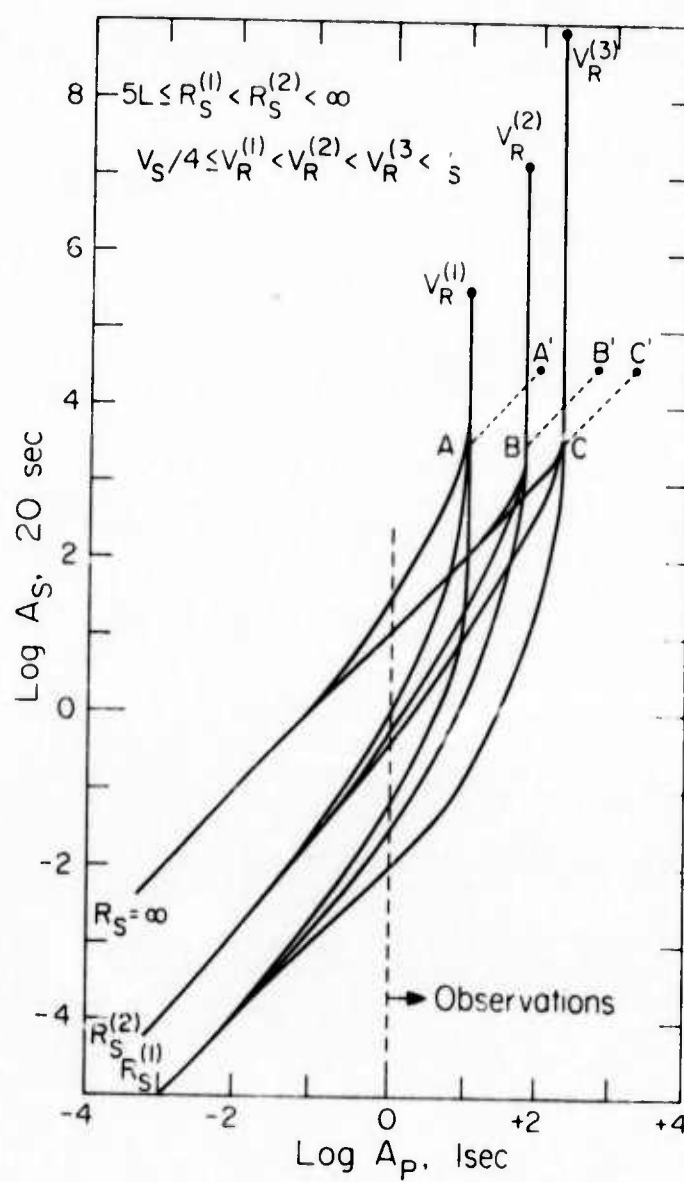sections. The distance was kept constant and equal to 100 km.

Fig. VII 5-1. Plot of S spectral amplitude at 20 seconds versus P spectral amplitude at 1 second period. Simulation of m_b / M_s plots.

The low magnitude part of the graph is controlled by R_s and the large magnitude part by the rupture velocity. The net result is that a band of possible observations is defined in the $m_b - M_s$ plane, which allows for much scatter in the data. In addition, a change of the prestress yields a shift of the whole graph along a direction inclined at $45°$ on the axes. Since there is an observational cut-off, we do not expect to observe the lower part of the curves. Furthermore, we pointed out in Chapter IV that R_s may equal many source dimensions for small events so that the observations should cluster towards the upper limit of the zone defined in figure VII-5-1 for low magnitudes.

The diagram predicts an upper bound for both m_b and M_s , at fixed prestress. In particular, the curves bend sharply upwards when the bound on m_b is reached. The bend occurs for a fault dimension between 5 km and 10 km, depending on the rupture velocity. This corresponds to a magnitude between 5 and 6. Of course, an increase in the prestress would bring the points A,B,C to A',B',C' respectively, and this complicates the problem. The latitude offered by the three parameters V_R , R_s , and the prestress level may account for the very large scatter of the observations (Evernden, 1973, personal communication).

The character of these curves provides an explanation as to why no earthquake with local magnitude larger than 6 ½ has been observed in Southern California (Hanks, 1973, personal communication). Furthermore, observations of a large number of events with widely differing locations and depths show that the m_b/M_s diagram does indeed exhibit this character, in spite of the scatter (Evernden, 1973, personal communication).

Figure VII-5-1 shows an upper bound for M_s as well, which agrees with the observations since no earthquake with magnitude greater than 9 has ever been recorded. However, when the rupture velocity equals the shear velocity, we saw earlier that the S-spectrum has a high frequency slope of ω^{-2} and thus M_s should be unbounded. But it seems difficult to envision a rupture propagating for 700 km or 800 km at the shear velocity since this would require very high stress levels on a large regional scale.

Let us again emphasize that spectral levels are not simply related to time domain amplitudes, so that we shall confine ourselves here to this qualitative discussion.

ii) Comparison with numerical models

Cherry (1973) constructed a two dimensional fault model for which the rupture propagation is controlled by a failure criterion such as the one described in Chapter III. A minimum of plastic work is required before failure, and a dynamic friction is imposed on the rupture surface. The radiation field is calculated by combining a finite element technique with a finite difference scheme for the time dependence.

Figure VII-5-2 shows the near-field radiation obtained by Cherry at a particular station. The components x and y are measured parallel and orthogonal to the fault line respectively. Also shown on the figure is the radiation spectrum calculated from our model, using the average rupture parameters obtained by Cherry. The agreement is very good at high frequency. In particular, both models predict an average slope of ω^{-3}. On the other hand, one observes a discrepancy at long periods.
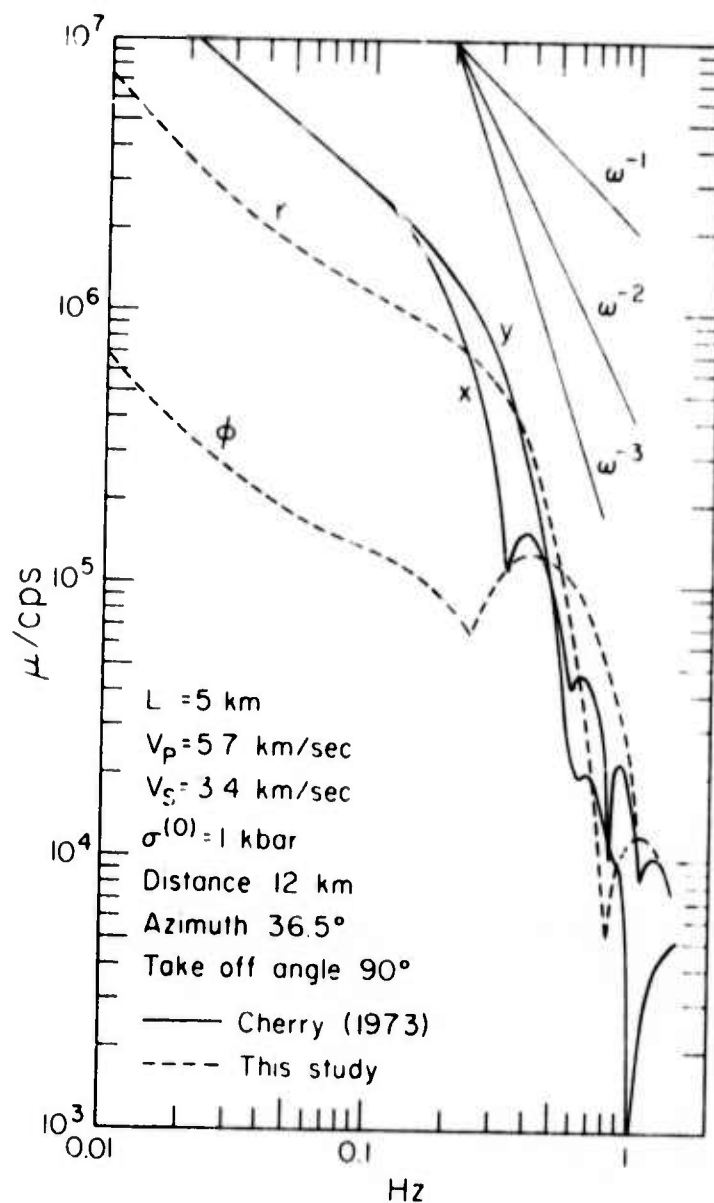
-389-

Figure VII-5-2. Comparison of spherical rupture model with results from a two-dimensional numerical finite difference code.

-390-

The field is practically radial for both models, but we predict a smaller relative long-period amplitude -- by a factor of 4 .

Recall however, that Cherry uses a two dimensional model, while we use a three dimensional one, and since the distance is about two rupture dimensions, the finiteness of the fault should not be neglected. Furthermore,Cherry assumes a significant hydrostatic pressure, while we have a pure shear prestress; it is also rather difficult to evaluate the effects due to different boundary conditions, both on the fault surface, and at large distances: Cherry "freezes" the fault when the relative velocity of the two lips vanishes--unless the shear stress exceeds the dynamic friction--and thus he may freeze the fault in an "overshot" configuration[†].

In spite of the extreme differences between the two models, the agreement shown on figure VII-5-2 is still excellent. The corner frequency chosen by Cherry (1973) at .3 cps is almost exactly that predicted by our model, and since the high frequency spectra are quite comparable, it is likely that the far-field spectra would also compare favorably.

iii) The Harris Ranch earthquake of 27 October 1969

Figure VII-5-3 shows an example of spectral data compared with

---

[†] Cherry (1973, personal communication) overestimated his spectral levels by a factor of 2π . Thus the two models can be better reconciled, since we must then scale our prestress to 160 bars, which is of the order of his static stress drop ($\sim$ 110 bars) and his dynamic stress drop ($\sim$ 250 bars). The long-period difference is thus geometrical.

-391-

a theoretical spectrum. The data were computed by McEvilly and Johnson (1973). This is a displacement amplitude spectrum computed for the Harris Ranch earthquake of 27 October 1969. This was a magnitude 4.6 strike-slip event on the San Andreas fault system; the focal depth was 12.5 km; the epicentral distance was 1.25 km; the spectrum shown corresponds to the EW component, and the entire wave train shown on figure VII-5-4b was used to compute it. The theoretical spectrum was simply obtained by use of the scaling laws from one of the cases computed earlier. We see that a good fit is obtained for a rupture length of 1.4 km, a rupture velocity of 3.0 km/sec, a prestress of 300 bars, and a relaxation radius of about 10 fault lengths. The interaction of the incident wave with the free surface was simply taken into account by doubling the free-space amplitude.

Of course, we are not capable of reproducing the high frequency details of the spectrum, which are most likely due to surface layering, and which come from the long coda shown on figure VII-5-4b. However, the general shape of the spectrum is matched reasonably well. It is probable that the slightly high spectral amplitude predicted by the model around 1 cps could be corrected by using, for example, a slightly lower rupture velocity. The fit is good at long periods, and a finite value of R_s is required to match the marked trough at 0.1 cps. Note that the very long-period slope of the observed spectrum is steeper than ω^{-1}, which suggests that there is significant contamination by long-period noise.

There is no doubt that this fit could be improved by suitable manipulation of the fault parameters. For instance, one could try a
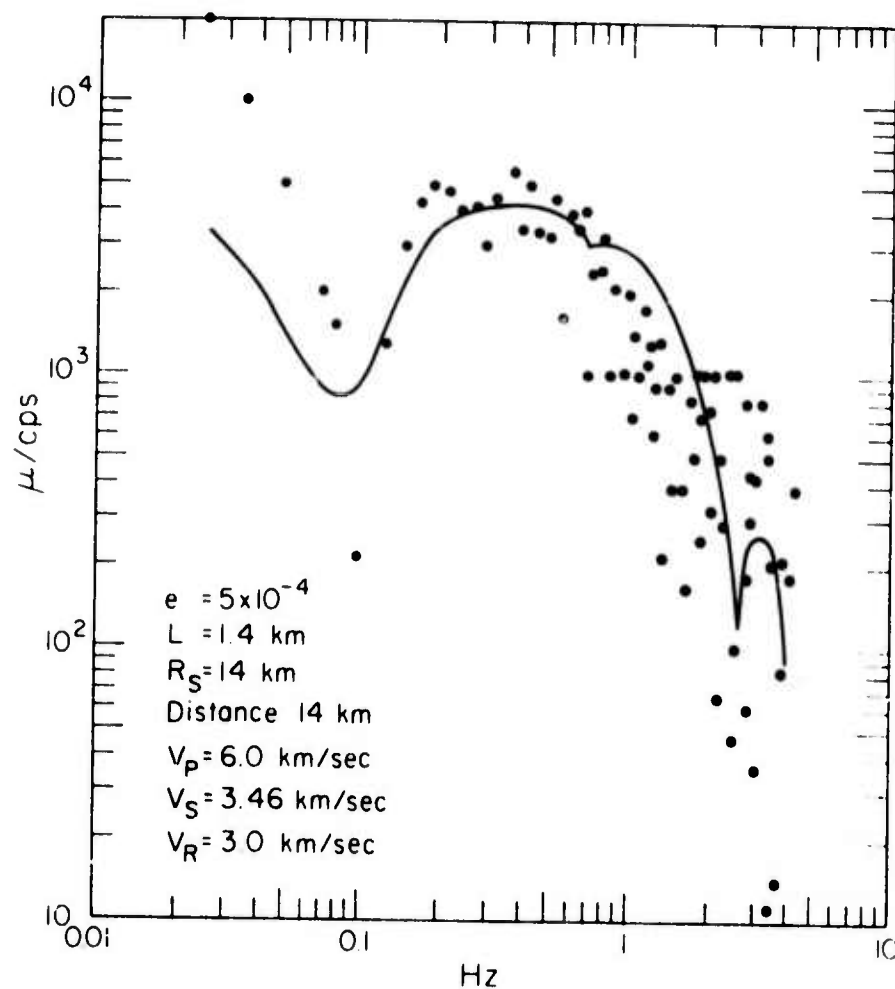
-392-

Figure VII-5-3.   Comparison of observed spectrum from the Harris Ranch earthquake of 27 October 1969 with theoretical spectrum from the propagating spherical rupture model.
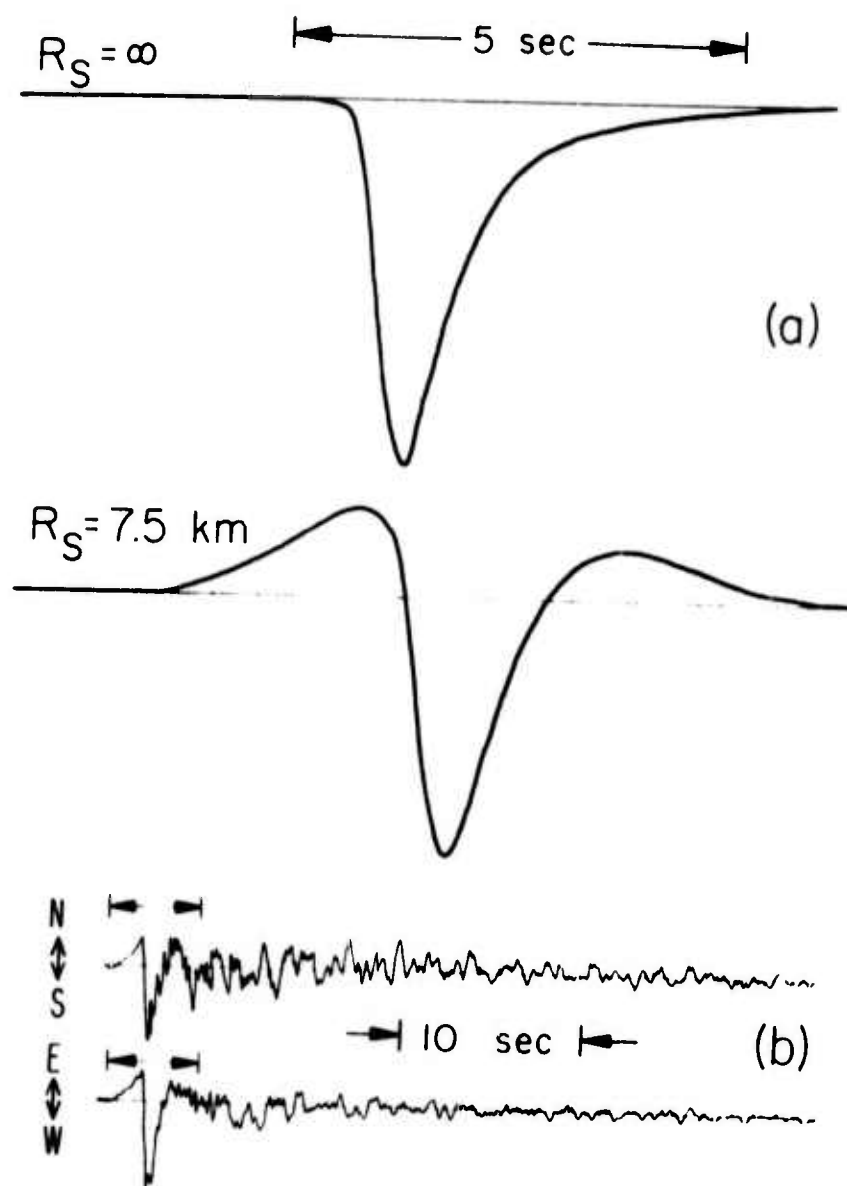
Figure VII-5-4. a) Wave forms computed for spherical rupture model with equilateral growth. b) Observed ground displacement from the Harris Ranch earthquake of 27 October 1969.

larger rupture dimension, combined with a smaller prestress, then a
smaller value of R_s would be required. But the results shown here are
sufficient for our present purposes. In particular, it seems that a
finite value of R_s is required in order to match the long-period
spectrum. The trough seen at about 0.1 cps is also present on the NS
component (McEvilly and Johnson, 1973). This feature should be translated
into a particular pulse shape in the time domain.

Figure VII-5-4 shows synthetic far-field pulses computed for a
stationary spherical rupture of radius 750 m. When R_s is infinite, the
pulse is unipolar (e.g., Molnar, et al., 1973). This is no longer the
case where R_s is finite. It is easy to compare qualitatively these
pulse shapes with the seismograms shown below them. McEvilly and
Johnson (1973) show that these records represent essentially the ground
displacement except at very long periods (tilts). It is clear that a
finite value of R_s is suggested by the time domain data as well.

The rather qualitative comparisons presented above are only
preliminary results in an effort to systematically compare model and
observations. We should make note of the fact that Tucker and Brune
(1973) observed flat spectra for many aftershocks of the San Fernando
earthquake, observed at close range. Thus their data suggest that R_s
should be very large compared with the fault dimensions for those events.
Although any precise statement concerning the comparison of data and
model would require a more complete study, we can nevertheless state
that the results of this section are very encouraging.

VI. PREVIOUS TECHNICAL REPORTS

Previous Technical Reports

1969 - Present

Teng, T. L., and Richards, P. G., 1969, Diffracted P, SV, and SH waves and their shadow boundary shifts: Jour. Geophys. Research, v. 74, no. 6, p. 1537-1555.

McGinley, J. R., Jr., and Anderson, D. L., 1969, Relative amplitudes of P and S waves as a mantle reconnaissance tool: Seismol. Soc. America Bull., v. 59, no. 3, p. 1189-1200.

Johnson, L. R., 1969, Array measurements of P velocities in the lower mantle: Seismol. Soc. America Bull., v. 59, no. 2, p. 973-1008.

McGinley, J. R., Jr., 1969, A comparison of observed permanent tilts and strains due to earthquakes with those calculated from displacement dislocations in elastic earth models: Ph.D. Thesis, California Institute of Technology, Pasadena, California.

Smith, M. L., and Franklin, J. N., 1969, Geophysical application of generalized inverse theory: Jour. Geophys. Research, v. 74, no. 10, p. 2783-2785.

Anderson, D. L., and Kovach, R. L., 1969, Universal dispersion tables, III, Free oscillation variational parameters: Seismol. Soc. America Bull., v. 59, no. 4, p. 1667-1693.

Anderson, D. L., and Julian, B. R., 1969, Shear velocities and elastic parameters of the mantle: Jour. Geophys. Research, v. 74, no. 12, p. p. 3281-3286.

Smith, S. W., McGinley, J. R., Jr., Johnson, L. R., and Scholz, C. H., 1969, Effects of large explosions on tectonic strain: Jour. Geophys. Research, v. 74, no. 12, p. 3308-3309.

Archambeau, C. B., Flinn, E. A., and Lambert, D. G., 1969, Fine structure of the upper mantle: Jour. Geophys. Research, v. 74, no. 25, p. 5825-5865.

Anderson, D. L., and Sammis, C. G., 1969, The low velocity zone: Geofisica Internac., v. 9, no. 1-3, p. 3-19.

Archambeau, C. B., and Sammis, C. G., 1970, Seismic radiation from explosions in prestressed media and the measurement of tectonic stress in the earth: Rev. Geophysics and Space Physics, v. 8, no. 3, p. 473-499.

Anderson, D. L., and Sammis, C. G., 1970, Partial melting in the upper mantle: Physics Earth and Planet. Interiors, v. 3, p. 41-50.

Arabasz, W. J., Brune, J. N., and Engen, G. R., 1970, Locations of small earthquakes near the trifurcation of the San Jacinto fault southeast of Anza, California: Seismol. Soc. America Bull., v. 60, no. 2, p. 617-627.

Jackson, D. D., and Anderson, D. L., 1970, Physical mechanisms of seismic-wave attenuation: Rev. Geophysics and Space Physics, v. 8, no. 1, p. 1-63.

Whitcomb, J. H., and Anderson, D. L., 1970, Reflection of P'P' seismic waves from discontinuities in the mantle: Jour. Geophys. Research, v. 75, no. 29, p. 5713-5728.

Julian, B. R., 1970, Regional variations in upper mantle structure beneath North America: Ph.D. thesis, California Institute of Technology, Pasadena, California.

Richards, P. G., 1970, A contribution to the theory of high frequency elastic waves, with applications to the shadow boundary of the earth's core: Ph.D. thesis, California Institute of Technology, Pasadena, California.

Wyss, Max, 1970, Observations and interpretations of tectonic strain release mechanisms: Ph.D. thesis, California Institute of Technology, Pasadena, California.

Archambeau, C. B., 1970, Theory of the seismic source: Proceedings of the Advanced Research Projects Agency Symposium on Discrimination of Earthquakes and Underground Explosions, Woods Hole, Massachusetts, July 20-23.

Gile, W. W., 1970, A mercury pendulum seismometer: IEEE Transactions on Geoscience Electronics (technical report).

Richards, P. G., 1971, Potentials for elastic displacement in spherically symmetric media: Acoust. Soc. America Jour., v. 50, no. 1, p. 188-197.

Richards, P. G., 1971, An elasticity theorem for heterogeneous media, with an example of body wave dispersion in the earth: Royal Astron. Soc. Geophys. Jour., v. 22, p. 453-472.

Liebermann, R. C., and Basham, P. W., 1971, Excitation of surface waves by the Aleutian underground explosion Milrow (October 2, 1969): Jour. Geophys. Research, v. 76, no. 17, p. 4030-4034.

Jordan, T. H., and Franklin, J. N., 1971, Optimal solutions to a linear inverse problem in geophysics: Natl. Acad. Sci. Proc., v. 68, no. 2, p. 291-293.

Hill, D. P., 1971, High frequency wave propagation in the earth: Theory and observation: Ph.D. thesis, California Institute of Technology, Pasadena, California.

Wyss, Max, Hanks, T. C., and Liebermann, R. C., 1971, Comparison of P-wave spectra of underground explosions and earthquakes: Jour. Geophys. Research, v. 76, no. 11, p. 2716-2729.

Hill, D. P., 1971, Velocity gradients and anelasticity from crustal body wave amplitudes: Jour. Geophys. Research, v. 76, no. 14, p. 3309-3325.

Jungels, P. H., and Anderson, D. L., 1971, Strains and tilts associated with the San Fernando earthquake, in The San Fernando, California, Earthquake of February 9, 1971: U.S. Geol. Survey Prof. Paper 733, p. 77-79.

Jordan, T. H., and Minster, J. B., 1971, An application of a stochastic inverse
    to the geophysical inverse problem: Workshop on Mathematics of Profile
    Inversion, Ames Research Center, Moffitt Field, California, July 12-16.

Hill, D. P., 1971, Velocity gradients in the continental crust from head wave
    amplitudes: Am. Geophys. Union Mon. Ser. 14, p. 71-75.

Whitcomb, J. H., 1971, Reflections of P'P' seismic waves from 0 to 150 km depth
    under the Ninety-East Ridge, Indian Ocean, and the Atlantic-Indian Rise:
    Am. Geophys. Union Mon. Ser. 14, p. 211-225.

McKenzie, Dan, and Julian, Bruce, 1971, The Puget Sound, Washington, earthquake
    and the mantle structure beneath the northwestern United States: Geol.
    Soc. America Bull., v. 82, p. 3519-3524.

Helmberger, D. V., 1972, Long period body wave propagation from 4 to 13°:
    Seismol. Soc. America Bull., v. 62, no. 1, p. 325-341.

Archambeau, C. B., 1972, The theory of stress wave radiation from explosions
    in prestressed media: Royal Astron. Soc. Geophys. Jour., v. 29, p. 329-366.

Hanks, T. C., and Wyss, Max, 1972, The use of body-wave spectra in the
    determination of seismic source parameters: Seismol. Soc. America
    Bull., v. 62, no. 2, p. 561-589.

Hanks, T. C. and Thatcher, W., 1972, A graphical representation of seismic
    source parameters: Jour. Geophys. Research, v. 77, no. 23, p. 4393-4405.

Alewine, R. W., 1972, Theoretical and observed distance corrections for
    Rayleigh wave magnitude: Seismol. Soc. America Bull., v. 62, no. 6,
    p. 1611-1619.

Helmberger, D. V., and Harkrider, D. G., 1972, Seismic source descriptions
    of underground explosions and a depth discriminate: Geophys. J. R. Astr.
    Soc., v. 31, p. 45-66.

Mizutani, H., and Abe, K., 1972, An earth model consistent with free oscillation
    and surface wave data: Phys. Earth Planet. Int., v. 5, p. 345-356.

Hill, D. P., 1972, Crustal and upper mantle structure of the Columbia Plateau
    from long-range seismic-refraction measurements: Geol. Soc. America Bull.,
    v. 83, p. 1639-1648.

Lambert, D. G., Flinn, E. A., and Archambeau, C. B., 1972, A comparative study
    of the elastic wave radiation from earthquakes and underground explosions:
    Geophys. Jour., v. 29, p. 403-432.

Mitchell, B. J., 1973, Radiation and attenuation of Rayleigh waves from the
    southeastern Missouri earthquake of October 21, 1965: Jour. Geophys.
    Research, v. 78, no. 5, p. 886-899.

Kurita, T., 1973, A procedure and formulation for elucidating fine structure
    of the crust and upper mantle from seismological data: Seismol. Soc.
    America Bull., v. 63, no. 1, p. 189-209.

Wiggins, R., and Helmberger, D. V., 1973, Upper mantle structure of
    western United States: Jour. Geophys. Research, v. 78, no. 11,
    p. 1870-1880.

York, J. E., and Helmberger, D. V., 1973, Low velocity zone variations
    in the southwestern United States: Jour. Geophys. Research, v. 78,
    no. 11, p. 1883-1886.

Whitcomb, J. H., 1973, Part I. A study of the velocity structure of the
    earth by the use of core phases. Part II. The 1971 San Fernando
    earthquake series focal mechanisms and tectonics; Ph.D. Thesis,
    California Institute of Technology.

Jordan, T. H., 1973, Estimation of the radial variation of seismic velocities
    and density in the earth: Ph.D. Thesis, California Institute of Technology.

Whitcomb, J. H., 1973, Asymmetric P'P' -- an alternative to P'dP' reflections
    in the upper mantle (0-110 km): Seismol. Soc. America Bull., v. 63,
    p. 133-143.

Helmberger, D. V., 1973, Numerical seismograms of long-period body waves from
    seventeen to forty degrees: Seismol. Soc. America Bull., v. 63, p. 633-
    646.

Kurita, T., 1973, Regional variations in the structure of the crust in the
    Central United States from P-wave spectra: Seismol. Soc. America
    Bull., v. 63, p. 1663-1687.

Mitchell, B. J., 1973, Surface-wave attenuation and crustal anelasticity in
    Central North America: Seismol. Soc. America Bull., v. 63, p. 1057-1071.

Mitchell, B. J., and Helmberger, D. V., 1973, Shear velocities at the base
    of the mantle from observations of S and ScS: Jour. Geophys. Research,
    v. 78, p. 6609-6020.

Niazi, M., 1973, SH travel times and lateral heterogeneities in the lower
    mantle: Seismol. Soc. America Bull., v. 63, p. 2035-2046.

PAPERS SUBMITTED FOR PUBLICATION

Hron, F., and Kanasewich, E. R., Synthetic seismograms for deep seismic
sounding studies using generalized ray theory: submitted to Seismol.
Soc. America Bull.

Minster, J. B., Transformation of multipolar expansions under rotation
of the coordinate system: submitted to Royal Astron. Soc. Geophys.
Jour.

Gile, W. W., and Taylor, R. A., Photon-coupled generated: submitted to
Electronic Design

Wiggins, R. A., and Helmberger, D. V., Synthetic seismogram computation
by expansion in generalized rays: submitted to Royal Astron. Soc.
Geophys. Jour.

Jordan, T. H., and Anderson, D. L., Earth structure from free oscillations
and travel times: submitted to Royal Astron. Soc. Geophys. Jour.

Kurita, T., Upper mantle structure in the central United States from P
and S wave spectra: Physics of the Earth and Planetary Interiors,
in press.